

HEIKI ERIKSON

Electrochemical reduction of oxygen
on nanostructured palladium and
gold catalysts



DISSERTATIONES CHIMICAE UNIVERSITATIS TARTUENSIS

147

HEIKI ERIKSON

Electrochemical reduction of oxygen
on nanostructured palladium and
gold catalysts



Institute of Chemistry, Faculty of Science and Technology University of Tartu,
Estonia

Dissertation is accepted for the commencement of the degree of Doctor of
Philosophy in Chemistry on June 18, 2015 by the Council of Institute of
Chemistry, University of Tartu.

Supervisors: Assoc. Prof. Kaido Tammeveski
Institute of Chemistry, University of Tartu, Estonia

Dr. Ave Sarapuu
Institute of Chemistry, University of Tartu, Estonia

Opponent: Prof. Elisabet Ahlberg
Department of Chemistry & Molecular Biology,
University of Gothenburg, Sweden

Commencement: August 28th, 2015, at 14:00 in Tartu, Ravila 14a, room 1021



European Union
European Social Fund



Investing in your future

ISSN 1406-0299
ISBN 978-9949-32-883-3 (print)
ISBN 978-9949-32-884-0 (pdf)

Copyright: Heiki Erikson, 2015

University of Tartu Press
www.tyk.ee

TABLE OF CONTENTS

1. LIST OF ORIGINAL PUBLICATIONS	7
2. ABBREVIATIONS AND SYMBOLS	9
3. INTRODUCTION	11
4. LITERATURE OVERVIEW	12
4.1. Oxygen reduction reaction	12
4.2. Oxygen reduction reaction on palladium	12
4.3. Oxygen reduction reaction on gold	17
4.4. Oxygen reduction reaction on palladium/gold bimetallic catalysts ..	19
5. EXPERIMENTAL	21
5.1. Electrode preparation	21
5.1.1. Preparation of thin Pd films	21
5.1.2. Preparation of electrodeposited Pd coatings	21
5.1.3. Preparation of electrodeposited Pd-Au coatings	21
5.1.4. Preparation of shape-controlled Pd nanoparticles	22
5.1.5. Preparation of shape-controlled carbon-supported Pd catalysts	22
5.1.6. Preparation of Au/C electrodes	22
5.1.7. Preparation of shape-controlled carbon-supported Au catalysts	23
5.2. Surface characterisation	24
5.3. Electrochemical measurements	24
6. RESULTS AND DISCUSSION	26
6.1. Oxygen reduction on thin Pd films	26
6.1.1. Surface characterisation of thin Pd films	26
6.1.2. Cyclic voltammetry of thin Pd films	27
6.1.3. ORR on thin Pd films in alkaline solution	29
6.1.4. ORR on thin Pd films in acidic solution	32
6.2. Oxygen reduction on electrodeposited Pd coatings	36
6.2.1. Surface characterisation of electrodeposited Pd coatings	36
6.2.2. Cyclic voltammetry and CO stripping	38
6.2.3. ORR on electrodeposited Pd electrodes in acidic solution	40
6.2.4. ORR on electrodeposited Pd electrodes in alkaline solution...	42
6.3. Oxygen reduction on electrodeposited Pd-Au coatings	44
6.3.1. Surface characterisation of Pd-Au coatings.....	45
6.3.2. Cyclic voltammetry of electrodeposited Pd-Au coatings	46
6.3.3. ORR on electrodeposited Pd-Au coatings in acidic solution...	47
6.3.4. ORR on electrodeposited Pd-Au coatings in alkaline solution	50
6.3.5. Hydrogen peroxide reactions on electrodeposited Pd-Au alloys in alkaline solution.....	52

6.4. Oxygen reduction on Pd nanocubes	53
6.4.1. Surface characterisation of Pd nanocubes	53
6.4.2. Cyclic voltammetry and CO stripping	54
6.4.3. ORR on Pd nanocubes in acidic solutions	56
6.4.4. ORR on Pd nanocubes in alkaline solution	58
6.5. Oxygen reduction on carbon-supported Pd nanocubes	59
6.5.1. Surface characterisation of carbon-supported Pd nanocubes ..	59
6.5.2. Cyclic voltammetry and CO stripping	60
6.5.3. ORR on shape-controlled Pd/C catalysts in acidic solution ...	61
6.6. Oxygen reduction on gold catalysts supported on carbon	63
6.6.1. Surface characterisation of Au/C catalysts	63
6.6.2. Cyclic voltammetry of Au/C catalysts	64
6.6.3. ORR on Au/C catalysts in acidic solution	65
6.6.4. ORR on Au/C catalysts in alkaline solution	67
6.7. Oxygen reduction on shape-controlled Au nanopartices supported on carbon	70
6.7.1. Surface characterisation of shape-controlled Au/C catalysts .	70
6.7.2. CO stripping on shape-controlled Au nanoparticles in alkaline solution	71
6.7.3. Cyclic voltammetry of shape-controlled Au/C catalysts	72
6.7.4. ORR on shape-controlled Au/C catalysts in acidic solution ...	73
6.7.5. ORR on shape-controlled Au/C catalysts in alkaline solution	76
7. SUMMARY	79
8. REFERENCES	81
9. SUMMARY IN ESTONIAN	94
10. ACKNOWLEDGEMENTS	96
11. PUBLICATIONS	97
CURRICULUM VITAE	193
ELULOOKIRJELDUS	195

I. LIST OF ORIGINAL PUBLICATIONS

This thesis consists of nine original articles listed below and a review. The articles are referred in the text by Roman numerals I-IX.

- I **H. Erikson**, A. Kasikov, C. Johans, K. Kontturi, K. Tammeveski, A. Sarapuu, Oxygen reduction on Nafion-coated thin-film palladium electrodes, *Journal of Electroanalytical Chemistry* 652 (2011) 1–7.
- II **H. Erikson**, M. Liik, A. Sarapuu, J. Kozlova, V. Sammelselg, K. Tammeveski, Oxygen reduction on electrodeposited Pd coatings on glassy carbon, *Electrochimica Acta* 88 (2013) 513–518.
- III **H. Erikson**, M. Liik, A. Sarapuu, M. Marandi, V. Sammelselg, K. Tammeveski, Electrocatalysis of oxygen reduction on electrodeposited Pd coatings on gold, *Journal of Electroanalytical Chemistry* 691 (2013) 35–41.
- IV **H. Erikson**, A. Sarapuu, J. Kozlova, L. Matisen, V. Sammelselg, K. Tammeveski, Oxygen electroreduction on electrodeposited PdAu nanoalloys, *Electrocatalysis* 6 (2015) 77–85.
- V **H. Erikson**, A. Sarapuu, K. Tammeveski, J. Solla-Gullón, J. M. Feliu, Enhanced electrocatalytic activity of cubic Pd nanoparticles towards the oxygen reduction reaction in acid media, *Electrochemistry Communications* 13 (2011) 734–737.
- VI **H. Erikson**, A. Sarapuu, N. Alexeyeva, K. Tammeveski, J. Solla-Gullón, J. M. Feliu, Electrochemical reduction of oxygen on palladium nanocubes in acid and alkaline solutions, *Electrochimica Acta* 59 (2012) 329–335.
- VII **H. Erikson**, A. Sarapuu, K. Tammeveski, J. Solla-Gullón, J. M. Feliu, Oxygen electroreduction on carbon-supported Pd nanocubes in acid solution, (manuscript in preparation).
- VIII **H. Erikson**, G. Jürmann, A. Sarapuu, R. J. Potter, K. Tammeveski, Electroreduction of oxygen on carbon-supported gold catalysts, *Electrochimica Acta* 54 (2009) 7483–7489.
- IX **H. Erikson**, A. Sarapuu, K. Tammeveski, J. Solla-Gullón, J. M. Feliu, Shape-dependent electrocatalysis: oxygen reduction on carbon-supported gold nanoparticles, *ChemElectroChem* 1 (2014) 1338–1347.

Author's contribution:

Paper I: The author has performed all electrochemical measurements, participated in the analysis of the data and participated in the writing of the paper.

Paper II: The author participated in the electrochemical measurements, analysed the data and is mainly responsible for writing the paper.

Paper III: The author participated in the electrochemical measurements, analysed the data and is mainly responsible for writing the paper.

- Paper IV:** The author performed all electrochemical measurements, analysed the data and is mainly responsible for writing the paper.
- Paper V:** The author made all the electrochemical measurements, analysed the data and participated in the writing of the paper.
- Paper VI:** The author made all the electrochemical measurements, analysed the data and participated in the writing of the paper.
- Paper VII:** The author prepared the catalyst materials and made all the electrochemical measurements, analysed the data and is mainly responsible for writing the paper.
- Paper VIII:** The author made all the electrochemical measurements.
- Paper IX:** The author made all the electrochemical measurements, analysed the data and is mainly responsible for writing the paper.

2. ABBREVIATIONS AND SYMBOLS

A_r	real electroactive surface area
AuNP	gold nanoparticles
AFM	atomic force microscopy
BE	binding energy
$C_{O_2}^b$	concentration of oxygen in the bulk solution
$C_{O_2}^f$	concentration of oxygen in the Nafion film
CV	cyclic voltammetry
CTAB	cetyltrimethylammonium bromide
D_{O_2}	diffusion coefficient of oxygen
D_f	diffusion coefficient of O_2 in the Nafion layer
E	potential
$E_{1/2}$	half-wave potential
EDX	energy dispersive X-ray spectroscopy
F	Faraday constant
<i>fcc</i>	face-centred cubic
GC	glassy carbon
HAADF	high angle annular dark field
HOPG	highly oriented pyrolytic graphite
HR-SEM	high resolution scanning electron microscopy
j	measured current density
j_d	diffusion-limited current density
j_f	limiting diffusion current density in the Nafion layer
j_{lim}	plateau current density
j_k	kinetic current density
k_i	heterogeneous electron transfer rate constant
K-L	Koutecky-Levich
L	thickness of the Nafion layer
MA	mass activity
n	number of electrons transferred per oxygen molecule
ORR	oxygen reduction reaction
PdNP	palladium nanoparticles
PVP	polyvinylpyrrolidone
RDE	rotating disk electrode
RHE	reversible hydrogen electrode
RMS	root mean square
SA	specific activity
SEM	scanning electron microscopy
SCE	saturated calomel electrode
STEM	scanning transmission electron microscopy
TEM	transmission electron microscopy
UPD	underpotential deposition

v	potential scan rate
XPS	X-ray photoelectron spectroscopy
XRD	X-ray diffraction
ν	kinematic viscosity of the solution
θ	electron take-off angle
ω	electrode rotation rate

3. INTRODUCTION

The oxygen reduction reaction (ORR) is one of the most important reactions in electrochemistry that is employed in several applications, for example in fuel cells, metal-air batteries and hydrogen peroxide electrosynthesis.

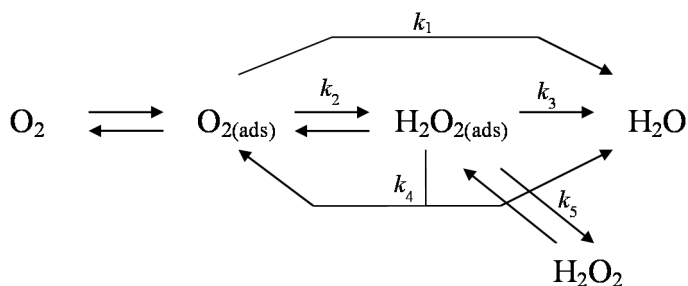
The ORR proceeds via two main pathways. The four-electron pathway is preferred in the fuel cell applications, while the two-electron pathway is employed in the electrochemical synthesis of hydrogen peroxide [1, 2]. Platinum-based catalysts are commonly used in the low-temperature fuel cells, as Pt is the most active metal catalyst for ORR and supports the 4-electron reduction. Due to the high price and scarcity of Pt, alternative catalysts are searched and palladium is a possible candidate, as the price of Pd is lower than that of Pt and the ORR proceeds mainly via the same mechanism on both metals [1]. In addition, oxygen reduction on palladium is a structure-sensitive reaction [3] and thus it is possible to tailor the catalysts through precise control of their morphology, in order to achieve the highest electrocatalytic activity. Addition of gold to palladium has been shown to increase the stability of the catalyst and also it may improve the electrocatalytic activity towards the ORR [1, 2].

The main aim of this research was to study the ORR on different nanostructured palladium and gold catalysts. In the first part of this study palladium was deposited onto glassy carbon (GC) substrate by vacuum evaporation and the effect of the nominal Pd film thickness on the ORR kinetics was evaluated in acid and alkaline media [I]. In the second part Pd was electrochemically deposited onto GC and Au substrates and the influence of the deposition time on the ORR activity was investigated [II, III]. As a continuation, Pd and Au were codeposited onto GC substrate at different Pd:Au ratios and the kinetics of the ORR on these nanoalloys was studied. In the next part the ORR on cubic Pd nanoparticles was investigated, in order to see if the results obtained on the single-crystal Pd electrodes are transferrable to nanoparticles [V–VII]. To study the effect of catalyst loading on the ORR activity, the Au/C catalysts at various layer thickness were employed [VIII]. In the final part the carbon-supported shape-controlled Au nanoparticles were used for oxygen reduction studies to demonstrate the shape effect of the nanostructured Au catalysts on the ORR kinetics [IX].

4. LITERATURE OVERVIEW

4.1. Oxygen reduction reaction

The oxygen reduction reaction is a process that can proceed via numerous pathways [4]. Oxygen may be reduced directly to water by a four-electron pathway, or it may be reduced to hydrogen peroxide via a two-electron pathway. Also H_2O_2 may be further reduced to water or it may disproportionate to H_2O and O_2 . These simplified reaction pathways are shown in Scheme 1 [5]:



Scheme 1. Simplified mechanism for the ORR in acid solutions. The rate constants (k_i) for the different steps are indicated in the Scheme. (ads) denotes the species in their adsorbed form.

The predominant reaction pathway depends on several factors, like electrode material, pH of the solution and the electrode potential [5, 6]. For example on Pt, Pd and Ag in alkaline media the ORR proceeds via direct four-electron pathway while carbon blacks and graphite catalyse the two-electron reduction of oxygen [1, 7].

4.2. Oxygen reduction reaction on palladium

Platinum is the best catalyst among pure metals for ORR and palladium is the next best [8]. This is due to the fact that Pd and Pt belong to the same group in the periodic table, have the same face-centred cubic (*fcc*) crystal structure and similar atomic size [1]. Also the price of Pd is lower as it is more abundant on Earth than platinum [1].

The oxygen reduction reaction on bulk Pd has been thoroughly studied. The ORR on polycrystalline Pd proceeds via a 4-electron pathway yielding water and the reaction mechanism has been proposed to be the same on Pd as on Pt [9, 10]. The electrocatalytic activity of Pd for ORR is strongly affected by the oxidation of Pd surface and therefore depends on the potential cycling conditions, cathodic sweeps generally showing lower currents than anodic sweeps

[9–11]. It has been suggested that the ORR proceeds mainly via a 4-electron pathway in the potential regions where Pd surface is either oxide free or oxidised to PdOH, but when PdO is present on the surface, then the ORR proceeds partly via peroxide intermediate [11]. The analysis of the ORR results on palladium have shown two distinct Tafel slope regions, at high current densities the slope is -120 mV and at low current densities a value of -60 mV is observed [9, 10]. However, the rate-determining step in both regions is suggested to be the transfer of the first electron to the O₂ molecule and the change in the slope value is due to the adsorption of oxygen species.

Very recently the role of oxides on Pd/C catalysts in the ORR activity has been studied in perchloric acid solution [12]. It was shown that strongly oxidised Pd nanoparticles are inactive for ORR until the initial oxides are reduced in the hydrogen underpotential deposition (H_{UPD}) region. During subsequent potential sweeps the remaining oxides are further reduced and thus the half-wave potential of the catalyst shifts positively until it stabilises.

Kondo et al. studied the ORR on the low-index planes, *n*(100)-(111) and *n*(100)-(110) series of Pd in perchloric acid solution [3]. They observed that platinum has higher activity than palladium, except of Pd(100) that had the highest current density at 0.9 V, nearly 3 times higher than that of the most active single-crystal facet of Pt. It is also important to note that the activity of the ORR increases in the order of Pd(110) < Pd(111) < Pd(100), that is the opposite direction of that of platinum in perchloric acid. Studying the stepped surfaces also supported the claim that Pd(100) is the most active plane for ORR and the stepped structures do not affect the activity of the ORR. Later Hitotsuyanagi et al. have studied the oxygen reduction reaction on *n*(111)–(100) series of Pd [13]. They observed that oxides are preferentially adsorbed on the step sites and do not affect the ORR activity at 0.9 V, suggesting that Pd(111) terraces are the active sites for ORR.

For practical applications nanostructured catalysts are needed, which can be prepared by several methods, for instance electrochemical [14–20], chemical [21, 22], physical [23–26], template assisted spontaneous procedures [27, 28], etc. Electrochemically deposited nanoporous palladium and platinum have shown increased ORR activity as compared to the commercial Pt/C catalyst [19]. The increased activity of these structures was suggested to arise from the structural effects, like porosity that facilitates the mass transport through the porous metal layer. Al Abass et al. have shown the increased activity of electro-deposited Pd nanoparticles (PdNPs) that could not be explained only by the increased electroactive surface area [20].

The oxygen reduction studies on thin palladium films in acid solutions have shown that the overall ORR activity of the electrodes decreases with decreasing the film thickness in sulphuric and perchloric acid solutions, mainly as a result of the decrease in the electroactive surface area [23]. The specific activity of the ORR was independent of the metal loading in perchloric acid, but in sulphuric acid it decreased with decreasing the film thickness. This activity decrease in

sulphuric acid was suggested to be due to the adsorption of (bi)sulphate on the active centres. Pd particles in the size range of 10–30 nm were spontaneously deposited onto Au substrate [28]. With increased deposition time higher number of Pd particles was formed and thus the half-wave potential of the ORR in perchloric acid shifted to more positive potentials [28]. The ORR on Pd deposited onto gold substrate proceeded partly through a $4e^-$ series pathway [28].

Salvador-Pascual et al. investigated the oxygen reduction reaction on PdNPs with average crystallite size of 4 nm [29]. Overall their catalyst showed poor ORR activity in sulphuric acid, but the reaction on nanostructured Pd proceeded via 4-electron pathway, while the transfer of the first electron to the oxygen molecule was the rate-determining step as on bulk Pd. Alvarez et al. evaluated the ORR activity of PdNPs prepared using different reducing agents like ethylene glycol, formaldehyde and sodium borohydride [21]. Different synthesis methods yielded particles with different morphologies and all catalysts showed agglomeration. The best results were achieved with particles synthesised with ethylene glycol as it had less agglomeration and thus the highest ORR activity, but it was still lower than that of commercial Pt/C catalyst. Jukk et al. have prepared PdNPs supported on multi-walled carbon nanotubes [22, 24, 25]. For chemically synthesised materials they obtained the specific activity (SA) of the ORR twice as high as that for bulk Pd in sulphuric acid and about three times higher in potassium hydroxide solution [22]. The activity of Pd nanolayers sputter-deposited onto carbon nanotubes was lower as compared to that of bulk Pd in acid solution, probably due to the adsorption of (bi)sulphate ions. In alkaline media the specific activity surpassed that of bulk Pd and was rather constant for the catalysts with different nominal thicknesses of the Pd film [25]. Also they showed that heat-treatment of the catalysts would improve their ORR activity [24]. Li and Zhao studied a similar system in the anion-exchange membrane fuel cell [26]. They suggested that sputter-deposition of Pd on the surface of carbon nanotubes with backing layer of carbon paper extends the electrochemical surface area and also facilitates the oxygen transport, thereby improving the fuel cell performance.

Jiang et al. have studied the Pd particle size effect on the oxygen reduction activity in alkaline media [30]. The SA of Pd/C increased continuously by a factor of 3 when the particle size increased from 3 to 16.7 nm. The mass activity increased by a factor of 1.3 when particle size increased from 3 to 5 nm, but then decreased with further increasing the particle size. It was suggested that lower activity of smaller particles might be due to the increased adsorption of OH^- , as has been suggested on platinum nanoparticles [31]. It was also reported that the reaction mechanism does not change with changing particle size and the ORR proceeds via four-electron pathway [30]. The particle size effect in acidic solution has been suggested to follow similar trend, the specific activity increasing with increasing the particle size and particles larger than 10 nm acting like bulk material [32, 33].

The substrate where metal nanoparticles are incorporated plays an important role in the electrocatalytic activity of the catalyst [34–38]. The pre-treatment of Vulcan XC-72R carbon has shown to affect the physical and chemical properties of the catalyst by changing the Brunauer–Emmett–Teller (BET) surface area, removing the impurities and influencing the agglomeration of PdNPs, which in turn affects the ORR activity [34]. Pd nanoparticles supported on graphene sheets had higher electrocatalytic activity towards the ORR than similar Pt particles on the same support in alkaline media, as the specific activity and mass activity were about 2 times higher for Pd than Pt catalysts [35]. In addition Carrera-Cerritos et al. compared the conventional carbon and the reduced graphene oxide as catalyst supports [36]. They found that Pd nanoparticles have higher electrocatalytic activity towards the ORR in acid when being deposited on reduced graphene oxide, while Pt nanoparticles had higher activity when on a conventional carbon support, showing that the interaction between metal nanoparticles and support material affects the activity of the catalyst. Similarly PdNPs on nitrogen-doped graphene nanosheets exhibited better ORR activity than bulk Pd [37]. Pd nanoparticles bound on the nitrogen-doped mesoporous graphitic carbon nanospheres have shown an increase in the ORR activity, but in addition to synergistic effects, ordered mesopores, large surface area, homogeneous budding of abundant Pd active sites and graphitisation were also suggested to improve the activity [38]. In contrast, it has been shown that for Pd nanoparticles supported on highly oriented pyrolytic graphite (HOPG) and on nitrogen-doped HOPG the electrocatalytic activity for ORR was similar, but the stability of the catalyst was smaller on N-doped HOPG [39]. It has been shown that the surface area of carbon support affects the stability of Pd-based catalysts, as with increasing the surface area the stability decreased [40]. It is obvious that the ORR activity of Pd nanoparticles depends also on the supporting material. In addition, the Tafel analysis has shown typical slope values for nanostructured Pd as has been observed on bulk Pd in respective solutions, thus indicating that the reaction mechanism on Pd catalyst does not depend on the support material [34, 36, 37].

The activity of the ORR can be improved by modifying Pd nanoparticles with polymers [41, 42]. For example Fu et al. prepared polyallylamine functionalised Pd icosahedra [41]. This catalyst exhibited superior electrocatalytic activity towards the ORR. In alkaline media the activity of Pd as compared to commercial Pt/C, which was suggested to arise from downshift of the d-band centre, lower OH coverage and high density of twinned defects of the Pd icosahedra. Also it was suggested that the polymer can act as a barrier for ethanol, which increases the ethanol tolerance in alkaline media. The change in the Pd electronic structure and steric blocking effect of oleylamine on Pd nanoparticles has been suggested to increase their tolerance to formic acid in the ORR in acidic media [42].

As the electrocatalytic activity of Pd for ORR is structure-sensitive [3], there are several studies of O₂ reduction on Pd nanoparticles of preferential surface

structure. For example Xiao et al. managed to prepare Pd nanorods which showed 10-fold increase in the ORR activity over the Pd nanoparticles [43]. The higher activity of nanorods was attributed to the Pd(110) facets that has later been shown to be the least active site for ORR [3]. Cai et al. proposed a method to prepare particles with preferential Pd(111) facet using bromide adsorption/desorption [44]. These particles showed higher specific activity and mass activity in comparison with untreated Pd/C catalyst. Recently it was shown that Pd nanowires and nanorods had higher specific activities and mass activities than those of commercial Pd/C in acidic as well as in alkaline solution [45].

Shao et al. systematically studied the ORR on preferentially shaped Pd nanoparticles [46]. They compared the activity of carbon-supported Pd nanocubes enclosed with (100) facets with that of octahedral Pd nanoparticles enclosed with (111) facet and commercial Pd/C and Pt/C catalysts in perchloric acid solution. Pd nanocubes exhibited 10 times higher specific activity than that of octahedral Pd nanoparticles and it was comparable to that of the state-of-the-art Pt electrocatalysts. Somewhat later Lee et al. prepared palladium nanocubes with different sizes (27, 48 and 63 nm) composed of (100) planes and investigated their electrocatalytic activity towards the ORR in 1 M NaOH [47]. The specific activity of the nanocubes was up to 1.5 times higher than that of 9 nm Pd nanoparticles. These nanocubes had more than 3 times higher specific activity for the ORR than spherical Pd nanoparticles in H₂SO₄ solution and it was retained in the presence of methanol [48]. In contrast, Shao et al. did not observe the structural dependence of ORR on Pd nanocubes with the size of 5–6 nm in alkaline media [49]. In sulphuric acid solution the ORR activity of Pd cubes was 17 times higher than that of Pd octahedra, which was explained by stronger adsorption of (bi)sulphate on the surface of octahedral nanocrystals in addition to OH_{ad}. However, for formic acid oxidation no advantage was observed on the shape-controlled Pd nanocrystals in comparison to conventional Pd catalysts [49]. As opposed to the findings by Shao and co-workers, Arjona et al. found that ~11 nm Pd cubes have higher catalytic activity than commercial Pd/C for methanol, ethanol and formic acid oxidation and also for the ORR in alkaline media [50]. In general Pd/C catalysts have displayed higher alcohol tolerance than Pt/C [2, 51].

The stability of Pd-based catalysts is a serious issue [2] and for shape-controlled particles it is even more important [52]. Zadick et al. demonstrated the effects of extensive potential cycling on Pd nanocubes in alkaline media [52]. It was shown that the oxide formation and its subsequent reduction does not significantly change the morphology of the particles and also hydrogen adsorption and desorption alone does not lead to the degradation of Pd nanocubes. The change in the shape of the Pd cubes was observed by cycling in the potential region where both surface oxidation and H_{UPD} take place, thus the degradation of Pd nanocubes was attributed to the electro-oxidation of hydrogen.

4.3. Oxygen reduction reaction on gold

The oxygen reduction reaction studies have shown that this process is strongly structure sensitive on gold as well as on palladium. The Au(100) is clearly the most active single crystal facet for ORR in alkaline media [53, 54]. The adsorption of anions changes the ORR pathway on Au(100) as Štrbac et al. showed with (bi)sulphate and OH^- [55]. The adsorbed OH^- has been suggested to be the most important key to determine the reaction pathway. Without OH^- adsorption (at $\text{pH} < 6$) the ORR begins as a 2-electron process and changes to a 4-electron reduction at certain potential depending on the pH of the solution. At $\text{pH} > 6$ the ORR starts as a 4-electron process in the potential region where specifically adsorbed OH^- anions are present. The increased activity of Au(100) has been suggested to arise from Aloha species that have stronger interaction with O_2 , HO_2^- and O_2^- [54, 56, 57]. Later it has been shown on the basis of spectroscopic data that the reaction intermediate on gold is HO_2^- , which reduces further to OH^- in alkaline media, but protonates fast in acid media, yielding H_2O_2 . Therefore, the ORR in alkaline solutions proceeds via $4e^-$ pathway, but in acid via $2e^-$ pathway [58]. In contrast, Kim and Gewirth have suggested that the ORR in alkaline media proceeds via superoxide species and the enhanced activity of Au(100) arises from a disproportionation mechanism [59]. Andoralov et al. determined that ORR on polycrystalline gold in acidic medium proceeds by different pathways that depend on the electrode potential [60]. Close to the steady-state potential peroxide is the main product and at negative potentials it can be further reduced. On nanostructured Au $2e^-$ and $4e^-$ pathways for ORR have been suggested [61].

It has been shown that modification of Au surface can change the ORR pathway. For instance, deposition of fullerenes onto Au surface increased the selectivity of O_2 reduction to hydrogen peroxide, which may be the result of steric blocking of the surface [62]. Cysteine has been shown to block Au(100) and Au(110) facets and on Au(111) the ORR proceeds via $2e^-$ pathway in alkaline media [63]. Metal ad-layers can also affect the ORR activity, for example Ag on Au(111) increases the reduction current and the reaction yields water [64].

The dependence of ORR on the size of Au nanoparticles has been described in several studies. Thin Au films in sulphuric acid solution have shown increased SA for the ORR as compared to bulk gold, whereas the SA and the reaction mechanism do not depend on the film thickness [65, 66]. Similar electrocatalytic behaviour was observed for nanostructured Au on boron-doped diamond electrode [67]. In both cases the H_2O_2 was partially further reduced to yield water. Such observations suggest that the ORR on Au depends on the particle size. However, Bron showed that in sulphuric acid solution the specific activity is neither dependent on the particle size in the range of 2.7–42.3 nm nor on the support material and the number of electrons involved in the reaction is 2

to 3 [68]. On the other hand, Inasaki and Kobayashi have demonstrated that the SA decreases with decreasing the particle size from 13.2 to 1.7 nm and the value of n increases with decreasing the particle size in sulphuric acid solution [69]. In contradiction to previous reports, Au nanoparticles on highly oriented pyrolytic graphite have shown that the SA increases with decreasing the particle size [70]. In addition, small Au clusters with less than 11 atoms have shown promising electrocatalytic activity towards the ORR [71].

Guerin et al. observed that the activity of Au nanoparticles in perchloric acid decreases when particle size drops below 3 nm [72]. Jirkovsky et al. found a maximum activity on 5.7 nm particles and that the selectivity for peroxide increases for particles smaller than 6 nm [73].

In alkaline media the kinetic current of ORR on 3 nm Au nanoparticles was found to be 2.5 times higher than that on 7 nm Au nanoparticles [74]. The reaction product on smaller particles was found to be water while on 7 nm particles it was HO_2^- . Chen and Chen also suggested that smaller particles are more active towards the ORR in alkaline media [75]. The report by Zhang et al. also showed that the intrinsic activity of the ORR increases with decreasing the particle size [76]. In contrast, the specific activity of thin Au films in alkaline solution decreased with decreasing film thickness [66]. Despite the number of different results it is obvious that the particle size does play an important role in the kinetics of the ORR on gold nanoparticles in sulphuric acid, perchloric acid and in alkaline media.

Ohsaka and co-workers have prepared several gold nanoparticle-modified electrodes using self-assembled monolayers and electrochemical deposition of Au [77–84]. In general they managed to deposit Au nanoparticles (AuNPs) with various morphologies and surface crystallographic orientations in the presence of different additives that blocked certain single crystal facets. The best ORR activities were obtained with particles that had Au(100)-like structure [79]. In addition to electrochemical deposition, electrochemical pre-treatment allows tailoring of Au and AuNPs to improve the ORR activity [85]. It was suggested that the pre-treatment forms a thick Au oxide layer that has an important role in the ORR activity.

The ORR activity and pathway on nanostructured Au catalysts also depends on the support material. On pure gold catalysts the ORR proceeds mainly via 2-electron pathway in acid, but when Au nanoparticles are supported on carbon black and SnO_x , which also catalyses the production of peroxide, the four-electron reduction of oxygen has been observed to prevail [86, 87]. Also enhancement of the ORR activity has been observed when Au was dispersed on nanotubular TiO_2 matrix [88]. Au/ TiO_2 composites on Ti surface have produced the voltammetric response similar to Au(100) facet [89]. AuNP composites with MnO_x have proved to catalyse the ORR to water, presumably by AuNPs catalysing the reduction of O_2 to HO_2^- and MnO_x catalysing the decomposition of the peroxide [90]. Synergistic effect between Au nanoparticles and graphene has been suggested to increase the ORR activity as compared to carbon black

supported Au nanoparticles [91]. Au nanoparticles on reduced graphene oxide have been demonstrated to have the onset potential of O₂ reduction comparable to that of commercial Pt/C, but superior methanol tolerance and enhanced stability [92]. AuNP supported on carbon nanotubes prepared by different approaches have shown high electrocatalytic activity towards the ORR in acidic media [93–96].

As it has been well established that Au(100) is the most active single crystal facet of Au for ORR [53, 55–57] then it is of great interest to prepare gold particles that have the (100) facet prevailing on their surface. Hernandez et al. have studied the electrochemical properties of various Au nanoparticles [97–100]. They employed microemulsion method to prepare nanoparticles with higher percentage of (100) and (111) facets, but also nanoparticles where these facets are almost absent [97]. The ORR on the former yielded OH⁻, whereas the latter had HO₂⁻ as the product. Au nanorods composed of (111) and (110) surface domains catalysed the two-electron reduction of O₂ [98]. They also synthesised Au nanocubes about 40 nm in size that had large quantity of wide (100) domains [99]. It was reported that water was the final product of the ORR on these particles in the whole range of potentials, while hydrogen peroxide was obtained only in the lower potentials as on Au(100) electrodes. It was also demonstrated that in alkaline media cubic AuNPs are more active than spherical AuNPs and the least active are short Au nanorods [101]. On the other hand, Jena et al. prepared gold nanoprisms and nanoperiwinkles that despite of dominant Au(111) facets showed excellent electrocatalytic activity towards the oxidation of methanol and the reduction of oxygen [102].

4.4. Oxygen reduction reaction on palladium/gold bimetallic catalysts

In order to increase the activity and stability of Pd-based catalysts, there have been several suggestions to the benefits of alloying [1, 2]. A series of studies by Kibler et al. has shown alloy formation when electrodepositing Pd onto Au monocrystals [14–16]. Submonolayers of Pd on Au(111) and Au(100) have shown to improve the electrodes' activity towards O₂ reduction and the monolayers of Pd were found to be more active than multilayers [103]. In alkaline media depositing a monolayer of Pd onto Pt(*hkl*) has increased its ORR activity 2–4 times, whereas an increase higher than an order of magnitude has been observed when Pd was vacuum evaporated onto Au(*hkl*) [104]. This enhancement of the activity was achieved with as little as 18 at.% of Pd on the surface and it saturated at less than a monolayer, the maximum activity per surface Pd atom was found between 20 and 50 at.% of Pd on the surface. The ORR on Pd-modified Au(*hkl*) was found to proceed via 4e⁻ pathway. Similarly, Dursun et al. reported largest positive shift in the O₂ reduction peak at 2/5 monolayer of Pd on Au(111) electrode in alkaline media [105].

Pd-Au core-shell particles have gained increasingly more attention since a cheaper and chemically more active ad-layer was suggested to be used as a sacrificial medium for noble metal deposition [106, 107]. Using galvanic replacement of Cu by Pd on Au surface the resulting Pd-Au catalyst showed higher electrocatalytic activity than either bare Au or Pd as a result of the interactions between the metals [107, 108].

Jirkowsky et al. attempted to gain higher activity and selectivity with Au-Pd nanoalloys to produce hydrogen peroxide [109]. They suggested that single Pd atoms, up to 8%, on gold nanoparticles would increase the peroxide yield up to 95%, but further increasing the Pd content leads to a drop in H₂O₂ production [109]. Pd-Au alloys are sensitive to different electrochemical pre-treatments [110–112]. Using pre-treatment has allowed fine-tuning of the Pd-Au alloy towards either Au rich or Pd rich surface [111, 112] and preparation of Pd-Au alloys with high peroxide yield in the oxygen reduction reaction [112].

Koenigsmann et al. demonstrated that PdAu nanowires had the specific activity twice higher than that of commercial Pt catalyst [113, 114]. They suggested that the increase is not only caused by the electronic changes resulting from the alloying, but also due to the small diameter of the nanowires. Porous Pd layers on Au nanoparticles showed a volcano plot-like activity-composition dependence, as particles with Pd:Au ratio of 1:0.61 were more active than these of 1:0.73 or 1:0.49 ratios, but it was suggested that this may originate also from porosity effects [115]. In addition, sponge-like PdAu structures showed higher electrocatalytic activity and stability than sponge-like Pd, commercial Pd/C and Pt/C catalysts in alkaline solution [116, 117].

A Pd-Au bimetallic catalyst supported on reduced graphene oxide displayed enhanced catalytic activity for ORR and better stability in alkaline media as compared to commercial Pd/C [118]. In addition it was suggested that Pd-Au clusters bind with graphene through Pd and synergetic effect between graphene and Au weakens the adsorption of anions, thus increasing the electrocatalytic activity of the alloy catalyst [119].

5. EXPERIMENTAL

5.1. Electrode preparation

Glassy carbon, bulk polycrystalline gold and palladium electrodes were prepared by mounting glassy carbon (GC-20SS, Tokai Carbon), Au (99.99%, Alfa Aesar) and Pd (99.95%, Alfa Aesar) disks (diameter 5 mm) into Teflon holders. The surface of the electrodes was polished to a mirror finish using 1.0 and 0.3 μm alumina slurries (Buehler) and for bulk Au and Pd electrodes, additional polishing on 0.05 μm alumina was used. After alumina polishing, the electrodes were sonicated in Milli-Q water (Millipore Inc.) for 5 min to remove polishing residues.

5.1.1. Preparation of thin Pd films

Thin Pd films with nominal thickness of 0.25–10 nm were deposited onto GC electrodes by electron beam evaporation from graphite crucible using Vacuum Service OY evaporation device at a base pressure of ca 1×10^{-6} Torr. The freshly prepared electrodes were coated with a 0.5 μm thick Nafion layer by applying a droplet of 0.5% Nafion solution in ethanol onto the electrode and allowing the solvent to evaporate in air. The Nafion solution was prepared from a commercial 5% Nafion solution in low molecular weight alcohols (Aldrich). The thickness of Nafion layer was calculated from the deposited mass and the surface area of the electrode, assuming a dry Nafion density of 2 g cm^{-3} [120].

5.1.2. Preparation of electrodeposited Pd coatings

The electrochemical deposition of palladium was carried out in deaerated 0.05 M H_2SO_4 solution containing 0.1 mM PdCl_2 (99.9%, Sigma-Aldrich) onto GC and gold substrates. During the deposition the electrode was continuously rotated at 960 rpm to ensure constant mass-transfer conditions. The deposition process was as follows: first, the electrode was kept at 1.1 V vs. RHE in order to avoid premature deposition of Pd, then the potential was scanned to 0.78 V at scan rate of 50 mV s^{-1} , where the electrode was kept for 300, 600 or 900 s. Immediately after that time the electrode was rinsed with Milli-Q water and transferred to another cell containing either 0.05 M H_2SO_4 or 0.1 M KOH, where the electrode was kept at 0.1 V for 5 min to ensure the desorption of chloride.

5.1.3. Preparation of electrodeposited Pd-Au coatings

The Pd-Au coatings were electrochemically deposited at constant potential of -0.15 V vs. SCE for 10 s. PdCl_2 and HAuCl_4 (Sigma-Aldrich) were used as precursors for electrodeposition. The precursor content in the deposition bath was 2 mM in 0.05 M H_2SO_4 . The Pd: Au ratio was 50:50; 75:25; 90:10 and also

1:0 and 0:1. After the electrodeposition the electrodes were thoroughly rinsed with Milli-Q water and placed to the next cell where the electrochemical characterisation was carried out.

5.1.4. Preparation of shape-controlled Pd nanoparticles

Pd nanocubes were synthesised using previously described methodology [121] in which H_2PdCl_4 solution was reduced with ascorbic acid in the presence of cetyltrimethylammonium bromide (CTAB) at 95 °C. The sample was centrifuged twice and redispersed in water. The PdNPs were then cleaned with strong basic aqueous solution followed by washing 3–4 times in ultrapure water to finally achieve a water suspension. The synthesis of spherical Pd nanoparticles has been adapted from the citrate method usually employed for the synthesis of gold nanoparticles [122]. In brief, the metal precursor (H_2PdCl_4) was reduced with ice-cold sodium borohydride in the presence of sodium citrate. Afterwards solid NaOH was added to precipitate the nanoparticles. After complete precipitation, the nanoparticles were washed 3–4 times with ultrapure water.

For electrochemical measurements an aliquot of the PdNPs suspension was pipetted onto the electrode and the solvent was allowed to evaporate in air.

5.1.5. Preparation of shape-controlled carbon-supported Pd catalysts

For the preparation of Pd/C catalysts three methods were used. Pd cubes with the size of ~24 nm were prepared using cetyltrimethylammonium bromide as a capping agent [121] and 14 nm particles and sub 10 nm Pd particles were synthesised by two methods developed by Xia and co-workers using polyvinylpyrrolidone (PVP) [123, 124]. After the reactions had finished, carbon powder (Vulcan XC-72, Cabot Corp.) was added to form 5, 20 and 50 wt% catalysts by continuously mixing to form uniform suspension. For cleaning the prepared Pd/C catalysts NaOH was added to the mixture [125], which was then filtrated and washed several times with water. Finally the sample was dried overnight at 75 °C.

For electrochemical measurements an aliquot of the catalyst suspension was pipetted onto the electrode and the solvent was allowed to evaporate in air.

5.1.6. Preparation of Au/C electrodes

20 wt% and 30 wt% Au nanoparticles supported on Vulcan XC-72R carbon black were supplied by Johnson Matthey. Carbon powder was used for comparison purposes. The catalyst suspension was prepared by mixing 4.7 mg of catalyst powder, 20 μl of 5 wt% Nafion solution and certain amount of ethanol, followed by sonication for 15 min. Then 5 μl of the catalyst suspension was dropped onto the glassy carbon disk resulting Au loading on the electrode

from 5.6 to 57 $\mu\text{g cm}^{-2}$, which corresponds to the Au/C catalyst layer thicknesses of 1.5 to 10 μm . The solvent was allowed to dry overnight.

5.1.7. Preparation of shape-controlled carbon-supported Au catalysts

The shape-controlled Au nanoparticles were prepared using different methodologies. In all synthesis the nominal gold content was kept at 20 wt%.

The quasi-spherical AuNPs (~5 nm) were prepared using previously described methods [101, 126]. Freshly prepared ice-cold NaBH_4 solution was added to aqueous solution of HAuCl_4 and trisodium citrate dehydrate at room temperature under vigorous stirring. After 30 s, the stirring was slowed down and the Au colloid solution was stirred gently at 40–45 $^\circ\text{C}$ for 15 min to ensure the reaction of excess NaBH_4 . Then appropriate amount of carbon powder (Vulcan XC-72R) was added under fast stirring for approximately 1 h, alternating between ultrasonic and magnetic. This process would disperse the carbon and allow uniform distribution of the nanoparticles on the support surface. Finally, NaOH pellets were added to the mixture to precipitate the sample and the synthesis mixture was left to stand overnight. After complete precipitation, the sample was filtered, rinsed with ultrapure water and dried at 70–80 $^\circ\text{C}$.

Quasi-spherical AuNPs (~30 nm) were synthesised using the standard citrate method [127], in which aqueous HAuCl_4 solution was heated to boiling and freshly prepared sodium citrate solution was added quickly with vigorous stirring. The mixture was refluxed for 20 min and then allowed to cool to room temperature. Then carbon powder was added as previously described. 1–2 NaOH pellets were added to the mixture that was left to precipitate for overnight. Finally, the sample was filtered, rinsed with ultrapure water and dried at 70–80 $^\circ\text{C}$.

Octahedral AuNPs (40–45 nm) were synthesised by the method described by Han et al. [128, 129]. The procedure was following: aqueous ascorbic acid was added to HAuCl_4 and CTAB aqueous solution. To this mixture NaOH solution was rapidly injected to ensure the formation of Au particles. The reaction temperature was kept at 25 $^\circ\text{C}$ and the reaction was allowed to proceed for 20–30 min. Subsequently appropriate amount of Vulcan XC-72R carbon was added. After that methanol solution in which 1–2 pellets of NaOH were dissolved was added to the mixture. Finally the sample was filtered, rinsed with ultrapure water and dried at 70–80 $^\circ\text{C}$.

The Au nanocubes were grown from spherical Au seeds [99–101, 130]. The Au seeds were prepared by the reduction of HAuCl_4 by ice-cold NaBH_4 in the presence of CTAB. The growth of the nanoparticles to yield nanocubes followed the next procedure: HAuCl_4 , CTAB and L-ascorbic acid were added to water. Then diluted Au seed solution was added to this growth solution. After 1 h the reaction was complete and the appropriate amount of carbon powder was added. The sample was washed with methanol solution containing 1–2

pellets of NaOH. Finally the sample was filtered, rinsed with ultrapure water and dried at 70–80 °C.

The corresponding unsupported AuNPs were prepared as described above, but without the carbon powder addition step. Furthermore, filtering and drying steps were unnecessary, and the AuNPs were simply washed 3–4 times with ultrapure water after precipitation.

For electrochemical measurements the catalyst suspension was prepared by mixing Au/C powder in ethanol containing 0.1% Nafion and an aliquot of this was pipetted onto the GC electrode. The solvent was left to dry overnight at room temperature.

5.2. Surface characterisation

Transmission electron microscopy (TEM) measurements were conducted on a Tecnai 12, JEM-2010 (JEOL) or Tecnai F20 TEM instrument and formvar/carbon coated copper grids were used as substrate. High-resolution scanning electron microscopy (HR-SEM) was conducted on Helios™ NanoLab 600 (FEI) equipped with INCA Energy 350 X-ray spectrometer (Oxford Instruments) for energy dispersive X-ray spectroscopy (EDX). The SEM measurements were carried out on GC disk that was removed from the Teflon holder after deposition process. Multimode atomic force microscope (AFM) images of Pd coatings on Au electrodes were obtained using Autoprobe CP II (Veeco) using UL20 (PSI) series cantilevers under ambient conditions in non-contact mode. X-ray photoelectron spectroscopy (XPS) measurements were conducted on SCIENIA SES-100 spectrometer. X-ray diffractograms (XRD) were recorded using a Bruker D8 advance diffractometer. The samples for XRD were prepared by evaporating a drop of catalyst suspension on Si substrate.

5.3. Electrochemical measurements

The electrochemical measurements were carried out either in 0.5 M or 0.05 M H₂SO₄ or 0.1 M KOH solutions. The solutions were prepared from 96% H₂SO₄ (Suprapur, Merck) or KOH pellets (p.a. quality, Merck). The solutions were made using Milli-Q water and were saturated with pure O₂ (99.999%, AGA), Ar (99.999%, AGA) or CO (99.97%, AGA) for CO stripping experiments. The electrochemical measurements were carried out in a three-electrode glass cell. The reversible hydrogen electrode (RHE) or saturated calomel electrode (SCE) was used as a reference electrode that was connected through a Luggin capillary. A Pt wire served as a counter electrode and it was separated from the main cell by a glass frit. The potential was applied using either Autolab potentiostat/galvanostat PGSTAT30 or PGSTAT128N (Eco Chemie B.V., The Netherlands) and the experiments were controlled using General Purpose Electrochemical System (GPES) software. An EDI101 rotator with CTV101

speed control unit (Radiometer, Copenhagen) was used for RDE experiments. All the experiments were carried out at room temperature (23 ± 1 °C).

Prior to O₂ reduction measurements, the electrodes were electrochemically pre-treated in deaerated solution for electrochemical characterisation and cleaning. To further clean the surface of Pd electrodes carbon monoxide was adsorbed onto the Pd by bubbling CO through the cell while keeping the potential at 0.1 V vs. RHE until complete blockage of the surface, which was monitored by scanning the electrode between 0.1 and 0.35 V [131]. After that the CO was removed from the solution by bubbling Ar for 45 min. Finally CO was oxidatively stripped from the surface. After these pre-treatments the electrode was transferred to another cell for the ORR studies.

6. RESULTS AND DISCUSSION

6.1. Oxygen reduction on thin Pd films

Oxygen reduction reaction was studied in potassium hydroxide and sulphuric acid solutions on thin palladium films prepared by electron beam evaporation onto glassy carbon substrate [1]. The objective of this study was to evaluate the ORR kinetics and determine the possible size effect of Pd nanoislands and the Pd film thickness on the oxygen reduction reaction.

6.1.1. Surface characterisation of thin Pd films

Figure 1 presents TEM micrographs of vacuum-evaporated thin Pd films of various nominal thicknesses. It can be observed that the palladium layer is not growing epitaxially, but very small Pd nanoparticles (nanoislands) are formed. This corresponds to Volmer-Weber growth mode. Similar phenomenon has been observed with thin Pt films prepared by the same method [132, 133]. The particle size was 2.0 ± 0.3 nm for 0.25 nm film and slightly increased with increasing the film thickness to 2.1 ± 0.3 nm for 0.5 nm film, 2.5 ± 0.4 nm for 1 nm film and 2.6 ± 0.4 nm for 2 nm film. It appears that the average particle size increases only slightly with nominal film thickness, but the number density of nanoparticles increases instead as can be observed in the TEM micrographs. The particles are in contact with each other forming dendritic structures and with increasing the nominal thickness of the film this trend increases. It is evident that the substrate material has a large influence on the surface morphology of the Pd films, as the size of the Pd nanoislands on Au substrate was considerably larger [23]. It is expected that for 5 nm and thicker films, the substrate is completely covered by Pd layer, as this has been observed for thin platinum films prepared by the same method [132].

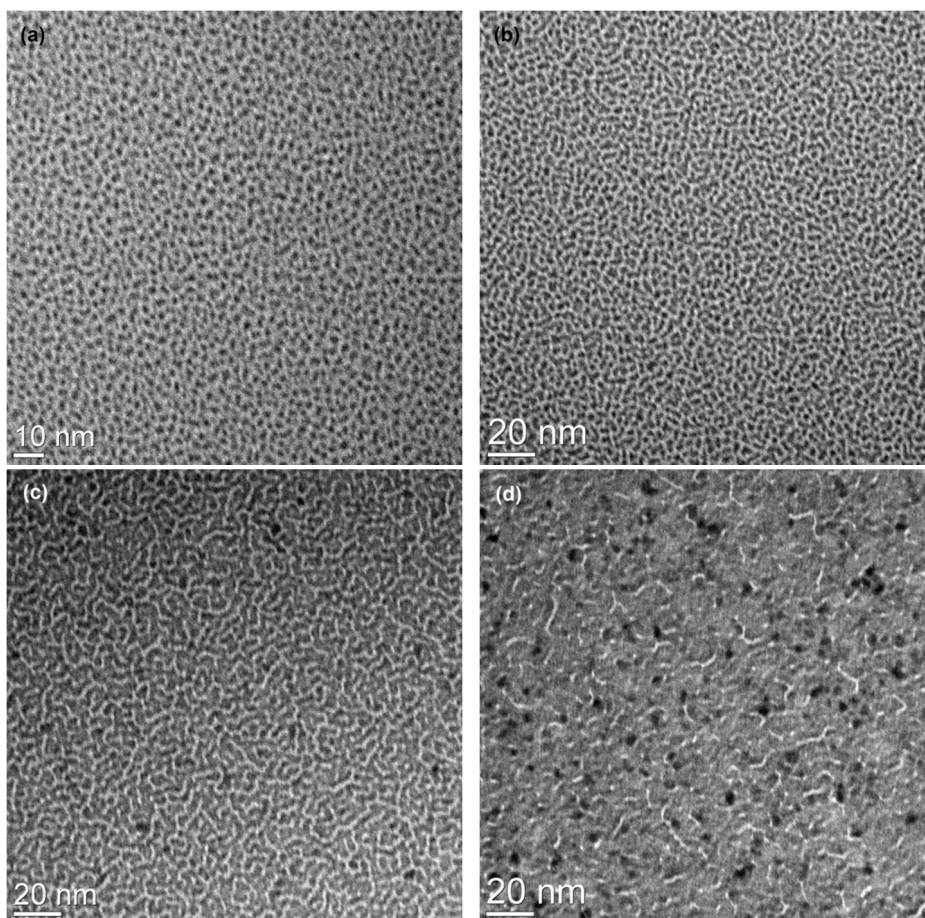


Figure 1. TEM images of thin Pd films. Nominal film thickness: (a) 0.25 nm; (b) 0.5 nm; (c) 1 nm and (d) 2 nm.

6.1.2. Cyclic voltammetry of thin Pd films

The thin palladium films and bulk polycrystalline Pd electrodes were subjected to potential cycling in Ar-saturated 0.1 M KOH solution prior to the oxygen reduction measurements in order to clean and electrochemically characterise the metal surface. The cyclic voltammetry (CV) response (Figure 2) shows the general features characteristic to palladium. The broad anodic peak at the potentials $E > 0.6$ V is associated with the formation of Pd surface oxides, while the well-defined cathodic peak between 0.9 and 0.5 corresponds to the reduction of these oxides. With decreasing Pd film thickness a significant shift of the oxide reduction peak potential towards negative direction can be observed

(Figure 2). The peak potential shift between the thinnest and thickest film is about 60 mV.

Similar phenomenon has been observed for platinum particles with decreasing particle size in acid solutions and it has been related to stronger adsorption of OH on smaller particles [31, 132, 134], which has also been confirmed by X-ray absorption spectroscopy [135]. Similarly, carbon-supported Pd nanoparticles exhibited same effect as the oxide reduction peak shifted about 50 mV towards negative potentials as Pd particle size decreased from 16.7 to 3 nm [30]. A small increase of the cathodic current can be observed at $E < 0.4$ V and anodic peak at about 0.5–0.6 V. These peaks are more pronounced for thicker films and can be attributed to the absorption or adsorption of hydrogen and its desorption, respectively [136].

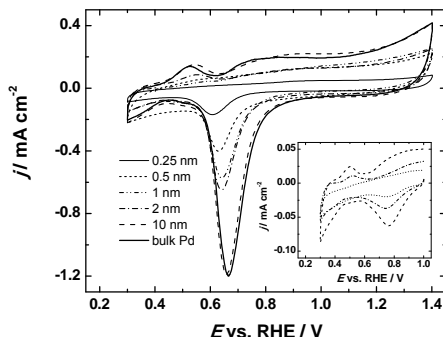


Figure 2. Cyclic voltammograms for Nafion-coated thin-film Pd electrodes and Nafion-coated bulk Pd in Ar-saturated 0.1 M KOH. $\nu = 100$ mV s⁻¹. Inset: $\nu = 10$ mV s⁻¹.

In order to calculate the real electroactive surface area of Pd the charge corresponding to the reduction of surface oxides was found. It has been suggested that the formation of the first monolayer of PdO is accomplished at ca 1.4–1.5 V vs. RHE [137], and therefore the positive potential limit was chosen to be 1.4 V for CV studies in this work. The value of $424 \mu\text{C cm}^{-2}$ was employed as the charge density for the reduction of a monolayer of PdO [137]. As expected, the real electroactive surface area (A_r) for Pd increased with increasing the film thickness for the thinner films, from 0.07 cm^2 for 0.25 nm film to 0.31 cm^2 for 2 nm film. For the 5 nm and thicker films, the GC surface is completely covered by Pd and the A_r was between 0.5 and 0.6 cm^2 , similar to that of bulk Pd electrode.

6.1.3. ORR on thin Pd films in alkaline solution

After CV studies the reduction of oxygen on thin-film Pd electrodes was investigated in alkaline solution. A representative set of the RDE polarisation curves at various electrode rotation rates is presented in Figure 3; the background current registered in O₂-free solution has been subtracted from these data. Only the cathodic sweeps are presented and were subjected for further analysis.

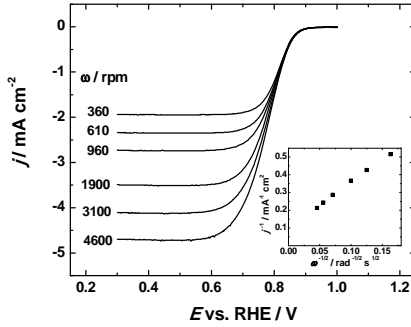


Figure 3. RDE results for O₂ reduction on Nafion-coated 0.5 nm Pd electrode in O₂-saturated 0.1 M KOH. $\nu = 10 \text{ mV s}^{-1}$. Inset: Koutecky-Levich plot for ORR at 0.3 V.

The RDE data were analysed using the Koutecky-Levich (K-L) equation, which in case of a thin Nafion layer on the electrode can be expressed as follows [120, 138, 139]:

$$\frac{1}{j} = \frac{1}{j_k} + \frac{1}{j_d} + \frac{1}{j_f} = \frac{1}{j_k} + \frac{1}{0.62nFD_{O_2}^{2/3}\nu^{-1/6}C_{O_2}^b\omega^{1/2}} + \frac{L}{nFC_{O_2}^fD_f} \quad (1)$$

where j is the measured current density, j_k is the kinetic current density, j_d is the diffusion-limited current density, j_f is the limiting diffusion current density in the Nafion layer, n is the number of electrons transferred per O₂ molecule, F is the Faraday constant ($96\,485 \text{ C mol}^{-1}$), ω is the rotation rate, $C_{O_2}^b$ is the concentration of oxygen in the bulk solution ($1.2 \times 10^{-6} \text{ mol cm}^{-3}$) [140], D_{O_2} is the diffusion coefficient of oxygen ($1.9 \times 10^{-5} \text{ cm}^2 \text{ s}^{-1}$) [140], ν is the kinematic viscosity of the solution ($0.01 \text{ cm}^2 \text{ s}^{-1}$) [141], L is the thickness of the Nafion layer, $C_{O_2}^f$ is the concentration of oxygen in the Nafion film and D_f is the diffusion coefficient of O₂ in the Nafion layer. According to Equation (1), the plots of j^{-1} vs $\omega^{-1/2}$ should be linear, with the intercept of $(1/j_k + 1/j_f)$. From the slope of the K-L plots (inset of Figure 3), the value of n was calculated. For the thicker films and for bulk Pd, n was close to four in the whole range of potentials studied, indicating that O₂ is fully reduced to water. This is in agreement with the earlier results in alkaline

solutions, where negligible production of peroxide was observed [30, 51]. For the 1 nm and thinner films, the value of n slightly decreased and was between 3.5 and 3.7. This can be attributed to a partial reduction of O_2 on the supporting GC surface, on which the ORR follows a two-electron pathway [142]. This explanation has also been given for the decreased values of n for the reduction of O_2 on a Pd/C catalyst [143].

Similar single-wave ORR polarisation curves with well-defined current plateaus were observed for all thin-film Pd electrodes and bulk Pd in alkaline solution (Figure 4). As expected for the electrodes coated with a Nafion layer, the plateau currents are lower than at bare Pd and also smaller than theoretically calculated value for a $4e^-$ reduction of O_2 in this solution at 1900 rpm (6.2 mA cm^{-2}). The plateau current density (j_{lim}) is determined by diffusion of oxygen in the solution as well as in the Nafion layer ($1/j_{lim} = 1/j_d + 1/j_r$). The small variations of j_{lim} are apparently due to the variation of j_r as a result of uneven thickness of Nafion layer on the electrodes.

The electrocatalytic activity of the thin Pd films decreases with decreasing film thickness below 2 nm (Figure 4) and the half-wave potential ($E_{1/2}$) shifts negative (Table 1). The main reason for this decrease is decreasing the A_r of palladium for the thinner films.

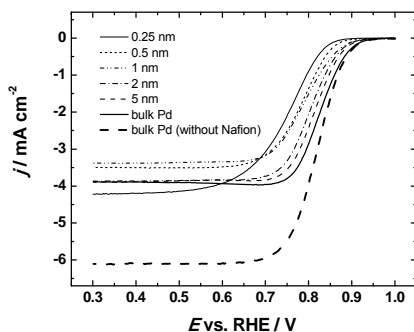


Figure 4. RDE voltammetry curves for O_2 reduction on Nafion-coated thin-film and bulk Pd electrodes in O_2 -saturated 0.1 M KOH. $\omega = 1900 \text{ rpm}$; $\nu = 10 \text{ mV s}^{-1}$.

To evaluate the influence of the surface morphology of Pd islands on their O_2 reduction activity, the specific activity of Pd at 0.85 V was calculated:

$$SA = I_k / A_r \quad (2)$$

where I_k is the kinetic current at this potential and A_r is the real surface area of Pd. It appears that the SA is rather constant in the range of Pd film thicknesses studied (Table 1). It has been shown that in alkaline solution, the specific activity of PdNPs towards the ORR decreases with decreasing the particle size

[30]. This has been attributed to the stronger adsorption of OH on smaller particles that block the active reaction sites [30]. Similar particle size effect has also been observed for Pt catalysts in alkaline solution [144, 145]. Indeed, the CV curves in Figure 2 show that the peak potential of the reduction of Pd surface oxides shifts to negative direction as the film thickness and Pd particle size decreases. However, when the CV curves were registered in the oxygen-free solution in the same conditions as the oxygen reduction measurements (starting at less positive potentials and using a lower scan rate), the oxide reduction peak appeared at much more positive potential, which did not show a remarkable dependence on the Pd film thickness (inset to Figure 2). It has been pointed out that the electrocatalytic activity of Pd for ORR depends on the coverage of surface oxides [103], which in turn is highly dependent on the conditions of the experiment, such as on the start potential if the potential is scanned to the negative direction [137]. Apparently, if the starting potential is as low as 1.0 V, surface oxides are formed that can be rather easily reduced, also at the thinnest Pd films that consist of very small Pd particles.

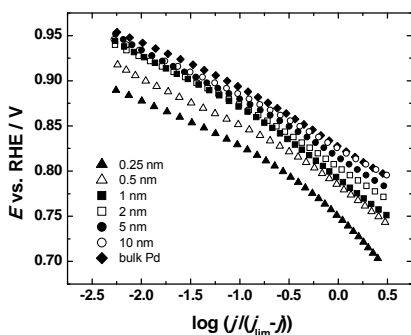


Figure 5. Mass-transfer corrected Tafel plots for O_2 reduction on Nafion-coated thin-film Pd electrodes and bulk Pd in 0.1 M KOH. $\omega = 1900$ rpm.

On the basis of the RDE data the mass-transfer corrected Tafel plots were constructed (Figure 5). For all electrodes except for the thinnest Pd film, these plots showed a single slope close to -60 mV (Table 1). For the O_2 reduction on Pt electrodes, characteristic slopes of -60 mV at low current densities and -120 mV at high current densities have been determined in many researches [6, 146, 147]. Similar slope values have also been found for Pd/C catalysts [30, 51]. The change in the slope has been attributed to the change from Temkin to Langmuir conditions for the adsorption of reaction intermediates [146, 147] or to the decreasing coverage of chemisorbed oxygen [148], but the transfer of the first electron to O_2 molecule is the rate-determining step in both regions. Apparently, on thin-film Pd electrodes the Pd oxides are reduced at potentials more negative than the range of Tafel analysis, which results in a single Tafel slope. The

gradual increase of the slope at negative potentials can be observed only in case of the thinnest Pd film (Figure 5). A single Tafel slope of -60 mV has also been observed on a bulk Pd electrode at pH 13.3 [9]. These results imply that the mechanism of oxygen reduction on thin Pd films in alkaline solution is similar to that on bulk Pd and Pt electrodes.

Table 1. Kinetic parameters of the ORR for the thin Pd films in 0.1 M KOH. $\omega = 1900$ rpm.

Electrode	Tafel slope [mV]	$E_{1/2}$ vs. RHE [V]	SA at 0.85 V vs. RHE [mA cm^{-2}]
0.25 nm Pd/GC	-51	0.75	0.45
0.5 nm Pd/GC	-55	0.78	0.53
1 nm Pd/GC	-63	0.79	0.51
2 nm Pd/GC	-54	0.80	0.59
5 nm Pd/GC	-57	0.82	0.47
10 nm Pd/GC	-54	0.82	0.51
Bulk Pd	-59	0.83	0.61
Bulk Pd (not coated with Nafion)	-55	0.82	0.72

6.1.4. ORR on thin Pd films in acidic solution

For comparison, the reduction of oxygen was studied on thin-film Pd electrodes also in acid solution. In Figure 6, a representative set of RDE voltammetry curves is shown and in Figure 7 the data at a single rotation rate for Pd films of various thicknesses is compared. The electrocatalytic activity of Pd towards O_2 reduction is lower in H_2SO_4 than in KOH solution, therefore, at 0.3 V the reduction of O_2 is still under mixed kinetic-diffusion control and the diffusion-limited current plateau is not reached. In case of Pt electrodes, this activity decrease has been attributed to the presence of adsorbed (bi)sulphate anions, which block the active sites and have a negative electronic effect on the ORR kinetics [149]. The influence of adsorbed anions on the ORR rate on polycrystalline Pt has been reported in an early work by Hsueh et al. [150].

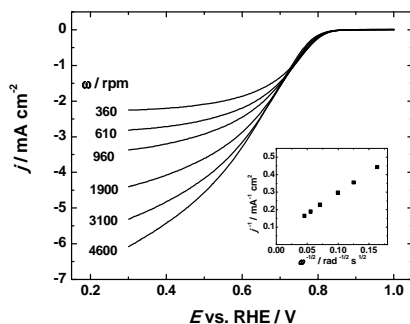


Figure 6. RDE results for O_2 reduction on a Nafion-coated 2 nm Pd electrode in O_2 -saturated 0.05 M H_2SO_4 . $v = 10 \text{ mV s}^{-1}$. Inset: Koutecky-Levich plot for O_2 reduction at 0.3 V.

The K-L plots were constructed (inset to Figure 6) and the number of electrons transferred per O_2 molecule was calculated from Eq. (1) using the literature data of $C_{O_2}^b = 1.26 \times 10^{-6} \text{ mol cm}^{-3}$ and $D_{O_2} = 1.93 \times 10^{-5} \text{ cm}^2 \text{ s}^{-1}$ for 0.05 M H_2SO_4 [151]. The values of n slightly lower than four (between 3.6 and 3.9) were found for thin-film Pd electrodes, which means that hydrogen peroxide is produced to some extent. The $4e^-$ reduction of oxygen has been observed on Pd single crystals [3], Pd nanoparticles [29] and on Pd monolayers on various metals [152]. Slightly lower n values in this work may be caused by the Nafion layer on the electrodes, as it has been pointed out that Nafion coating increases the peroxide formation on Pt catalysts [153].

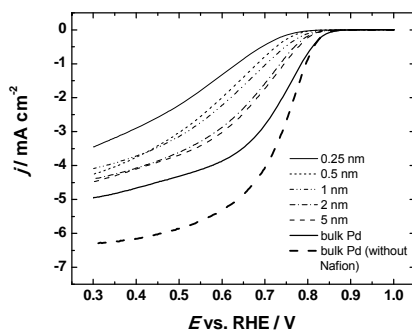


Figure 7. RDE voltammetry curves for O_2 reduction on Nafion-coated thin-film and bulk Pd electrodes in O_2 -saturated 0.05 M H_2SO_4 . $\omega = 1900 \text{ rpm}$; $v = 10 \text{ mV s}^{-1}$.

A comparison of mass-transfer corrected Tafel plots of O_2 reduction on thin Pd films in acid solution is presented in Figure 8 and Tafel slopes are given in

Table 2. At high and low current densities, the average Tafel slope values of -146 and -59 mV, respectively, were found. This is in agreement with the results obtained for bulk Pd [9], Pd/C catalysts [34] and thin Pd films on Au [23], where Tafel slopes close to -120 and -60 mV have been observed. For Pd nanoparticles, however, a single Tafel slope of -120 mV has been reported [29]. The Tafel slope values of -60 and -120 mV are also characteristic for O₂ reduction on Pt catalysts [6, 147, 154]. These results suggest that the reaction mechanism on thin-film Pd electrodes is the same as on bulk Pd and Pt and does not depend on the Pd film thickness.

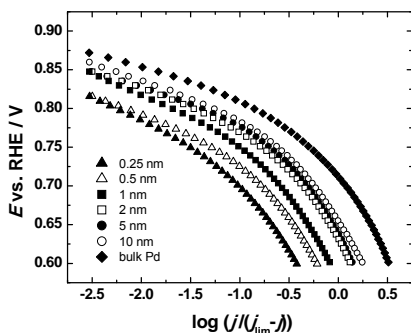


Figure 8. Mass-transfer corrected Tafel plots for O₂ reduction on Nafion-coated thin-film Pd electrodes and bulk Pd in 0.05 M H₂SO₄. $\omega = 1900$ rpm.

The specific activities of O₂ reduction on thin Pd films in acidic solution were also calculated using Eq. (2) and are given in Table 2. The values of j_k were obtained from $1/j_k = 1/j - 1/j_d - 1/j_f$, where j_d was found from the slopes of K-L plots and j_f was calculated from the difference of intercepts of K-L plots at 0.3 V for Nafion-coated and uncoated bulk Pd. Unlike in alkaline solution where the SA was nearly constant for all the electrodes studied, a decrease in the SA value with decreasing film thickness is in evidence. It is noteworthy that the same trend was also observed for Pd films on Au in H₂SO₄ solution [23]. For Pt catalysts, the particle size effect on the ORR activity has been extensively investigated [31, 154, 155] and due to the structural similarity of these metals it is also expected for Pd catalysts. Assuming a cubo-octahedral model shape of a Pt particle, the fraction of Pt(111) sites increases as the particle size decreases [154]. As on these sites the (bi)sulphate ions show the strongest adsorption, thereby blocking the sites of O₂ adsorption, the ORR activity decreases with decreasing particle size [155]. Although the crystallographic orientation of Pd islands on the thin-film electrodes is not known, it is expected that the morphological differences of the Pd films and most likely decreasing particle size are the reasons for the decreased activity for the thinnest films. Adsorbed OH has also been considered as a spectator species for O₂ reduction on Pt [149],

but considering that in alkaline solution the SA values are rather constant for all film thicknesses, it can be speculated that the main reason for decreasing the O₂ reduction activity for thinner Pd films in H₂SO₄ is the surface-specific adsorption of (bi)sulphate anions and not OH⁻.

Comparing the values of SA of Nafion-coated and uncoated bulk Pd indicates that the Nafion layer on the electrode surface slightly decreases the electrocatalytic activity for O₂ reduction. The solubility of O₂ is higher in Nafion film than in the solution, which should increase the kinetic current [138]. However, the enhancement in kinetic current decreases with decreasing the electrolyte concentration and approaches unity at very low acid concentrations [139]. As a result, in the kinetic region no differences in the O₂ reduction kinetics on Nafion-coated and bare Pt surfaces in dilute acid solutions were found [139]. On the other hand, Nafion slightly decreases the electrochemical surface area of Pt and therefore may block some active sites on Pt [120, 138]. Therefore, the influence of Nafion coating on the electrocatalytic activity of Pt in the kinetic region is not clear. For bulk Pt electrodes, the kinetic currents at the Nafion-coated electrodes were found to be higher than at the bare Pt electrodes [138]. However, the specific activity of the Nafion-Pt/C composite catalyst was either lower than that of bulk Pt [120] or similar to this [153].

Understanding the effects of metal particle size and morphology on their electrocatalytic activity is very important from both fundamental and practical point of view, as it will help to design and optimise the catalysts for the fuel cell cathodes. High activity of small Pd particles in alkaline solution makes this metal a promising alternative to platinum in alkaline anion exchange membrane fuel cells.

Table 2. Kinetic parameters for oxygen reduction on Pd/GC electrodes in 0.05 M H₂SO₄. $\omega = 1900$ rpm.

Electrode	Tafel slope [mV] Region I ^a	Tafel slope [mV] Region II ^a	$E_{1/2}$ vs. RHE [V]	SA at 0.8 V vs. RHE [mA cm ⁻²]
0.25 nm Pd/GC	-62	-151	0.48	0.04
0.5 nm Pd/GC	-49	-158	0.49	0.04
1 nm Pd/GC	-62	-125	0.53	0.10
2 nm Pd/GC	-59	-129	0.56	0.12
5 nm Pd/GC	-53	-144	0.59	0.11
10 nm Pd/GC	-59	-148	0.62	0.13
Bulk Pd	-65	-158	0.69	0.25
Bulk Pd (not coated with Nafion)	-52	-128	0.74	0.35

^a Region I corresponds to low current densities and Region II to high current densities.

6.2. Oxygen reduction on electrodeposited Pd coatings

In continuation to [I] the oxygen reduction reaction was studied on electrochemically deposited palladium electrodes in acid as well as in alkaline solution [II, III]. Palladium was deposited at constant potential of 0.78 V onto glassy carbon [II] and gold [III] substrates and in what follows these electrodes are designated as Pd/GC and Pd/Au, respectively. The electrochemical deposition was carried out in 0.05 M H₂SO₄ solution containing 0.1 mM PdCl₂.

6.2.1. Surface characterisation of electrodeposited Pd coatings

HR-SEM micrographs of Pd coatings on GC deposited for 300, 600 and 900 s are presented in Figure 9. It can be seen that after 300 s of Pd deposition (Figure 9a) there are small nanoparticles and also some larger agglomerates. After 600 s (Figure 9b) more agglomerates have been formed. After 900 s (Figure 9c) Pd has been deposited on multiple layers, but still some uncoated GC surface can be seen with some small Pd islands on it. The size of small Pd particles was in the range of 3 to 10 nm and the larger agglomerates were up to 100 nm in diameter. With these deposition parameters Pd grows in the form of nanoparticles as suggested by Bliznakov et al. [156].

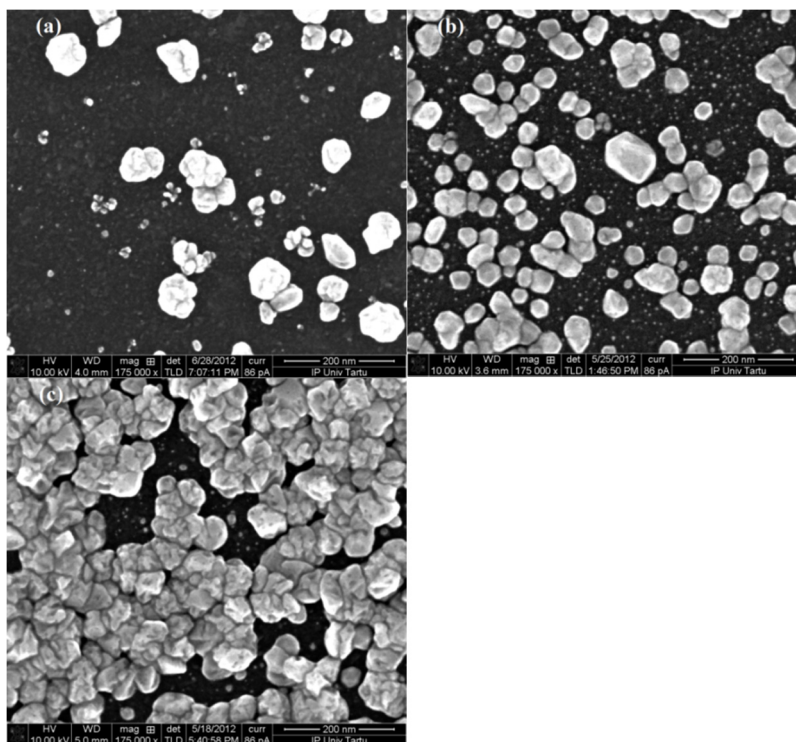


Figure 9. HR-SEM micrographs of electrodeposited Pd on GC. Deposition time: (a) 300, (b) 600 and (c) 900 s.

The surface morphology of electrodeposited Pd on gold substrate was studied using atomic force microscopy and Pd coatings deposited using different deposition times on gold are presented in Figure 10. For all electrodeposited Pd/Au it can be observed that the Au surface is covered with island-like structures of Pd (Figure 10). The root mean square (RMS) roughness was found to decrease as compared to clean polished Au surface. The corresponding RMS roughness values were: 4.1 ± 0.9 nm, 3.6 ± 0.5 nm, 3.6 ± 0.6 nm and 2.2 ± 0.5 nm for polished Au, 300, 600 and 900 s deposited Pd, respectively. This decreasing trend of RMS roughness can be explained by preferred growing of Pd particles on Au surface defects caused by polishing and subsequent fulfilment of these scratches. It was also found that the average size of Pd particles was 19 ± 2 nm and it does not depend on deposition time. In comparison with electrodeposited Pd/GC the size of the Pd nanoparticles on gold was more uniform and there were no large agglomerates.

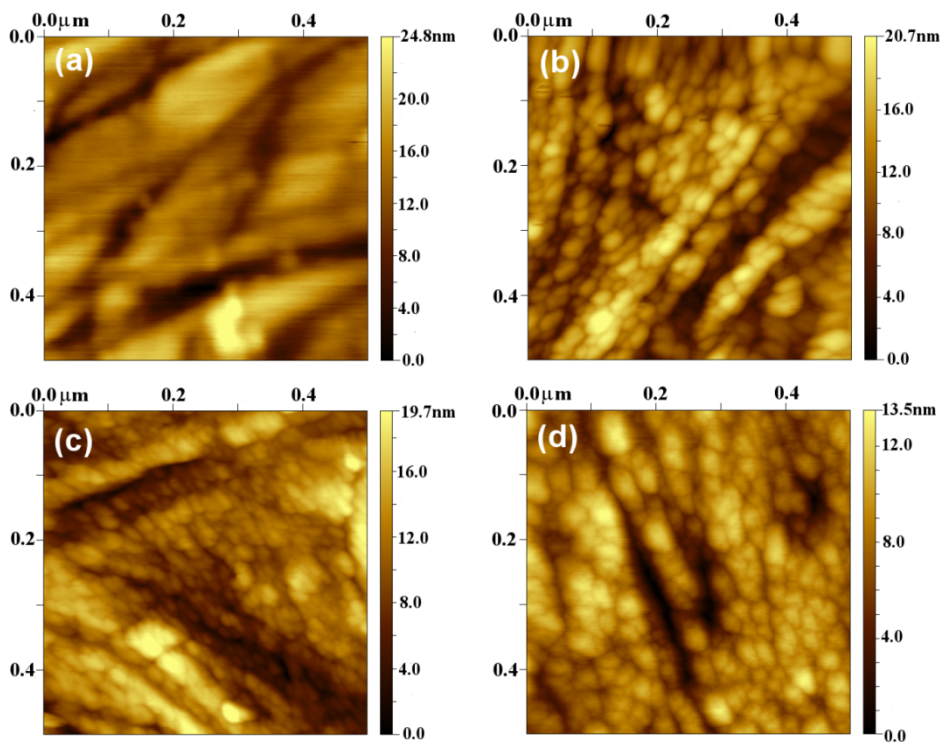


Figure 10. AFM micrographs of (a) bulk Au and electrodeposited Pd coatings of various deposition times: (b) 300, (c) 600 and (d) 900 s.

6.2.2. Cyclic voltammetry and CO stripping

As with thin Pd films, prior to oxygen reduction measurements the electrodeposited palladium and bulk Pd electrodes were subjected to potential cycling in deaerated solution in order to clean and electrochemically characterise the electrode surface. The cyclic voltammograms of Pd/GC presented in Figure 11 show general features characteristic to palladium electrodes. The main characteristics are similar in acid and in alkaline solutions. The broad anodic peak at the potentials $E > 0.6$ V is associated with the formation of Pd surface oxides and reduction of these oxides gives a well-defined cathodic peak between 0.6 and 0.9 V. The current increase between 0.4 and 0.1 V is attributed to hydrogen adsorption and desorption. A small contribution of hydrogen absorption into Pd is also possible, but it has been shown that in case of thin Pd films at $E > 0.1$ V this charge is small, as compared to the adsorption charge [157, 158]. In acidic media peaks in the hydrogen region are better defined than in alkaline solution. This has been attributed to the influence of adsorbed (bi)sulphate ions [159].

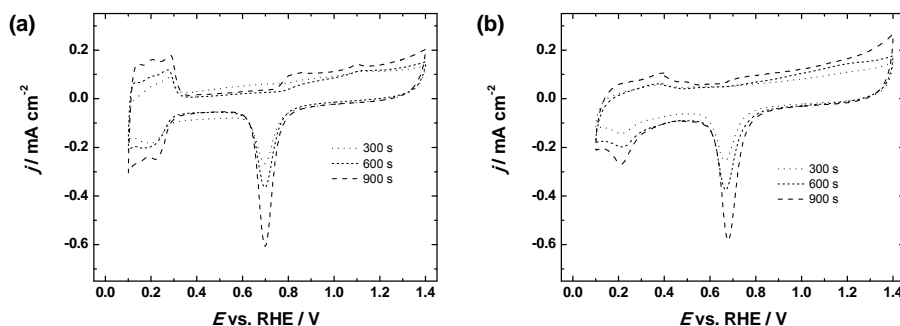


Figure 11. Cyclic voltammograms for Pd/GC electrodes in Ar-saturated solutions: (a) 0.05 M H_2SO_4 and (b) 0.1 M KOH. $\nu = 50 \text{ mV s}^{-1}$.

The Pd/Au electrodes were subjected to CO stripping experiments (Figure 12). In acid medium well-defined CO stripping peaks in the range of 0.9 to 0.95 V can be observed. In alkaline medium the CO stripping peak is located at 0.81 V for thicker Pd coatings, but the 300 s deposited Pd coating did not show a characteristic sharp CO stripping peak; the reason for that might be the formation of Pd-Au surface alloy. In acidic solution a shift of the CO stripping peak is in evidence, which is most likely caused by alloying with Au as shown previously [160]. The increased current at more positive potentials than the CO stripping peak can be attributed to Pd surface oxidation and the cathodic peak at 0.7 V is due to their reduction; the increased current at $E < 0.35$ V is due to the adsorption of hydrogen. The CVs registered after CO stripping experiments showed increased symmetry and better definition of hydrogen adsorption/desorption peaks, which were evidences for increased cleanliness of surface of

the electrode. The CVs of Pd/Au electrodes (Figure 13) were very similar to these of bulk Pd and Pd/GC in acid solution, but in alkaline medium there was a small wave prior to Pd surface oxide reduction for 300 s deposited Pd/Au, which was absent when using GC as substrate and suggests Pd-Au alloy formation. Also noteworthy is a broad cathodic peak at approximately 1.15 V which is due to the reduction of gold surface oxides that are formed on Au substrate surface uncovered by Pd layer. The hydrogen adsorption/desorption features of Pd/Au electrodes were similar to those of electrodeposited Pd/GC.

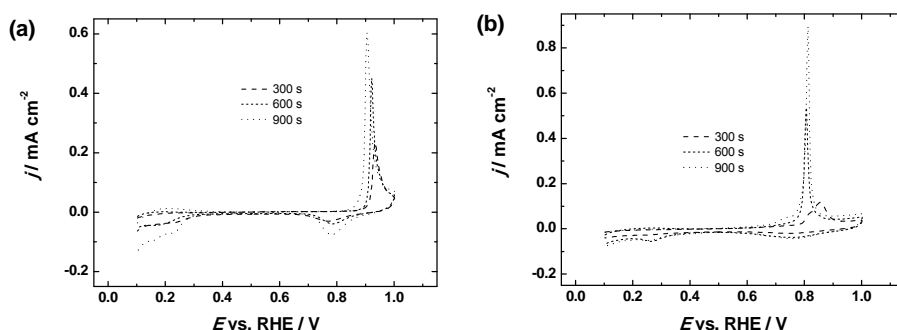


Figure 12. CO stripping voltammograms of Pd/Au electrodes recorded in Ar-saturated (a) 0.05 M H₂SO₄ and (b) 0.1 M KOH solutions. $\nu = 20 \text{ mV s}^{-1}$.

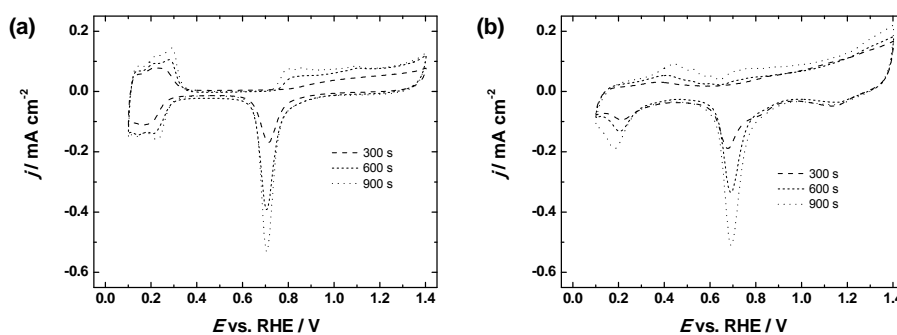


Figure 13. Cyclic voltammograms of Pd/Au electrodes recorded in Ar-saturated solutions: (a) 0.05 M H₂SO₄ and (b) 0.1 M KOH. $\nu = 50 \text{ mV s}^{-1}$.

The real electroactive surface area of Pd was determined using the same methodology as for thin Pd films in previous part [I]. As predicted, the A_r value increased with increasing the electrodeposition time at constant potential and it did not depend on the substrate material.

6.2.3. ORR on electrodeposited Pd electrodes in acidic solution

After the pre-treatment procedures the electrodeposited Pd coated electrode was transferred to another electrochemical cell where the solution was saturated with oxygen. For all Pd/GC and Pd/Au electrodes the ORR polarisation curves were single-waved. Only the cathodic sweeps are presented and were subjected to further analysis and background currents registered in O₂-free solution were subtracted from this data. A comparison of the RDE polarisation curves (Figure 14) shows increasing ORR activity of the Pd coatings with increasing deposition time. It has been shown that the adsorption of (bi)sulphate anions decreases the ORR activity of Pt [149]. The same effect has also been observed on epitaxial films of palladium on Pt(111) [161] and on thin Pd films [23]. In addition to strongly adsorbed anions the real electroactive surface area affects the $E_{1/2}$ value. In order to compare the intrinsic catalytic activity of the electrodeposited Pd electrodes the specific activities were calculated using Eq. (2). The SA values for Pd/GC electrodes were rather similar at 0.8 V, but small increase with increasing deposition time was observed and for thicker coatings the specific activities were comparable to that of bulk palladium (Table 3). In comparison, the SA values for Pd/Au catalysts prepared with shorter deposition time were similar, but the SA was higher for the coating prepared with the longest deposition time and even surpassed that of bulk Pd. It is evident that the SA value increases with Pd loading and this is more noticeable on GC substrate. This electrocatalytic behavioural tendency has also been observed on vacuum-evaporated thin Pd films ([I] and [23]) and explained by stronger adsorption of (bi)sulfate anions on smaller Pd particles. Therefore, the higher specific activity of 900 s deposited Pd/Au could arise from morphological effects.

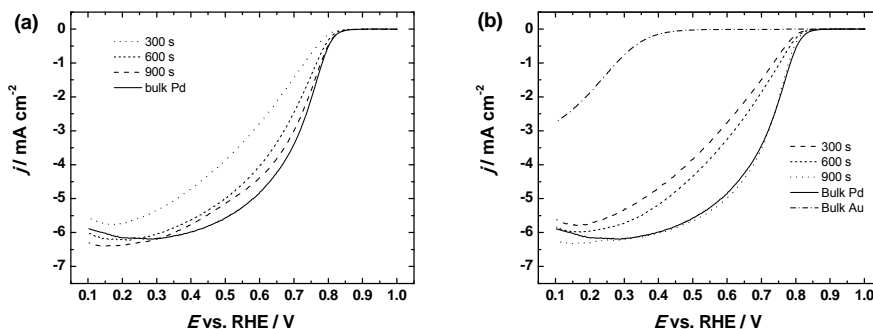


Figure 14. Comparison of RDE voltammetry curves of O₂ reduction on (a) Pd/GC and (b) Pd/Au in O₂-saturated 0.05 M H₂SO₄. $\omega = 1900$ rpm, $\nu = 20$ mV s⁻¹.

The analysis of RDE data was made using the Koutecky-Levich equation [162]:

$$\frac{1}{j} = \frac{1}{j_k} + \frac{1}{j_d} = -\frac{1}{nFkC_{O_2}^b} - \frac{1}{0.62nFD_{O_2}^{2/3}v^{-1/6}C_{O_2}^b\omega^{1/2}} \quad (3)$$

where $C_{O_2}^b$ is 1.22×10^{-6} mol cm⁻³ [163]. Using Eq. (3) the number of electrons transferred per O₂ molecule was found. For all Pd/Au electrodes the value of n was close to 4, showing that the reaction yielded mainly water. In case of GC support the n value was also close to 4 for 600 s and 900 s deposited Pd coatings, but for the thinnest coating it was somewhat lower, being between 3.5 and 3.9 at negative potentials. These values suggest that some H₂O₂ is produced. As in the measured potential region the reduction of oxygen is suppressed on pure GC surface [164], the value of $n < 4$ may not be attributed to the two-electron reduction of O₂ on GC, but it may be caused by a decreased activity of H₂O₂ reduction on Pd nanoparticles in H₂SO₄ solution [165]. On bulk Pd electrodes the ORR proceeded via 4-electron reduction pathway in the whole range of potentials studied.

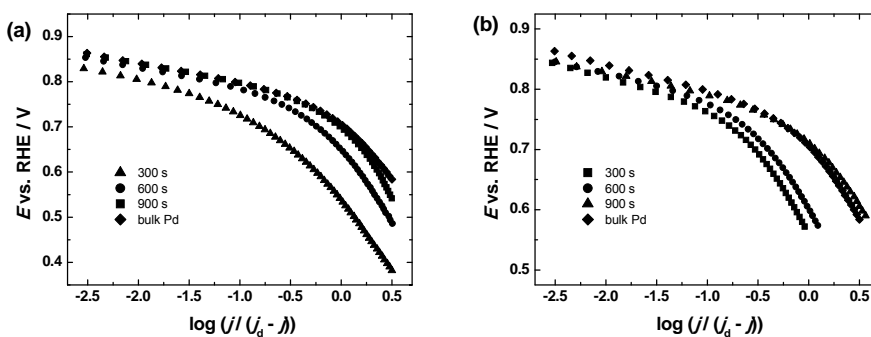


Figure 15. Mass-transfer corrected Tafel plots for oxygen reduction on (a) Pd/GC and (b) Pd/Au with comparison to bulk Pd electrodes in 0.05 M H₂SO₄. $\omega = 1900$ rpm. Data derived from Figure 14.

On the basis of the RDE data on ORR at 1900 rpm the mass-corrected Tafel plots were constructed (Figure 15). The Tafel slope values of the ORR on electrodeposited Pd at low current densities were close to -60 mV, but reached up to -150 mV at high current densities (Table 3). The Tafel slope values at high current densities on Pd/GC were somewhat lower than those on Pd/Au. The Tafel slope value of -60 mV at low current densities has been reported to arise from adsorbed oxygen-containing species on the surface of Pd catalysts [9]. At higher overpotentials the surface oxide coverage is significantly lower and typical Tafel slope value (-120 mV) is obtained, which indicates that the ORR rate is determined by the transfer of the first electron to O₂ molecule.

Table 3. Kinetic parameters for oxygen reduction on electrodeposited Pd and bulk Pd in 0.05 M H₂SO₄. $\omega = 1900$ rpm.

Catalyst	Tafel slope [mV] (Region I) ^a	Tafel slope [mV] (Region II) ^a	$E_{1/2}$ vs. RHE [V]	SA at 0.8 V vs. RHE [mA cm ⁻²]
300 s deposited Pd/GC	-55 ± 6	-123 ± 14	0.55 ± 0.02	0.19 ± 0.04
600 s deposited Pd/GC	-54 ± 1	-136 ± 1	0.65 ± 0.01	0.24 ± 0.02
900 s deposited Pd/GC	-57 ± 5	-138 ± 8	0.67 ± 0.03	0.25 ± 0.01
300 s deposited Pd/Au	-52 ± 1	-146 ± 4	0.54 ± 0.03	0.18 ± 0.03
600 s deposited Pd/Au	-51 ± 1	-156 ± 10	0.58 ± 0.02	0.19 ± 0.03
900 s deposited Pd/Au	-47 ± 2	-152 ± 7	0.71 ± 0.03	0.39 ± 0.04
bulk Pd	-53 ± 3	-128 ± 5	0.71 ± 0.01	0.24 ± 0.02

^a Region I corresponds to low current densities and Region II to high current densities

6.2.4. ORR on electrodeposited Pd electrodes in alkaline solution

The ORR on freshly prepared electrodeposited Pd coatings was also tested in 0.1 M KOH solution (Figure 16). In alkaline medium the ORR polarisation curves showed sharper current increase than in acid solution and well-defined diffusion-limited current plateaus. The RDE data was analysed using Eq. (3) and the values of $D_{O_2} = 1.9 \times 10^{-5}$ cm² s⁻¹ and $C_{O_2}^b = 1.2 \times 10^{-6}$ mol cm⁻³ [140]. The value of n was close to 4 for all electrodeposited Pd electrodes, except for 300 s deposited Pd/GC for which it was between 3.7 and 3.9. This indicates that some hydrogen peroxide is formed, possibly on uncovered GC surface as the ORR on bare GC electrodes is a two-electron process [142, 166]. There are several studies where 4-electron pathway for the ORR in alkaline solutions has been reported [35, 104, 143], but also somewhat smaller n values have been determined on Pd nanoparticles [30]. It has been suggested that on Pt group metals this reaction proceeds at least partially via peroxide intermediate [167].

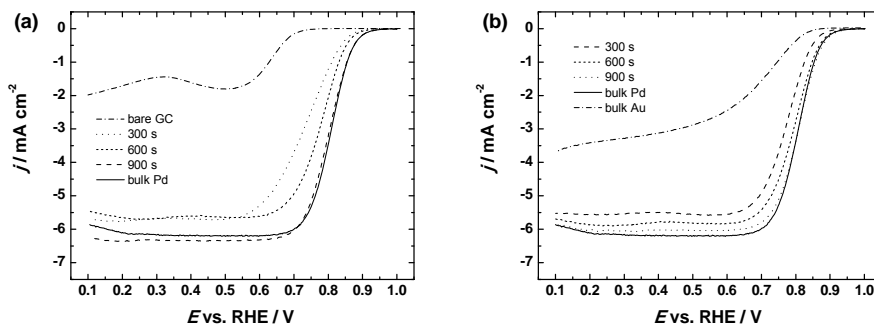


Figure 16. Comparison of RDE voltammetry curves for O_2 reduction on (a) Pd/GC and (b) Pd/Au in O_2 -saturated 0.1 M KOH. $\omega = 1900$ rpm, $\nu = 20$ mV s^{-1} .

A clear positive shift of $E_{1/2}$ with increasing deposition time is evident and the $E_{1/2}$ values of 900 s deposited Pd coatings coincide with that of bulk Pd (Table 4). The specific activities were found by using Eq. (2) at 0.85 V (Table 4). The SA values on Pd/GC electrodes remained lower than that of bulk Pd, but higher specific activities were observed for Pd/Au coatings. In either case the SA values were rather constant: near 0.4 mA cm^{-2} on Pd/GC and near 0.6 mA cm^{-2} on Pd/Au, in agreement with the results obtained for vacuum-evaporated thin Pd films (paper [I]). Jiang et al. have shown that the SA value of Pd/C catalysts increases continuously by a factor of 3 with increasing the particle size from 3 to 16.7 nm [30]. Such behaviour was not observed in this study, which can be due to the fact that the Pd particle size is relatively large as can be observed from SEM and AFM measurements. The higher SA values of Pd/Au might be caused by possible formation of Pd-Au surface alloy [15, 16]. However, this can also be due to the electronic effect of the substrate, as a monolayer of Pd on Au(111) has been shown to increase the ORR kinetics in alkaline solution by an order of magnitude [104].

Mass-transfer corrected Tafel plots were constructed for ORR in 0.1 M KOH (Figure 17). All Pd/Au electrodes and Pd/GC electrodes with thicker coatings showed one rather constant Tafel slope value of -60 mV. For 300 s deposited Pd two different Tafel slope regions were observed: at low current densities the slope was close to -60 mV, but at high current densities it increased to -120 mV. These values are in agreement with previous studies [30, 47, 51] and thus it can be concluded that the mechanism of the ORR on electrodeposited Pd coatings in alkaline media is the same as on bulk Pd.

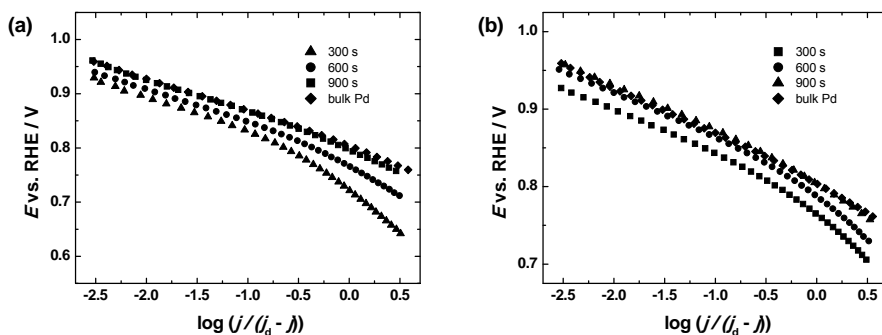


Figure 17. Mass-transfer corrected Tafel plots for oxygen reduction on (a) Pd/GC and (b) Pd/Au and bulk Pd electrodes in 0.1 M KOH. $\omega = 1900$ rpm. Data derived from Figure 16.

Table 4. Kinetic parameters for oxygen reduction on electrodeposited Pd and bulk Pd in 0.1 M KOH. $\omega = 1900$ rpm.

Catalyst	Tafel slope [mV]	$E_{1/2}$ vs. RHE [V]	SA at 0.85 V vs. RHE [mA cm ⁻²]
300 s deposited Pd/GC	-58 ± 2	0.71 ± 0.01	0.39 ± 0.01
600 s deposited Pd/GC	-57 ± 2	0.77 ± 0.01	0.38 ± 0.02
900 s deposited Pd/GC	-56 ± 3	0.79 ± 0.01	0.43 ± 0.09
300 s deposited Pd/Au	-58 ± 2	0.77 ± 0.01	0.60 ± 0.10
600 s deposited Pd/Au	-59 ± 1	0.79 ± 0.01	0.64 ± 0.02
900 s deposited Pd/Au	-60 ± 1	0.81 ± 0.01	0.60 ± 0.09
bulk Pd	-57 ± 2	0.79 ± 0.02	0.48 ± 0.02

6.3. Oxygen reduction on electrodeposited Pd-Au coatings

As the Pd/Au system in paper [III] showed increased ORR activity in alkaline solution, then palladium and gold were co-deposited onto GC support with different Pd:Au ratios in order to evaluate the ORR activity of Pd-Au alloys [IV]. The studied electrodes were prepared using different Pd:Au ratios in the deposition bath (50:50; 75:25; 90:10) and these are designated as 1-PdAu, 2-PdAu and 3-PdAu, respectively. For comparison purposes pure Pd and Au were electrochemically deposited.

6.3.1. Surface characterisation of Pd-Au coatings

HR-SEM micrographs of Pd-Au coatings are presented in Figure 18. From these images it can be observed that the size and distribution of Pd-Au particles are independent of the deposition bath content. The electrodeposited Pd-Au and Pd had rather uniform particle size of 6 ± 2 nm and these small particles formed some larger agglomerates. In contrast, the electrodeposited Au had different morphology and larger particles, even up to 45 nm, were formed.

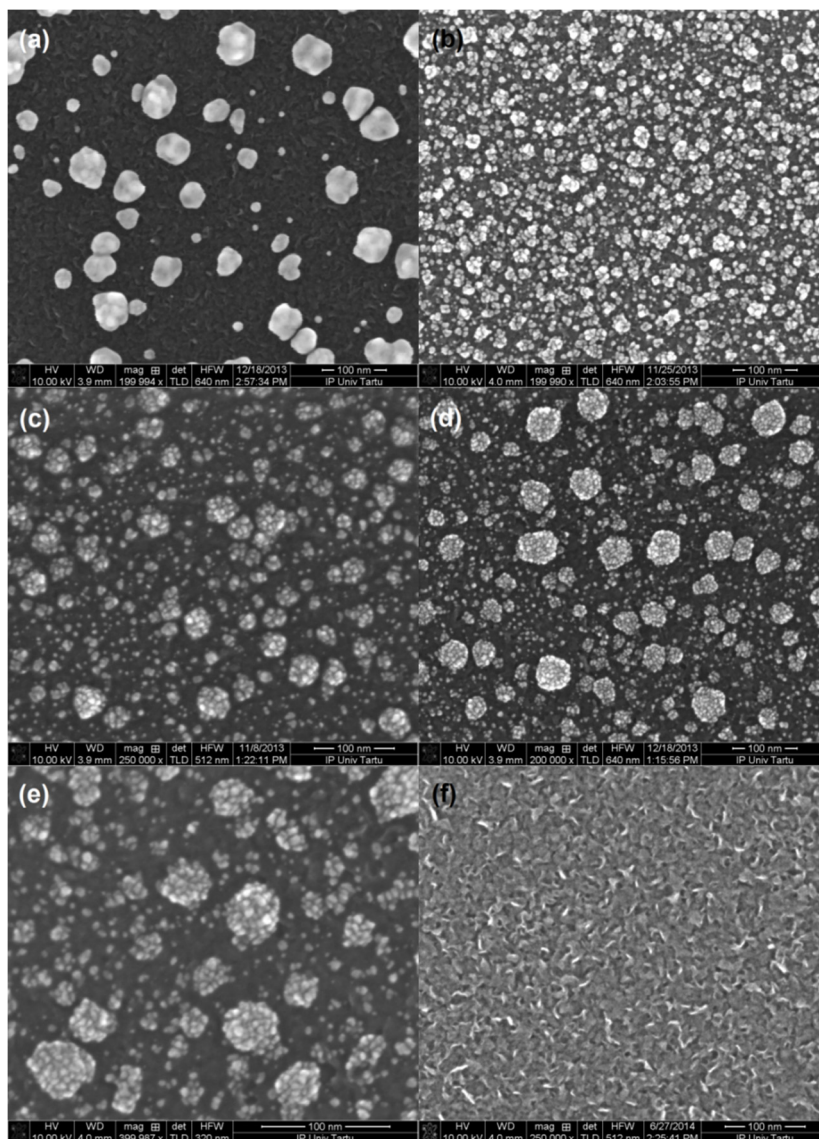


Figure 18. SEM micrographs of electrodeposited (a) Au, (b) Pd, (c) 1-PdAu, (d) 2-PdAu, (e) 3-PdAu, (f) bare GC.

In order to evaluate the distribution of Pd and Au and the real alloy composition, the energy dispersive X-ray spectroscopy was used. The metal distribution was found to be rather uniform. The 1-PdAu, 2-PdAu and 3-PdAu coatings contained 25 wt%, 55 wt% and about 75 wt% of Pd, respectively. Therefore it can be safely concluded that the deposition of Au is more facile than Pd in these conditions.

The X-ray photoelectron spectroscopy (XPS) measurements were carried out in order to analyse the valence state and surface composition of the electrodeposited Pd-Au coatings (Figure 19). For all Pd-Au coatings the Au4f spectra had a doublet at 83.4 and 87.1 eV. 1-PdAu and 2-PdAu had the Pd3d doublet at 334.4 and 340.1 eV, but for 3-PdAu a shift in binding energy (BE) was observed, as it had the corresponding XPS peaks at 334.6 and 340.2 eV.

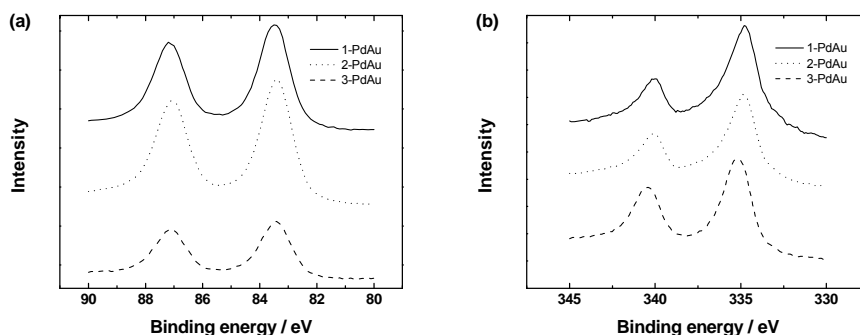


Figure 19. XPS spectra of electrodeposited Pd-Au coatings in the (a) Au4f and (b) Pd3d regions.

The BE values of Au4f obtained in this study coincide with those obtained by Xu et al. who explained the decrease in the BE of Au in Pd-Au alloy with electron transfer from Pd to Au [168]. In the case of 3-PdAu the Pd3d doublet is located at higher BE values, because palladium content is higher and probably not all Pd is alloyed.

6.3.2. Cyclic voltammetry of electrodeposited Pd-Au coatings

Cyclic voltammetry was used to characterise and clean the freshly prepared electrode surface. In order to avoid the recombination of the metals the upper potential limit was kept at 0.8 V prior the ORR studies and later it was increased to 1.4 V for three CV scans to determine the real electroactive surface area (Figure 20). The CVs of electrodeposited Pd were rather similar to that of bulk Pd, showing the H_{UPD} peaks at low potentials ($E < 0.3$ V) and peaks corresponding to the surface oxidation of Pd ($E > 0.8$ V) and reduction of PdO ($0.6 < E < 1.0$) at higher potentials. When the upper potential limit was in-

creased to 1.7 V, the characteristics for oxidation and reduction of gold were also observed. As it has been shown that for single Pd atoms on Au nanoparticles the hydrogen adsorption/desorption region does not appear [109], then it may be assumed that Pd in these Pd-Au coatings exists at least partially in larger clusters, as also the XPS and EDX studies suggest. From Figure 20 it can be observed that the Pd oxide reduction peak shifts to lower potentials with increasing Pd content in the coatings. This observation is in agreement with the results obtained by Lukaszewski and Czerwinski, who observed that for the co-deposited palladium-gold alloys the peak potential of oxide reduction depends on the alloy composition and it shifts to negative potentials during potential cycling as a result of the Pd segregation [111]. In this study the shift of PdO reduction peak was not observed during the potential cycling, which suggests that the segregation of Pd is negligible, probably due to the narrower potential range used during the CV studies. The Pd segregation can be utilised to gain certain surface composition by employing different pre-treatment conditions [112].

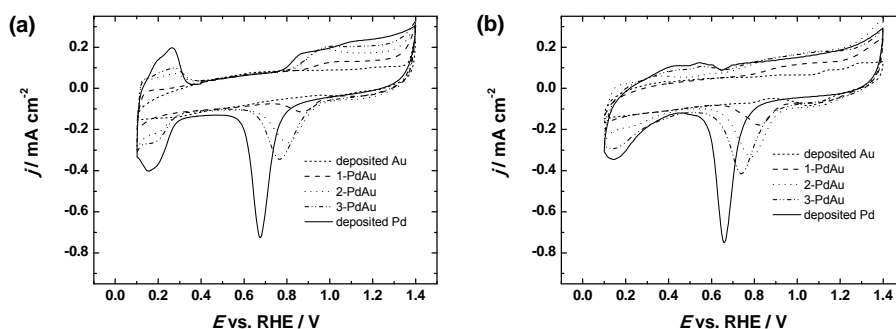


Figure 20. Cyclic voltammograms of electrodeposited Pd-Au coatings in Ar-saturated (a) 0.05 M H_2SO_4 and (b) 0.1 M KOH solution. $\nu = 50 \text{ mV s}^{-1}$.

The real electroactive Pd surface area of Pd-Au coatings was found by integrating the charge under the Pd oxide reduction peak and using the value of $424 \mu\text{C cm}^{-2}$ for the charge density of the reduction of a monolayer of PdO [137]. The surface areas for 1-PdAu, 2-PdAu and 3-PdAu were 0.04, 0.12 and 0.16 cm^2 , respectively. However, it has to be noted that for pure noble metal electrodes the surface area determination is more accurate than for Pd-Au alloys [111].

6.3.3. ORR on electrodeposited Pd-Au coatings in acidic solution

After CV experiments the ORR activity of electrodeposited Pd-Au coatings was evaluated. The RDE results for 1-PdAu are presented in Figure 21a. For all

electrodeposited coatings similar ORR polarisation curves were obtained (Figure 22). It can be observed from the comparison that the onset and half-wave potentials of the ORR are strongly affected by the alloy composition. With increasing the Pd content, a considerable positive shift of the onset potential and $E_{1/2}$ is evident (Table 5). From the Koutecky-Levich analysis (Figure 21b), the number of electrons transferred per O_2 molecule was determined. The value of n was close to 4 for electrodeposited pure Pd and for 3-PdAu, but a slightly lower value of n was obtained for 1-PdAu and 2-PdAu coatings, indicating that the ORR does not proceed selectively to water formation on these Pd-Au coatings. The n value was close to 2 for bulk Au and electrodeposited gold and therefore the reaction yielded H_2O_2 as expected. Since the Pd content in Pd-Au coatings is relatively high, it is expected that the H_2O_2 yield is low, as it has been demonstrated that in perchloric acid solution the hydrogen peroxide production decreases to 10% when Pd content increases up to 50% [109]. In addition, small amounts of spontaneously deposited Pd on polycrystalline gold have been shown to catalyse the four-electron reduction of oxygen to water in perchloric acid [28].

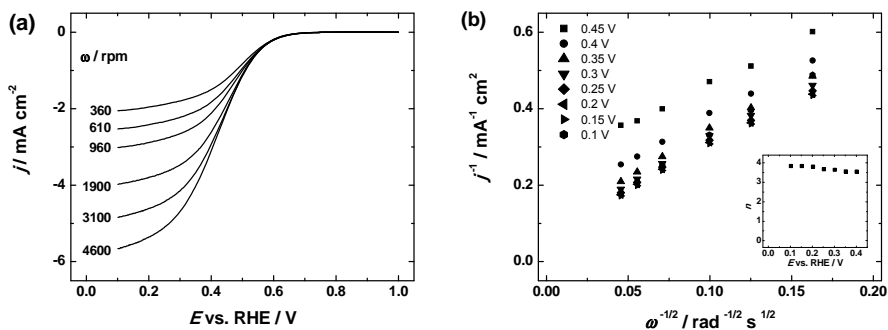


Figure 21. (a) A set of RDE results on 1-PdAu in O_2 -saturated 0.05 M H_2SO_4 solution and (b) the corresponding K-L plots. Inset shows the potential dependence of n .

The $E_{1/2}$ values of the ORR are strongly dependent on the alloy composition and $E_{1/2}$ shifts positively with increasing Pd content (Table 5). This behaviour is expected as the $E_{1/2}$ of gold is rather negative and even small amount of more active metal shifts significantly the half-wave potential [109]. Also it is evident that the diffusion-limited current depends on the alloy composition (see Figure 22) and thus the value of n is lower than 4 for Au-rich alloys.

In order to compare the intrinsic activity of the electrodes the SA values were calculated using Eq. (2), taking into account the electroactive surface area of Pd. As the onset potentials differ considerably, then it is difficult to compare the specific activities at a single potential. However, the SA values were calculated at 0.6 V (Table 5) and they differed only slightly. The electro-

deposited pure Pd had about two times higher SA value as compared to 3-PdAu coating, which might be due to the more favourable particle distribution, as pure Pd had no big agglomerates. The SA of bulk Pd was in turn twice as high as that of electrodeposited palladium. This effect is similar to that of thin Pd films, which had lower SA than that of bulk Pd (paper [I]) and it may be due to the morphological differences. For Pt catalysts, the particle size effect on the ORR activity has been extensively investigated [154, 155] and due to the similar crystal structure it is also expected for Pd catalysts. Assuming the cubo-octahedral model shape of the Pt particles, the fraction of Pt(111) sites increases with decreasing the particle size [154]. As the (bi)sulphate ions show the strongest adsorption on Pt(111) sites and block O₂ adsorption sites [155], a similar effect on Pd surface in H₂SO₄ solution is expected, which causes lower SA of Pd nanoparticles compared to bulk Pd. In addition, decreasing SA value with decreasing particle size below 11 nm has been observed for Pd/C catalysts in HClO₄ solution [32].

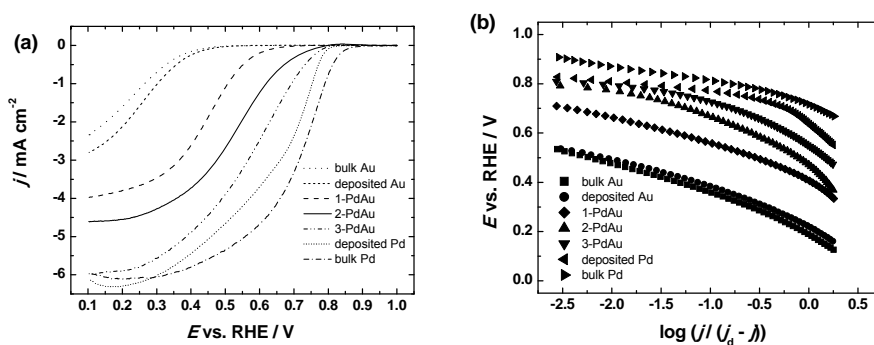


Figure 22. (a) A comparison of RDE results for O₂ reduction on electrodeposited Pd-Au coatings in O₂-saturated 0.05 M H₂SO₄ solution. (b) Tafel plots derived from (a).

On the basis of RDE data the Tafel analysis was carried out and the corresponding plots are presented in Figure 22b. The Tafel slope value at low current densities was close to -60 mV for Pd containing coatings, as is typical for Pd-based catalysts in this region [9, 23, 34], but with increasing Au content the slope value increased slightly (Table 5). The Tafel slope value of -60 mV has been agreed to originate from oxygen-containing species on Pd surface at low overpotentials [9]. For bulk gold and electrodeposited gold this value was higher than previously shown on gold catalysts [65, 66]. Nevertheless, the Tafel slope values obtained in this study show that the rate-determining step for the ORR is the sluggish transfer of first electron to O₂ molecule.

Table 5. Kinetic parameters of oxygen reduction on Pd-Au alloys in 0.05 M H₂SO₄. $\omega = 1900$ rpm.

Electrode	A_r [cm ²]	Tafel slope [mV]	$E_{1/2}$ vs. RHE [V]	SA at 0.6 V vs. RHE [mA cm ⁻²]
deposited Au		-122 ± 6	0.28 ± 0.01	
bulk Au		-104 ± 7	0.25 ± 0.01	
1-PdAu	0.04 ± 0.005	-88 ± 10	0.42 ± 0.05	1.8 ± 0.6
2-PdAu	0.12 ± 0.003	-84 ± 15	0.47 ± 0.04	1.5 ± 0.4
3-PdAu	0.16 ± 0.004	-49 ± 10	0.53 ± 0.04	2.4 ± 0.9
deposited Pd	0.31 ± 0.010	-48 ± 10	0.62 ± 0.04	4.3 ± 0.7
bulk Pd	0.52 ± 0.03	-53 ± 3	0.71 ± 0.01	7.5 ± 0.1

6.3.4. ORR on electrodeposited Pd-Au coatings in alkaline solution

Freshly prepared Pd-Au electrodes were also tested for ORR activity in alkaline media. Gold is a rather active catalyst for ORR in alkaline solution and thus the onset potentials of different coatings are within 50 mV (Figure 23a). Also from the comparison it can be seen that different Pd-Au electrodes have almost coinciding polarisation curves with well-defined diffusion limiting current plateaus. The difference of $E_{1/2}$ values between bulk Pd and 1-PdAu is only about 20 mV. Cha *et al.* observed the onset potential and half-wave potentials to differ more than 70 mV with different Au/Pd ratios [117].

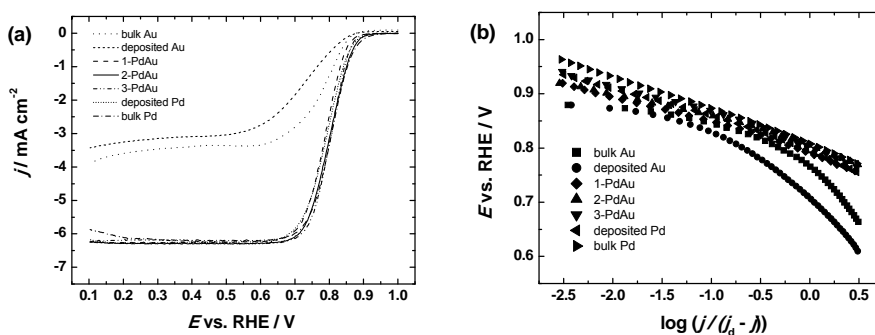


Figure 23. (a) A comparison of RDE results of electrodeposited Pd-Au coatings in O₂-saturated 0.1 M KOH solution. (b) Tafel plots derived from (a).

The Koutecky-Levich analysis (Eq. (3)) revealed that for electrodeposited Au and bulk Au the value of n was below 3, but on all coatings that contained Pd the reaction proceeded via 4-electron pathway. These results show that the reaction product is OH^- on Pd-containing coatings, but on pure gold the final product is peroxide that is partially reduced further. In comparison, the Au nanochain networks have the n value about three, but after modifying these particles with Pd shell the value of n increases to four [117], showing that a small amount of Pd is needed for the four-electron reduction of oxygen.

It should be noted that the specific activities here are calculated on the basis the electroactive surface area of Pd and thus these SA values can be considered as apparent specific activities, since gold is also electrochemically active in alkaline media. Unfortunately, the determination of the surface area of Au is not possible in present case, as this would change the surface composition [111]. As 1-PdAu has the smallest A_r , then it is expected that it possesses the highest SA value. In general, the SA values decrease with increasing the Pd content. The electrodeposited Pd has a little higher SA than that of bulk Pd. The higher electrocatalytic activity has been previously suggested to arise from structural and electronic effects on Pd-Au alloy catalysts [113–115] and these effects are most likely the cause of the change in the ORR activity of our catalysts. Similarly, the electronic interaction between Au and Pd has been suggested to be the reason for higher activity and stability for Pt/PdAu/C materials [169].

The Tafel analysis revealed a single Tafel slope region with the slope value of approximately -60 mV for all the studied electrodes (Table 6, Figure 23b). This value suggests that the ORR mechanism is the same as on typical Pd catalysts [24, 25, 30, 143, 170] and the rate-determining step is the transfer of the first electron to O_2 molecule.

Table 6. Kinetic parameters of oxygen reduction on Pd-Au alloys in 0.1 M KOH. $\omega = 1900$ rpm.

Electrode	A_r [cm^2]	Tafel slope [mV]	$E_{1/2}$ vs. RHE [V]	SA at 0.85 V vs. RHE [mA cm^{-2}]
deposited Au		-54 ± 11	0.71 ± 0.01	
bulk Au		-64 ± 9	0.77 ± 0.01	
1-PdAu	0.07 ± 0.01	-71 ± 9	0.81 ± 0.02	2.6 ± 0.2
2-PdAu	0.16 ± 0.02	-60 ± 10	0.81 ± 0.02	1.9 ± 0.1
3-PdAu	0.24 ± 0.02	-52 ± 11	0.81 ± 0.04	1.4 ± 0.2
deposited Pd	0.32 ± 0.02	-63 ± 5	0.79 ± 0.01	0.48 ± 0.1
bulk Pd	0.55 ± 0.03	-58 ± 6	0.80 ± 0.03	0.48 ± 0.02

6.3.5. Hydrogen peroxide reactions on electrodeposited Pd-Au alloys in alkaline solution

As hydrogen peroxide is the intermediate in the ORR process, the study of electrocatalytic behaviour of peroxide on Pd-Au catalysts is an important task. The reactions of hydrogen peroxide were studied in Ar-saturated 0.1 M KOH containing 1 mM of H_2O_2 . In Figure 24a a set of RDE results of peroxide reduction and oxidation on 1-PdAu alloy coating is presented. The results showed that the half-wave potentials of HO_2^- reduction on various Pd-Au catalysts are rather close to each other (Figure 24b), similarly to these of the ORR in alkaline media. As expected, the Pd-Au catalysts are highly active for HO_2^- reduction and oxidation in alkaline media. The collected RDE data were analysed employing the K-L equation (Eq. (3)) and using the value of the HO_2^- diffusion coefficient of $8.75 \times 10^{-6} \text{ cm}^2 \text{ s}^{-1}$ [171]. The number of electrons transferred per HO_2^- anion was found to be 2 for all the electrodes containing Pd. The electrodeposited Au showed a modest activity towards HO_2^- reduction. This is in accordance with the results of the oxygen electroreduction in alkaline solution, where only partial further reduction of peroxide was observed on electrodeposited Au. At pH 7 it has been shown that the onset potential of the peroxide reduction on Pd-Pt or Pd-Au codeposits does not depend on the electrode composition, but the overall activity decreases with increasing the Au content and increases with increasing the Pt content [172]. When Au was electroplated with Pd the same effect was in evidence [173]. On the basis of the RDE results, Son et al. have stated that Pd/Au catalyst has higher electrocatalytic activity towards peroxide reduction than that of commercial Pd/C and Pt/C [116]. The results obtained in this work show that electrodeposited Pd-Au coatings are promising electrocatalysts for hydrogen peroxide reduction and oxidation.

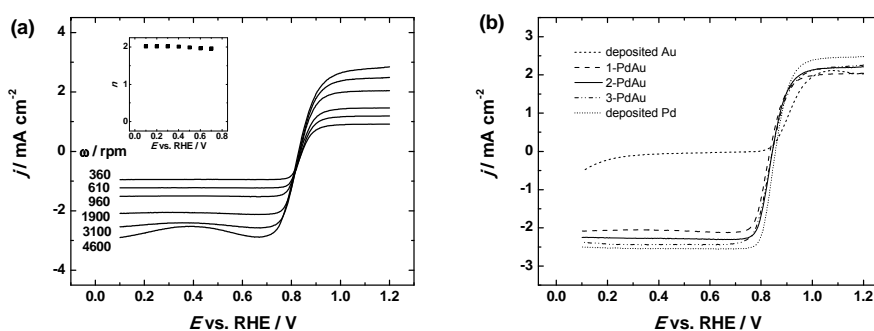


Figure 24. (a) A set of RDE results of HO_2^- oxidation and reduction on 1-PdAu alloy, inset shows the potential dependence of n for HO_2^- reduction. (b) A comparison of HO_2^- oxidation and reduction on Pd-Au coated electrodes at $\omega = 1900$ rpm in Ar-saturated 0.1 M KOH solution containing 1 mM HO_2^- .

6.4. Oxygen reduction on Pd nanocubes

Based on the literature data the electrocatalytic activity of different Pd single crystal facets for ORR is different in perchloric acid and Pd(100) is the most active facet [3]. The ORR was studied on Pd nanocubes as they have predominant Pd(100) plane and the results were compared to those of ordinary spherical nanoparticles [V, VI].

6.4.1. Surface characterisation of Pd nanocubes

The prepared Pd nanoparticles were examined using TEM (Figure 25). Figure 25a shows a high percentage of Pd nanocubes for which the (100) preferential surface structure is expected. For comparison, the quasi-spherical PdNPs can be observed in Figure 25b, these particles can be considered as polyoriented, non-specifically structured nanoparticles. The average particle size was determined from the TEM images and it was 26.9 ± 3.9 and 2.8 ± 0.4 nm for cubic and spherical PdNPs, respectively.

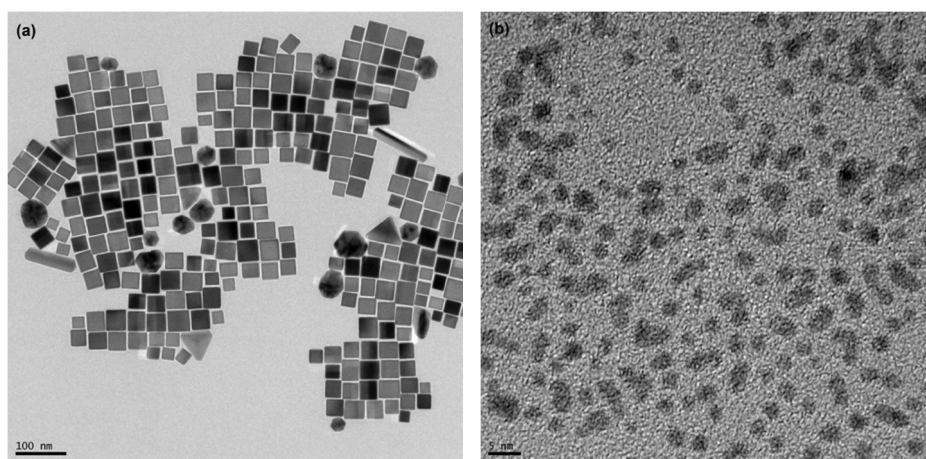


Figure 25. TEM micrographs of Pd catalysts: (a) cubic PdNPs and (b) spherical PdNPs.

In order to evaluate the crystallographic structure of the particles the X-ray diffraction (XRD) patterns were recorded (Figure 26). All the diffraction peaks can be well-indexed to face-centred cubic (*fcc*) palladium metal. Remarkably, the XRD pattern of Pd nanocubes shows an abnormally intense (200) peak, which is not observed for the Pd spheres, suggesting that most of the Pd nanocubes are preferentially oriented with their (100) facets parallel to the substrate surface. This feature has been previously observed with $\sim 50\text{--}70$ nm Pd nanocubes [121, 174, 175]. However, this abnormally intense (200) peak was

not observed for 6–7 nm Pd nanocubes [46], ~60 nm [176] and ~24 nm Pd nanocubes [177]. Additional experiments are required to clarify these discrepancies.

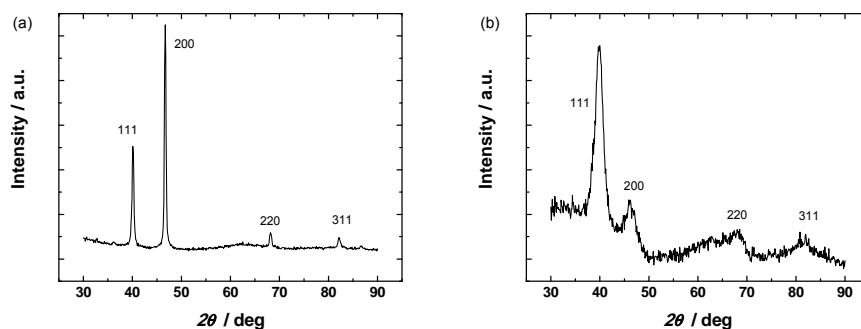


Figure 26. XRD patterns of Pd catalysts: (a) cubic PdNPs and (b) spherical PdNPs.

6.4.2. Cyclic voltammetry and CO stripping

In order to clean the surface of PdNPs without altering their initial structure, residual impurities on the surface of the particles were displaced by adsorption of CO, followed by its oxidation [131]. Typical CO stripping voltammograms in acid and alkaline media are presented in Figure 27. In acid solution, a well-defined stripping peak of adsorbed CO was observed at 0.88 V for cubic PdNPs and at 0.91 V for spherical PdNPs. The second anodic peak at 0.94 V can be attributed to the surface oxidation on Pd(100) terraces. This characteristic signal has been well-studied in Pd(S)-[n(100)x(111)] [178] and Pd(S)-[n(100)x(110)] [179] electrodes and its charge has been reported to exclusively depend on the terrace atom density without contributions from step sites. The cathodic peak at ca 0.77 V corresponds to the reduction of Pd surface oxides. The CV response of PdNPs recorded after CO stripping (inset of Figure 27) showed improved definition and symmetry of the CV peaks as a result of increased cleanliness of the surface. The voltammetric profile of the cubic PdNPs resembles that characteristic of a Pd(100) single crystal and shows well-defined peaks at 0.35 and 0.22 V [178, 179]. In alkaline solution (Figure 27b) sharp CO stripping peaks appear at the potentials of 0.72 and 0.75 V for Pd nanocubes and spherical Pd nanoparticles, respectively. The peaks of hydrogen adsorption and desorption on CVs recorded after CO stripping are not as well-defined as in acid solution, but the CV peak characteristic to Pd(100) terraces can be observed at ca 0.55 V [136].

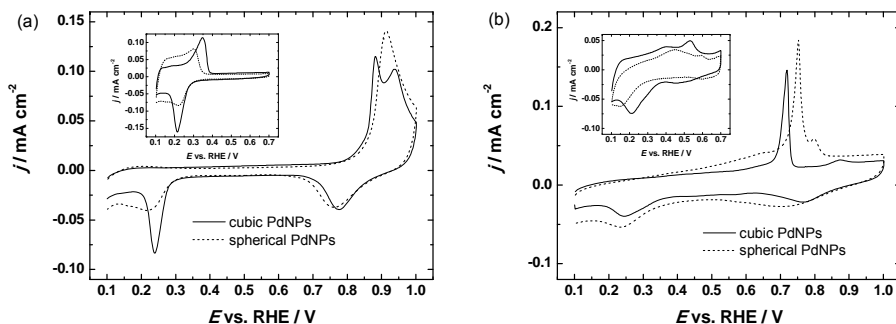


Figure 27. Oxidation of pre-adsorbed CO on PdNP modified GC electrodes in Ar-saturated (a) 0.05 M H_2SO_4 and (b) 0.1 M KOH. $\nu = 20 \text{ mV s}^{-1}$. Insets: CV curves for PdNPs recorded after CO stripping, $\nu = 50 \text{ mV s}^{-1}$. Current densities are normalised to the real surface area of Pd.

After the ORR measurements, the CVs were again recorded in Ar-saturated solutions by extending the anodic potential to 1.4 V. The anodic peaks at $E > 0.7 \text{ V}$ and the cathodic peaks at ca 0.65–0.7 V correspond to the formation of Pd surface oxides and to their reduction, respectively (Figure 28). For cubic PdNPs in alkaline solution (Figure 28b), characteristic peaks of hydrogen desorption and oxide formation on Pd(100) terraces are in evidence at the potentials of 0.58 and 0.87 V, respectively [136]. The real electroactive surface area was determined by integrating the charge of the PdO reduction peak, assuming the value of $424 \mu\text{C cm}^{-2}$ as the charge density for the reduction of a monolayer of PdO [137]. For comparison, the real surface area of PdNPs was also determined from the H_{UPD} desorption peaks on the CV curves registered in Ar-saturated 0.05 M H_2SO_4 (using the charge density of $212 \mu\text{C cm}^{-2}$) [180] and the A_r values obtained by these two methods were in a good agreement with each other.

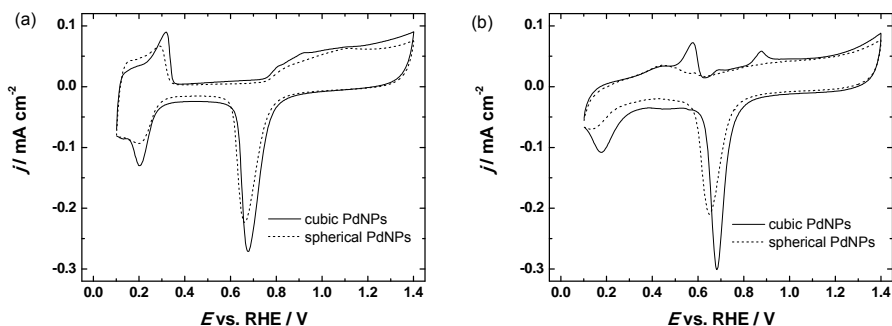


Figure 28. Cyclic voltammograms for PdNP modified GC electrodes after ORR in Ar-saturated (a) 0.05 M H_2SO_4 and (b) 0.1 M KOH. $\nu = 50 \text{ mV s}^{-1}$. Current densities are normalised to the real surface area of Pd.

6.4.3. ORR on Pd nanocubes in acidic solutions

The electroreduction of oxygen on Pd nanoparticles and bulk Pd was studied using the RDE method in 0.5 M and 0.05 M H₂SO₄ solutions on gold and GC support, respectively. Similar single-wave polarisation curves were obtained in both solutions for Pd nanocubes, spherical Pd nanoparticles and for bulk Pd.

It can be observed that the cubic Pd nanoparticles are considerably more active for ORR than bulk Pd or spherical PdNPs, as the onset potential of the ORR on Pd nanocubes is about 60 mV more positive than that of bulk Pd and spherical Pd nanoparticles (Figure 29a). It is well known that the electrocatalytic activity of Pt towards the ORR in sulphuric acid solution is strongly dependent on the crystallographic structure and the activity increases in the following order: Pt(111) < Pt(100) < Pt(110) [181, 182]. The lowest activity of Pt(111) is most likely due to the strong adsorption of (bi)sulphate anions on this plane because of the matching symmetry [181, 182]. Thus far the ORR activity of Pd single crystals has been systematically studied only in perchloric acid solution, where the activity was found to increase in the following order: Pd(110) < Pd(111) < Pd(100) [3]. On Pd, the adsorption of anions is even stronger than on Pt [2], therefore it is also expected that the presence of Pd(111) sites decreases the ORR activity on polyoriented PdNPs and bulk Pd as compared to cubic PdNPs that have mostly (100) facets on the surface. This is also supported by an infrared reflection absorption spectroscopy study, which shows that the coverage of (bi)sulphate anions on Pd(100) is lower than that of Pd(111) [183].

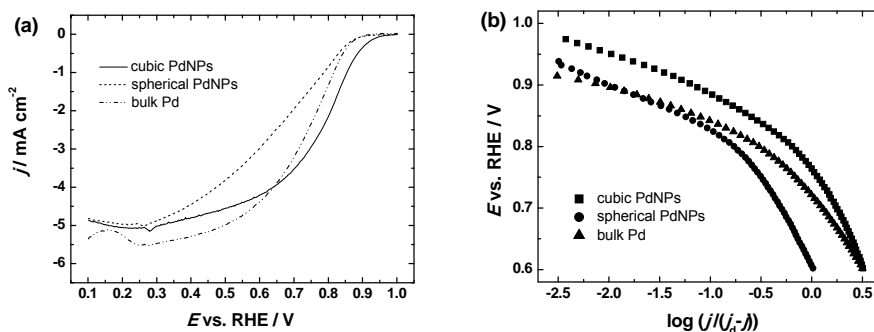


Figure 29. (a) A comparison of RDE voltammetry curves of oxygen reduction on PdNPs and bulk Pd in O₂-saturated 0.5 M H₂SO₄. $\omega = 1900$ rpm, $\nu = 10$ mV s⁻¹. (b) Tafel plots for oxygen reduction on Pd catalysts in 0.5 M H₂SO₄. Data derived from (a).

This suggests that the highest ORR activity of Pd nanocubes observed in this study is due to the predominance of Pd(100) surface sites. The specific activities were calculated at 0.85 V using Eq. (2). The SA value of cubic PdNPs is about three times higher than that of the spherical Pd nanoparticles (Table 7). This

effect is in accordance with the results obtained with platinum nanocubes, which had SA values two times higher than commercial Pt catalyst [184]. Additionally Shao et al. showed that the activity of the ORR is about 10 times higher than that of carbon-supported octahedral Pd nanoparticles and about 6 times higher than that of commercial Pd/C catalyst [46]. The SA of spherical Pd nanoparticles is somewhat lower than that of bulk Pd, similarly the thin Pd films had lower specific activity than that of bulk Pd [I]. This change in SA may be attributed to the influence of Pd particle size and/or morphology.

The Koutecky-Levich analysis (Eq. (3)) showed that on Pd nanoparticles the n value was close to four at negative potentials, which is in agreement with previous studies [3, 23, 29, 34, 185]. At potentials $E > 0.7$ the value of n decreased to about 3.5, indicating that hydrogen peroxide is produced to some extent. This change in the n value might be due to the decreased activity of H_2O_2 reduction on PdNPs in sulphuric acid solution [165]. On bulk Pd the ORR proceeds via 4-electron pathway in the whole range of potentials studied.

On the basis of RDE data at 1900 rpm (Figure 29a) the Tafel plots were constructed (Figure 29b) and the Tafel slopes were determined (Table 7). At low current densities the Tafel slope value was slightly higher than -60 mV, which is the typical value for nanostructured Pd catalysts as well as for bulk polycrystalline Pd [9, 21, 23, 34]. At high current densities the reported Tafel slope values are usually close to -120 mV [9, 23, 34], but also constantly changing Tafel slope has been observed [21]. Similar Tafel slope values (-60 and -120 mV) for the ORR are also characteristic for Pt catalysts [148]. The Tafel slope values at high current densities were even higher than -300 mV on nanostructured Pd that implies a possible change in the reaction mechanism and may correspond to the adsorption of molecular O_2 as the rate-determining step [148].

Table 7. Kinetic parameters for oxygen reduction on PdNPs and bulk Pd in H_2SO_4 solutions. $\omega = 1900$ rpm.

Electrode	In 0.5 M H_2SO_4 , Au support		In 0.05 M H_2SO_4 , GC support	
	Tafel slope [mV] ^a	SA at 0.85 V vs. RHE [$mA\ cm^{-2}$]	Tafel slope [mV] ^a	SA at 0.85 V vs. RHE [$mA\ cm^{-2}$]
Cubic PdNPs	-75 ± 8	0.36 ± 0.05	-67 ± 11	0.35 ± 0.09
Spherical PdNPs	-73 ± 11	0.11 ± 0.01	-81 ± 12	0.15 ± 0.02
Bulk Pd	-65 ± 7	0.12 ± 0.02	-61 ± 1	0.20 ± 0.02

^a At low current densities

6.4.4. ORR on Pd nanocubes in alkaline solution

The oxygen reduction reaction on Pd nanoparticles on GC was also studied in 0.1 M KOH solution. As the other Pd-based catalysts (papers [I-IV]), the Pd nanocubes were electrocatalytically more active in alkaline media and a well-defined diffusion-limited current plateau was formed. The K-L plots were constructed and from Eq. (3) the value of n was found to be 4 for Pd nanocubes as well as for spherical Pd nanoparticles and bulk palladium over the whole range of potentials studied. The 4-electron reduction of oxygen in alkaline solutions has been reported in numerous studies [30, 35, 51], but it has been suggested that on Pt-group metals the ORR proceeds at least partially via peroxide intermediate [167].

In Figure 30a, the RDE results at 1900 rpm on Pd nanocubes in comparison to spherical PdNPs and bulk Pd are presented. The onset potential of the ORR on all the studied electrodes is similar and the sharpest increase in current was observed for bulk Pd. The specific activities were calculated at 0.95 V and these are presented in Table 8. The calculated SA values increase in the same order as in acid solutions: spherical PdNPs < bulk Pd < Pd nanocubes and it is most likely due to the morphological differences of PdNPs. Thus far the ORR on palladium single crystals has not been systematically studied in alkaline media, but in perchloric acid the most active single crystal facet is Pd(100) and least active is Pd(110) [3]. A smaller SA for spherical PdNPs might arise partially from the size effect as Jiang et al. have shown that the activity of the ORR on Pd nanoparticles in alkaline media decreases about a factor of 3 with decreasing the particle size from 16.7 to 3 nm [30]. This effect has been attributed to the stronger adsorption of OH on smaller particles that blocks the active surface sites [30]. The lowest OH coverage on Pd nanocubes has also been proposed to be the reason for their high activity in perchloric acid [46]. On the other hand, it has been claimed that on Pd single crystals in HClO₄ solution the oxide coverage is not relevant to the ORR and the activity depends only on the width of terraces in which Pd(100) is the most active single crystal plane [3, 13]. Taking that into account it is most likely that the high electrocatalytic activity of the Pd nanocubes is due to the dominating Pd(100) surface sites.

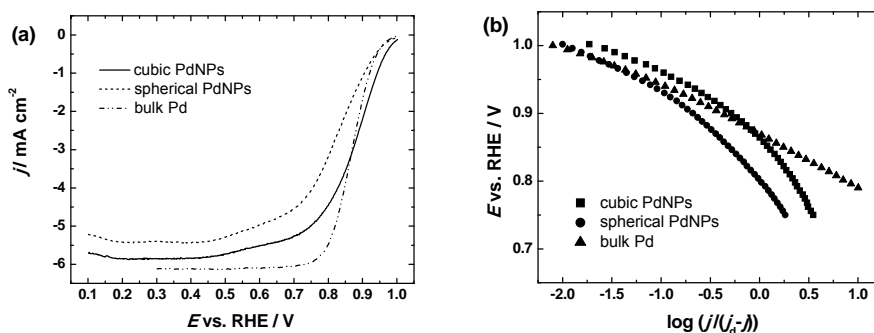


Figure 30. (a) A comparison of RDE voltammetry curves of oxygen reduction on PdNPs and bulk Pd in O₂-saturated 0.1 M KOH. $\omega = 1900$ rpm, $\nu = 10$ mV s⁻¹. (b) Tafel plots for oxygen reduction on Pd catalysts in 0.1 M KOH. Data derived from (a).

The mass-transfer corrected Tafel plots were constructed (Figure 30b) from the RDE data and the values of Tafel slope were determined (Table 8). At low current densities, the Tafel slopes are similar for PdNPs and bulk Pd and slightly higher than -60 mV that is usually observed on Pd nanocatalysts [30, 51, 170]. For PdNPs, the slope value gradually increases at more negative potentials, up to about -180 mV. For bulk Pd, however, the slope is rather constant in the range of Tafel analysis, similarly to the results obtained by Vracar et al. in strongly alkaline solutions [9]. On Pt electrodes, two Tafel slope values (-60 and -120 mV) have been confirmed in many researches and it has been suggested that the ORR mechanism is the same on Pd [167].

Table 8. Kinetic parameters for oxygen reduction on PdNPs and bulk Pd in 0.1 M KOH. $\omega = 1900$ rpm.

Electrode	Tafel slope [mV] I region ^a	Tafel slope [mV] II region ^a	SA at 0.95 V vs. RHE [mA cm ⁻²]
Cubic PdNPs	-79 ± 3	-180 ± 26	0.28 ± 0.06
Spherical PdNPs	-77 ± 13	-181 ± 11	0.073 ± 0.005
Bulk Pd	-75 ± 3		0.13 ± 0.01

^a Region I corresponds to low current densities and Region II to high current densities

6.5. Oxygen reduction on carbon-supported Pd nanocubes

As in practical fuel cells the catalyst material is supported on high surface area carbon, then in continuation to [V, VI], palladium nanocubes of different size supported on high-area carbon powder were prepared and their electrocatalytic properties were investigated in sulphuric acid solution [VII]. Carbon-supported Pd nanocubes with the size of ~ 30 , ~ 10 and ~ 7 nm and nominal Pd content of 20 wt% in the catalyst are designated as PdCub1-20, PdCub2-20, PdCub3-20, respectively. In case of ~ 30 nm Pd cubes 5 and 50 wt% catalysts were also prepared for comparison, designated as PdCub1-5, PdCub1-50, respectively. The results were also compared to these of ~ 2 nm spherical PdNPs (PdSphere).

6.5.1. Surface characterisation of carbon-supported Pd nanocubes

A representative set of TEM micrographs of Pd nanocubes prepared by different methods is presented in Figure 31. It can be observed that the particles are mainly cubic in shape and their size is determined by the synthesis method used. For the samples prepared using CTAB, the particle size is ~ 30 nm (Figure 31a–b) and the methods using PVP yielded smaller particles, ~ 10 nm (Figure

31c) and ~ 7 nm (Figure 31d). The spherical PdNPs were about 2–5 nm in size. It can also be observed that the distribution of Pd on Vulcan XC-72R carbon is rather uniform. It has been previously established that on nanocubes, Pd(100) facet prevails [VI].

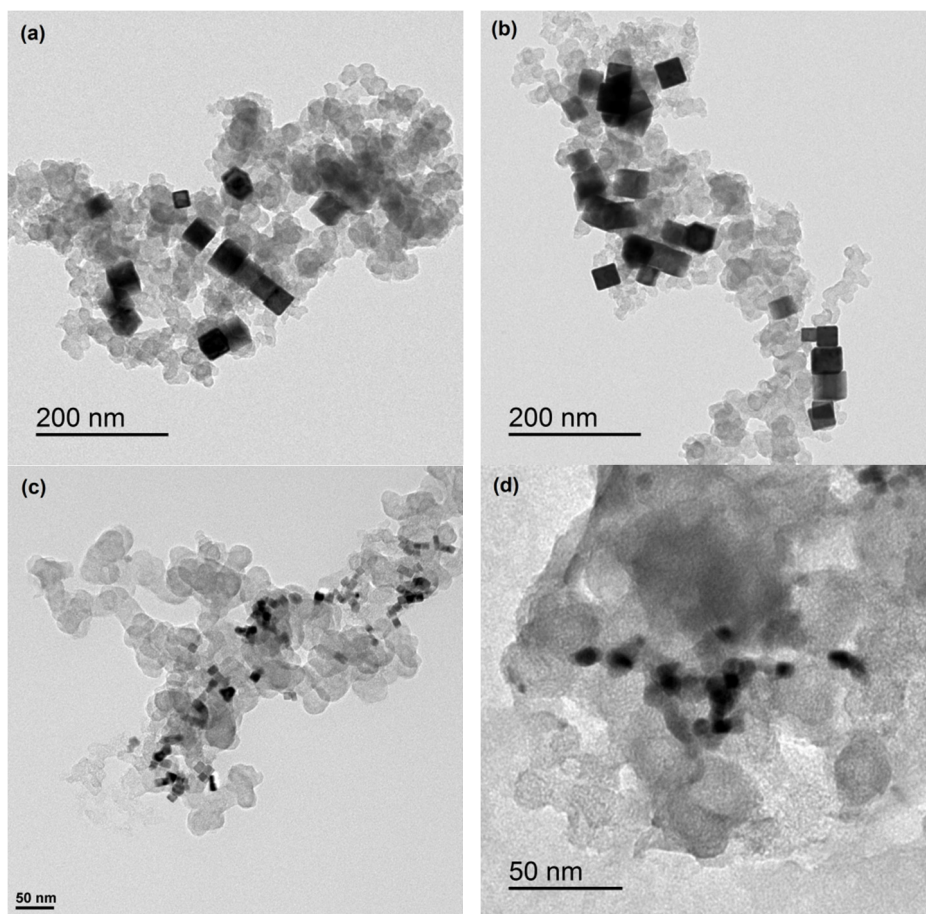


Figure 31. TEM images of carbon-supported Pd nanocubes (a) PdCub1–20, (b) PdCub1–50, (c) PdCub2–20 and (d) PdCub3–20.

6.5.2. Cyclic voltammetry and CO stripping

Cyclic voltammetry and carbon monoxide adsorption-oxidation experiments were carried out in order to electrochemically clean and characterise the Pd/C catalysts. The CO stripping voltammograms are presented in Figure 32a. It can be assumed that the Pd nanoparticle surface was fully covered by CO, as the hydrogen desorption peaks were absent and there was no current until the start of the

oxidation of CO at about 0.85 V. The CO stripping peaks were positioned between 0.91 and 0.94 V and the adsorbed CO was removed with a single cycle to 1 V. The CV curves of Pd nanocubes on carbon after CO stripping experiments are presented in Figure 32b. The shape of these curves is similar to that of Pd(100) single-crystal electrodes with distinctive hydrogen adsorption and desorption peaks. Scanning to more positive potentials was avoided in order to prevent the dissolution of Pd and resulting change of the shape and size of the PdNPs [52]. The distinctive peaks observed on cyclic voltammograms at 0.22 and 0.3 V in the H_{UPD} region are characteristic to Pd(100) facet [178]. The hydrogen adsorption/desorption region was not well defined for the sample containing 5% of Pd, which is most likely due to the high amount of carbon and low Pd content. It is noteworthy that in case of the PdCub1-50 the Pd(100) peaks are much better defined as compared to the catalysts with lower Pd content; this suggests that higher carbon content decreases the efficiency of the surface cleaning.

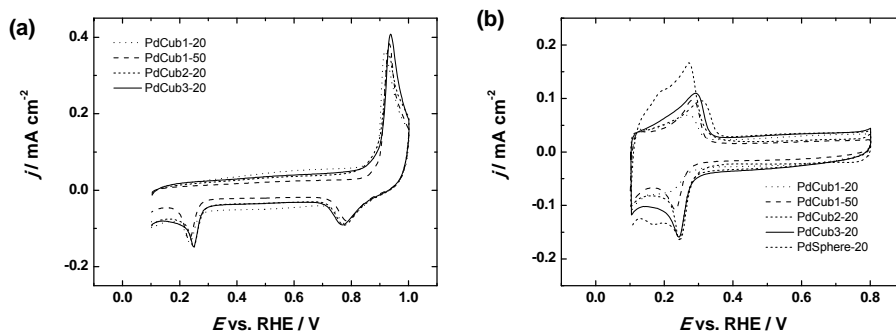


Figure 32. (a) Oxidation of pre-adsorbed CO ($v = 20 \text{ mV s}^{-1}$) and (b) cyclic voltammograms ($v = 50 \text{ mV s}^{-1}$) of Pd nanocubes in Ar-saturated 0.5 M H_2SO_4 . Current densities are normalised to the real surface area of Pd.

6.5.3. ORR on shape-controlled Pd/C catalysts in acidic solution

The ORR measurements were carried out in 0.5 M H_2SO_4 solution employing the RDE technique. For all Pd/C catalysts typical single-wave polarisation curves were obtained (Figure 33a). By comparing the j - E curves of 5, 20 and 50 wt% Pd nanocubes (Figure 33a) it is obvious that the onset potential and half-wave potential of O_2 reduction increase with increasing the Pd content. The $E_{1/2}$ values increase in the following order: PdCub1-5 < PdCub1-20 < PdCub2-20 < PdSphere-20 < PdCub3-20 < PdCub1-50. The specific activities calculated using (Eq. (2)) were about 2–3 times higher for cubic Pd nanoparticles than that for spherical PdNPs. Also some decrease in the SA value was observed with decreasing particle size. The lower activity may partially come from the fact that the ratio of the most active (100) facets to (111) and (110) facets is lower for smaller nanocubes that tend to be more truncated. Another reason may

be that PVP cannot be completely removed from the catalyst surface and the residues block the active sites of PdNPs from the access of O₂ molecules [186]. As the mass of the metal in the catalyst is important then the mass activities (MA) were found:

$$MA = I_k / m \quad (4)$$

where m is the mass of metal in the catalyst layer, calculated theoretically from the mass of the catalyst dropped onto the electrode. In general, the MA values increased with decreasing the particle size, as it is to be expected.

For all Pd/C catalysts the n value was close to 3.5, indicating that the main product of oxygen reduction is water. The reason why n is lower than 4 might be that the ORR on carbon support proceeds via a 2-electron reduction pathway, but it has also been suggested that Nafion coating increases the peroxide yield on Pt catalysts [153]. Recently such behaviour was observed on Pd catalysts, which also showed decreasing diffusion-limited current plateau with increasing Nafion content [187].

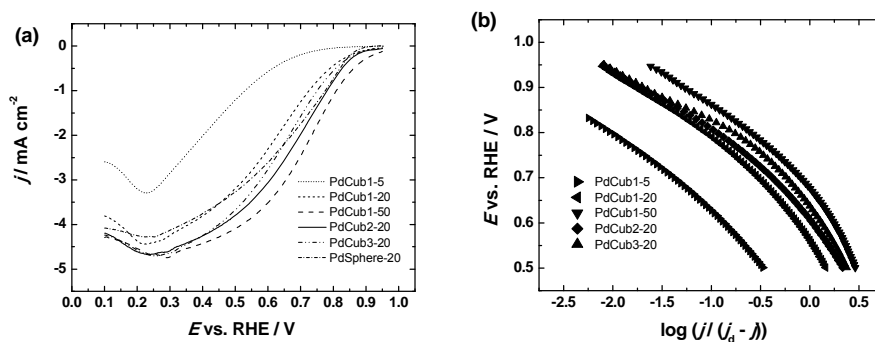


Figure 33. (a) A comparison of RDE voltammetry curves on Pd/C catalysts in O₂-saturated 0.5 M H₂SO₄. $\omega = 1900$ rpm, $\nu = 10$ mV s⁻¹. (b) Tafel plots for oxygen reduction on Pd/C catalysts in 0.5 M H₂SO₄. Data derived from (a).

The Tafel analysis (Figure 33b) was carried out and a tendency of increasing the Tafel slope value with increasing the loading of Pd nanocubes was in evidence. For the Pd nanocubes prepared using CTAB, the Tafel slope values were -128, -139 and -147 mV for the catalysts containing 5, 20 and 50 wt% of Pd, respectively. These values are somewhat higher than -120 mV that is usually observed for Pd catalysts [9, 23, 34], but on unsupported Pd nanocubes we have previously observed the slope values up to -150 mV [VI]. For PdCub2-20 the slope was -125 mV, but for PdCub3-20 it was -105 mV. The spherical Pd nanoparticles had the Tafel slope value of -65 mV that increases to -120 mV at higher current densities. Similarly, Salvador-Pascual et al. have observed one

Tafel slope region with the value of -120 mV for Pd nanoparticles [29]. In addition, Alvares et al. observed the Tafel slope values near -60 mV and suggested that this corresponds to oxide covered electrodes [21]. Thus, it may be assumed that the carbon-supported Pd nanocubes prepared in this study have lower coverage of oxides than spherical Pd nanoparticles and the smallest Pd nanocubes, as the Tafel slope value was below -120 mV.

6.6. Oxygen reduction on gold catalysts supported on carbon

The oxygen reduction reaction was also studied on commercial Au/C catalyst layers of various thicknesses [VIII]. The aim of this part of the work was to evaluate the effect of the thickness of Au/C catalyst layer on the kinetics of the ORR in acid and alkaline solutions.

6.6.1. Surface characterisation of Au/C catalysts

The surface morphology of Au/C catalyst was analysed using transmission electron microscopy and a representative set of TEM micrographs is presented in Figure 34. The particle size was determined by measuring 264 and 123 particles of 20 wt% and 30 wt% catalysts, respectively. A rather wide size distribution was obtained with the average particle size being 11.0 ± 1.7 nm and 14.0 ± 1.7 nm for 20 wt% and 30 wt% Au/C, respectively.

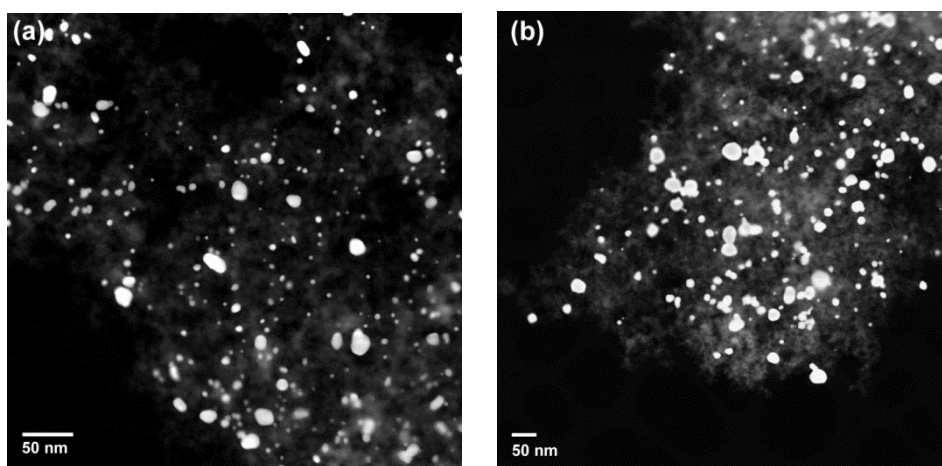


Figure 34. High-angle annular dark field TEM images of Au/C catalysts. (a) 20 wt% catalyst, (b) 30 wt% catalyst.

For comparison purposes the XRD measurements (Figure 35) were carried out to estimate the Au particle size. Four major peaks with 2θ values of 38.2° , 44.4° , 64.6° and 77.6° corresponding to the (111), (200), (220) and (311) planes of the bulk Au, respectively, were observed, which can be assigned to the Au face-centered cubic structure. The broad peak at about 25° is due to the graphitic regions of carbon support. The Rietveld analysis was carried out to calculate the crystallite size of Au particles and the average values of $d = 16.8$ nm and $d = 26.3$ nm were obtained for 20 wt% and 30 wt% Au/C catalysts, respectively. These values are larger than those obtained from TEM images. This is most probably due to the wide size distribution of Au particles, as the small number of large Au particles contains a significant fraction of all gold and therefore have a higher contribution to the XRD response.

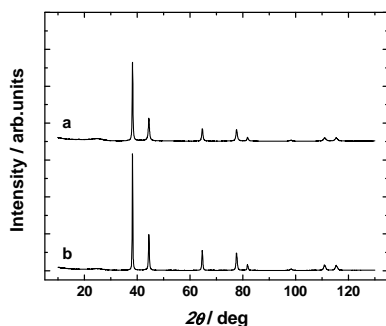


Figure 35. XRD pattern for (a) 20 wt% Au/C catalyst and (b) 30 wt% Au/C catalyst.

6.6.2. Cyclic voltammetry of Au/C catalysts

The thin-layered Au/C electrodes were first subjected to pre-treatment and characterisation by cyclic voltammetry in Ar-saturated 0.5 M H₂SO₄. The stable CVs are presented in Figure 36. The anodic current increase at $E > 1.1$ V vs. SCE corresponds to the formation of Au surface oxides and the cathodic peak at ca 0.89 V corresponds to their reduction [188]. The large background current is mainly due to the supporting carbon black and it increases proportionally with catalyst loading. The further current increase at $E > 1.3$ V is apparently caused by the oxidation of the carbon surface. The pair of peaks at ca 0.3 V is related to the oxidation and reduction of some functional groups on the carbon surface, such as quinone-type species [164]. These peaks increase with potential cycling due to the oxidation of the carbon surface.

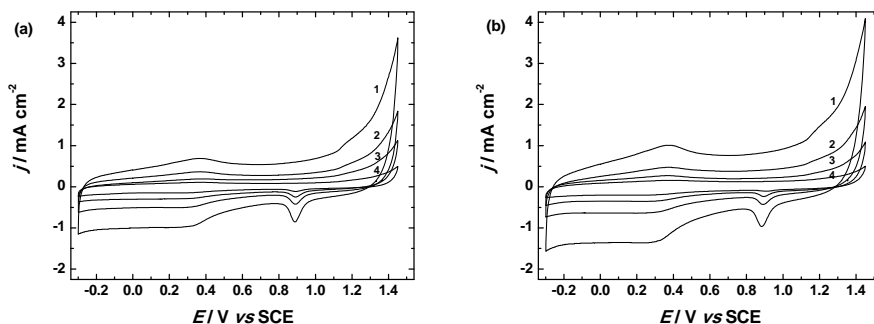


Figure 36. Cyclic voltammograms for (a) 20 wt% Au/C catalyst and (b) 30 wt% Au/C catalyst in Ar-saturated 0.5 M H₂SO₄. Catalyst layer thickness: (1) 10; (2) 6; (3) 3 and (4) 1.5 μm . $\nu = 100 \text{ mV s}^{-1}$.

The electroactive surface area of gold was determined from the stable cyclic voltammograms by charge integration under the oxide reduction peak and by using the value of $400 \mu\text{C cm}^{-2}$ as the charge density for the reduction of Au oxide monolayer [188]. The A_r increased linearly with increasing the Au/C loading, which indicates that the accessibility of the gold nanoparticles is not affected by changing the layer thickness.

6.6.3. ORR on Au/C catalysts in acidic solution

Both gold and carbon are rather inactive electrocatalysts towards the ORR in acid solution. For all Au/C electrodes studied, single-wave ORR polarisation curves with no well-defined current plateaus were registered using the RDE method (Figure 37a). The Koutecky-Levich equation (Eq. (3)) was employed for analysing the RDE data. From the slopes of the K-L plots the value of n was determined. The n values were close to 2 at the foot of the polarisation curve, showing that H₂O₂ is the final product at these potentials. The n value increases gradually at more negative potentials, as the formed hydrogen peroxide is further reduced. At $E = -0.3 \text{ V}$ the value of n slightly depended on the catalyst loading, increasing from 2.5 to 3 with increasing the catalyst layer thickness. This observation is in accordance with previous studies [65, 66, 68].

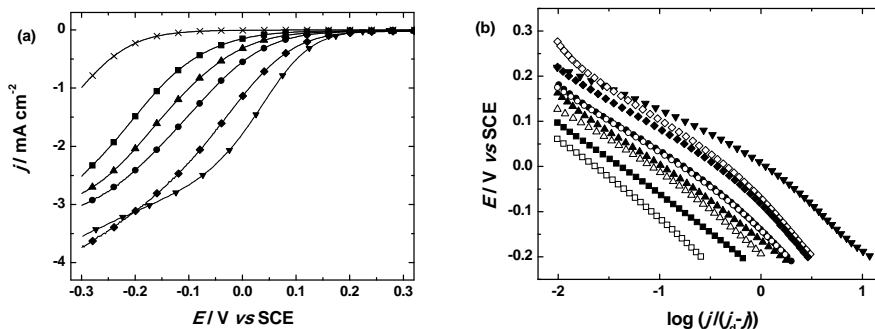


Figure 37. (a) RDE voltammetry curves for O_2 reduction on 20 wt% Au/C catalyst in O_2 -saturated 0.5 M H_2SO_4 . (b) Mass-transfer corrected Tafel plots for O_2 reduction on 20 wt% Au/C catalyst (closed symbols); on 30 wt% Au/C (open symbols) and on bulk Au (\blacktriangledown) in O_2 -saturated 0.5 M H_2SO_4 . Catalyst layer thickness: (\blacksquare, \square) 1.5 μm ; ($\blacktriangle, \triangle$) 3 μm ; (\bullet, \circ) 6 μm and (\blacklozenge, \lozenge) 10 μm and (\times) 3 μm layer of carbon powder. $\omega = 1900$ rpm; $\nu = 10$ mV s^{-1} .

The overall electrocatalytic activity of Au/C electrodes towards the ORR increased almost proportionally with increasing the catalyst loading and the $E_{1/2}$ shifted to positive potentials (Figure 37a). The SA values were calculated at $E = 0$ V and are given in Table 9. At this potential the carbon support powder is inactive towards the ORR and the reaction occurs only at gold particles. It is evident that the SA value has no significant dependence on the layer thickness, also the specific activities of 20 wt% and 30 wt% Au/C are similar. The mass activities were calculated from Eq. (4). The MA values were smaller for 30 wt% catalyst, as a result of the larger particle size.

The mass-transfer corrected Tafel plots were constructed (Figure 37b) from the RDE data at a single electrode rotation rate and the slope values are given in Table 9. The Tafel slope value close to -120 mV has been previously reported on bulk gold, indicating that the rate-determining step of the reaction is the transfer of the first electron to the O_2 molecule [65, 66]. However, the Au/C catalysts tested here had higher Tafel slope values, about -160 mV. This value is also higher than that obtained by Bron for electrodes coated with Au/C catalyst layers with the thickness of 7.6 μm [68].

Table 9. Kinetic parameters of oxygen reduction on Au/C catalysts in 0.5 M H₂SO₄. $\omega = 1900$ rpm.

Catalyst	Au/C layer thickness [μm]	Au loading [$\mu\text{g cm}^{-2}$]	A_r [cm^2]	Tafel slope [mV]	$E_{1/2}$ vs. SCE [V]	SA at 0 V vs. SCE [mA cm^{-2}]	MA at 0 V vs. SCE [A g^{-1}]
20% Au/C	1.5	5.8	0.026	-157	-0.24	1.2	27
	3	11.5	0.047	-152	-0.16	1.5	30
	6	23	0.097	-154	-0.14	1.3	28
	10	38	0.16	-165	-0.08	1.9	41
30 % Au/C	1.5	8.6	0.014	-169	-	1.2	9.6
	3	17.3	0.036	-151	-0.19	1.5	16
	6	34.5	0.068	-151	-0.14	1.6	15
	10	57	0.21	-181	-0.07	1.9	35
Bulk Au	-	-	0.64	-107	0.01	1.1	-

6.6.4. ORR on Au/C catalysts in alkaline solution

As opposed to acidic solution, gold is a rather active catalyst for ORR in alkaline media, especially Au(100) facet [6, 56]. In alkaline media the polarisation curves of the ORR showed two waves (Figure 38). It is known that at the first wave the ORR proceeds via 2-electron pathway forming mainly HO₂⁻ and at more negative potentials the ORR proceeds to yield OH⁻; on some catalysts a current maximum can be obtained at low overpotentials. Thorough ORR studies on Au single crystals have revealed that this is caused by the considerably high electrocatalytic activity of Au(100) plane, on which the four-electron reduction of O₂ proceeds in the certain potential range at low overpotentials [56]. As in acid solution, the activity of the electrodes increased with catalyst loading as the half-wave potential shifted to positive potentials (Figure 39a). A current maximum appears at ca -0.4 V vs. SCE for the thickest Au/C layers, this behaviour is similar to that of bulk Au electrode.

The Koutecky-Levich analysis revealed that the number of electrons transferred per O₂ molecule depends on the potential. At the potentials near to the current maximum, the value of n was close to 3 for the bulk gold and the thicker layers and ca 2.5 for the thinner layers. The n value decreased until 2 at more negative potentials, indicating that peroxide is the final reduction product. At the

potentials $E < -0.6$ V the further reduction of peroxide begins on all electrodes and the value of n increases again up to about four at the most negative potentials.

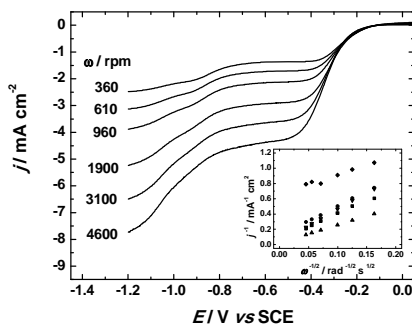


Figure 38. RDE voltammetry curves for O_2 reduction on $3 \mu\text{m Au/C}$ (20 wt%) in O_2 -saturated 0.1 M KOH. $v = 10 \text{ mV s}^{-1}$. Inset: Koutecky-Levich plots for O_2 reduction on $3 \mu\text{m Au/C}$ (20 wt%) in 0.1 M KOH at various potentials: (♦) -0.3 V; (●) -0.4 V; (▼) -0.6 V; (■) -0.8 V and (▲) -1.2 V.

The supporting carbon powder also shows considerable electrocatalytic activity towards the ORR in alkaline solution (Figure 39a). However, at $E = -0.2$ V the reduction current on carbon support is still negligible and thus the SA of gold may be calculated at this potential. As in acid solution, the SA values for 20 wt% and 30 wt% Au/C in 0.1 M KOH are similar for all layer thicknesses and are slightly higher than that of bulk Au (Table 10). The MA values are lower for 30 wt% Au/C due to the larger particle size.

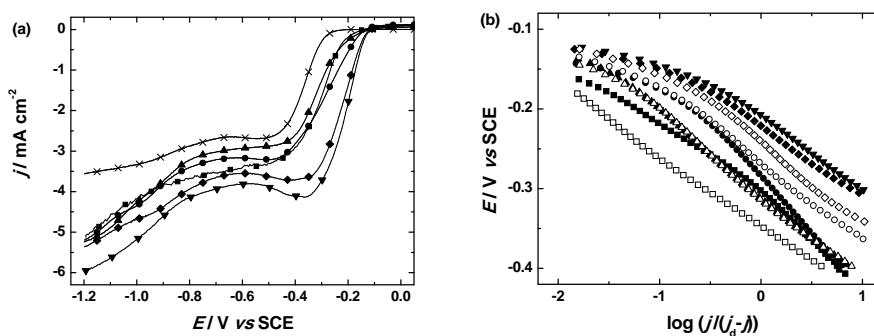


Figure 39. (a) RDE voltammetry curves for O_2 reduction on 20 wt% Au/C catalyst in O_2 -saturated 0.1 M KOH. (b) Mass-transfer corrected Tafel plots for O_2 reduction on 20 wt % Au/C catalyst (closed symbols); on 30 wt% Au/C (open symbols) and on bulk Au (▼) in 0.1 M KOH. Catalyst layer thickness: (■, □) 1.5 μm ; (▲, Δ) 3 μm ; (●, ○) 6 μm ; (♦, ◇) 10 μm and (×) 3 μm layer of carbon powder. $\omega = 1900 \text{ rpm}$; $v = 10 \text{ mV s}^{-1}$.

From the Tafel analysis (Figure 39b) the Tafel slope values close to -120 mV were determined for Au/C catalysts, which is the typical value for polycrystalline Au. This slope value indicates that the rate-determining step for the ORR on the studied catalyst is the transfer of the first electron to the O₂ molecule [66, 189].

The fact that the SA values are independent of catalyst layer thickness in both solutions indicates that at least at low overpotentials, where the SA was determined, the transport of reactants through the catalyst layer does not limit oxygen reduction and the reduction occurs also on Au particles that are located in the inner layers, close to the GC substrate. The Tafel plots are parallel even at more negative potentials, in the mixed kinetic-diffusion region, suggesting that the limitation also does not occur at these potentials. The SA values are similar for 20 wt% and 30 wt% Au/C catalysts, as expected for Au particles of larger size.

Table 10. Kinetic parameters of oxygen reduction on Au/C catalysts in 0.1 M KOH. $\omega = 1900$ rpm.

Catalyst	Au/C layer thickness [μm]	Au loading [$\mu\text{g cm}^{-2}$]	A_r [cm^2]	Tafel slope [mV]	$E_{1/2}$ vs. SCE [V]	SA at -0.2 V vs. SCE [mA cm^{-2}]	MA at -0.2 V vs. SCE [A g^{-1}]
20% Au/C	1.5	5.8	0.030	-100	-0.30	1.5	37
	3	11.5	0.047	-111	-0.31	1.2	25
	6	23	0.074	-135	-0.28	1.7	27.5
	10	38	0.20	-91	-0.22	1.9	48
30 % Au/C	1.5	8.6	0.010	-90	-0.34	1.2	7.4
	3	17.3	0.036	-115	-0.31	1.6	17
	6	34.5	0.077	-109	-0.27	1.6	18
	10	57	0.21	-114	-0.24	1.8	33
Bulk Au	-	-	0.64	-93	-0.21	1.0	-

6.7. Oxygen reduction on shape-controlled Au nanoparticles supported on carbon

The oxygen reduction reaction was studied on carbon-supported shape-controlled Au nanoparticles in acid and alkaline media [IX]. The ORR on Au catalysts is a structure sensitive process [53, 56] and thus in this part of the study the Au nanocubes, octahedra and spherical Au nanoparticles of two different size supported on carbon were used to evaluate the ORR activity.

6.7.1. Surface characterisation of shape-controlled Au/C catalysts

Figure 40 shows a representative set of TEM micrographs of the carbon-supported Au nanoparticles synthesised and used in this work. In all samples, the AuNPs are well-dispersed. However, in terms of particle size, remarkable differences are found as expected from the different synthesis methods. The Au nanoparticles prepared by the reduction of HAuCl_4 with ice-cold NaBH_4 in the presence of citrate shows a quasi-spherical particle shape with an average particle size of approximately 5 nm (Figure 40a). A similar quasi-spherical particle shape is also found for AuNPs prepared by the standard citrate method. However, as expected, the particle size is much larger and about 30 nm (Figure 40b). The Au nanoparticles prepared in the presence of CTAB and ascorbic acid by addition of NaOH show a well-defined octahedral shape, but also with a certain degree of truncation. The average particle size of these octahedral AuNPs is ca 40–45 nm (Figure 40c). This particle size fits well with the expected particle size at the used reaction temperature [128]. Finally, the AuNPs prepared using the seed-mediated growth method show a preferential cubic shape and a particle size about 40–45 nm (Figure 40d).

It is important to point out that TEM data provide valuable information about the nanoparticle size and shape as well as about the nanoparticle dispersion on the carbon substrate, but not about their surface structure. However, as shown in previous contributions [190–192], shape is expected to be a prerequisite for a particular surface structure. Thus, quasi-spherical nanoparticles can be considered as a polyoriented, non-specifically-surface-structured catalyst material, since no predominant facets are exposed. However, octahedral AuNPs represent a catalytic material having a preferential (111) surface orientation, and cubic AuNPs can be considered as catalytic material containing a preferential (100) surface orientation. Therefore, different electrocatalytic activity for ORR is expected for these samples as a consequence of their different surface structure.

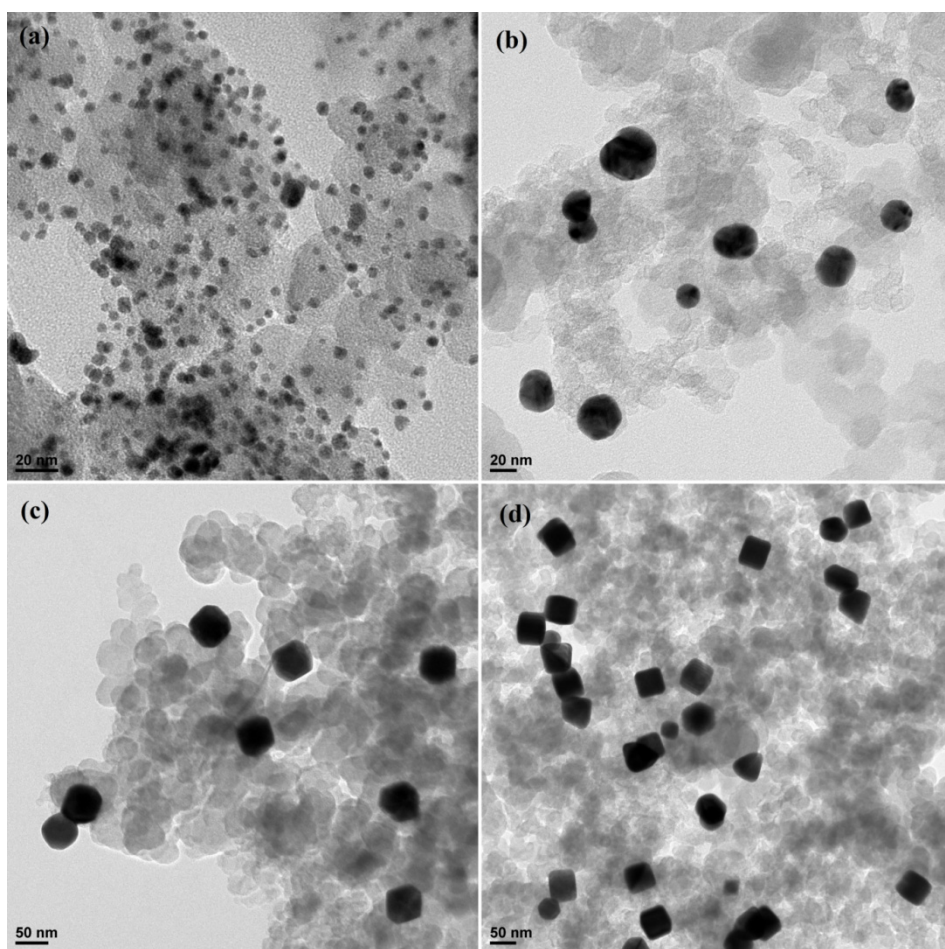


Figure 40. Representative TEM images of carbon-supported Au nanoparticles: (a) ~5 nm Au spheres, (b) ~30 nm Au spheres, (c) Au octahedra and (d) Au nanocubes.

6.7.2. CO stripping on shape-controlled Au nanoparticles in alkaline solution

Carbon monoxide effectively blocks the hydrogen H_{UPD} on platinum and palladium, but on gold there are no hydrogen-related adsorption/desorption processes and thus CO adsorption cannot be confirmed [131]. Still, it is expected that CO adsorbs onto the Au surface and covers the surface. Previously Koper and co-workers have found an unusual behaviour of adsorbed CO on single-crystalline gold electrodes in alkaline media [193]. They detected a reversible pair of peaks at around 0.4 V vs RHE on Au(111) and hex-Au(100), which were associated with OH adsorption induced by the CO adsorption on the surface. This behaviour has not been observed on Au(110) single crystal surface [193, 194].

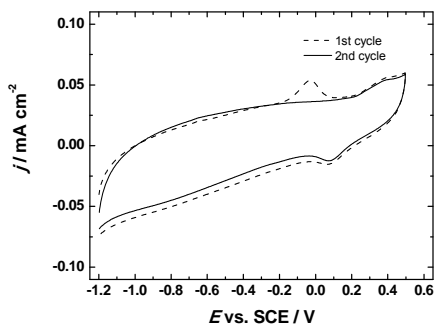


Figure 41. CO stripping voltammograms on unsupported 5 nm Au spheres in Ar-saturated 0.1 M KOH solution. $\nu = 20 \text{ mV s}^{-1}$.

In this work, gold nanoparticles without carbon support were used for pre-adsorbed CO oxidation experiments. The adsorbed CO was oxidised in a single sweep that was confirmed by the absence of peaks in the subsequent sweep (Figure 41). For all different shaped Au nanoparticles the CO stripping voltammograms were similar; the pair of peaks observed previously by Rodriguez et al. at 0.4 V vs RHE on Au(111) and Au(100) with adsorbed CO in 0.1 M NaOH solution [193, 194] was not detected. The CO stripping peak appeared at ca. 0 V vs. SCE as shown previously [193–195]. The size effect of AuNPs on the electro-oxidation of CO has been studied and the CO oxidation peaks in both cathodic and anodic sweeps have been observed [195]. In the present work CO was oxidised by applying a single potential cycle. The second cycle showed the same CV characteristics as bulk gold in O₂-free electrolyte. The electroactive area of gold increased upon CO oxidation, which could be attributed to the improved surface cleanliness, since there is probably some surfactant remaining on the nanoparticles from their synthesis. CO stripping experiments were also carried out with carbon-supported Au nanoparticles, but for those catalysts the CO stripping peaks were not observed, probably due to low Au loading.

6.7.3. Cyclic voltammetry of shape-controlled Au/C catalysts

The CVs of the Au/C catalysts (Figure 42) were in general similar to those obtained in previous part. In acid solution the anodic peak at $E > 1.1 \text{ V vs. SCE}$ corresponds to the formation of Au surface oxides and the cathodic peak at ca. 0.9 V corresponds to the reduction of these oxides. The current increase at $E > 1.3 \text{ V}$ can be due to the carbon support. The oxidation and reduction of the oxygen-containing species on carbon produces a pair of peaks at ca. 0.4 V vs. SCE. In alkaline solution the processes related to Au surface oxidation and reduction are also evident. The increase in anodic current at $E > 0.1 \text{ V}$ is due to

the oxidation of Au surface and the cathodic peak of Au oxide reduction is centred at ca 0.05 V (Figure 42b).

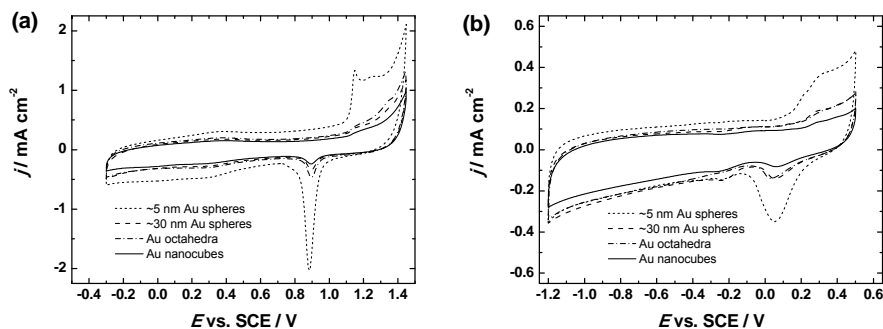


Figure 42. Cyclic voltammograms of Au/C catalysts in Ar-saturated (a) 0.5 M H₂SO₄ and (b) 0.1 M KOH solutions. $\nu = 50 \text{ mV s}^{-1}$.

The real electroactive surface area of gold catalyst was determined from stable cyclic voltammograms in acid solution by charge integration under the oxide reduction peak and using a value of $400 \mu\text{C cm}^{-2}$ as the charge density for the reduction of an oxide monolayer [188].

6.7.4. ORR on shape-controlled Au/C catalysts in acidic solution

Gold is a modest electrocatalyst for ORR in acid media; however, its electrocatalytic activity is considerably higher than that of unmodified carbon materials. For all Au/C catalysts studied, single-wave oxygen reduction polarisation curves with no well-defined current plateau were obtained using the RDE method (Figure 43). The K-L equation (Eq. (3)) was used to analyse the RDE data and the potential dependence of n was found. Similarly to the previous part, the value of n changed with potential. At the beginning of the polarisation curve n was close to two and increased up to 3.5 at negative potentials, showing that H₂O₂ is produced at positive potentials and at negative potentials it is further reduced to yield water. Such behaviour is typical for O₂ reduction on nanostructured gold electrodes in acidic media [65, 66, 94, 96, 196].

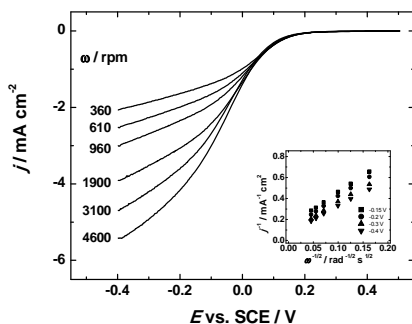


Figure 43. RDE voltammetry curves for oxygen reduction on carbon-supported ~ 5 nm Au spheres in O_2 -saturated 0.5 M H_2SO_4 solution. $v = 10$ $mV\ s^{-1}$. Inset: Koutecky-Levich plots for O_2 reduction.

A comparison of different Au catalysts is presented in Figure 44a. It is important to note that for the nanoparticle-modified electrodes with the fixed mass of nanocatalyst per unit area, the electrocatalytic activity is determined by the size and shape of the catalyst particles [197]. Thus, the $E_{1/2}$ of O_2 reduction is most positive for ~ 5 nm spherical AuNPs, being slightly higher than that of bulk Au. The other Au/C catalysts exhibit lower $E_{1/2}$ values. This observation can be explained by the differences in the real electroactive surface area, which is highest for ~ 5 nm Au spheres and bulk Au (Table 11). The rest of Au/C catalysts studied in this work (~ 30 nm Au spheres, octahedra and nanocubes) have a smaller electroactive surface area and thus the $E_{1/2}$ value is more negative. Differences in the $E_{1/2}$ value between larger Au spheres and octahedra apparently arise from differences in crystallographic orientation. Au nanocubes have the smallest electroactive surface area, but similar $E_{1/2}$ value, showing that the crystallographic orientation has an essential contribution to the electrocatalytic activity, as previously suggested [98–101]. For better comparison the specific activities (Eq. (2)) and mass activities (Eq. (4)) for O_2 reduction were calculated (Table 11). The mass of Au on the electrode was calculated on the basis of the nominal Au loading.

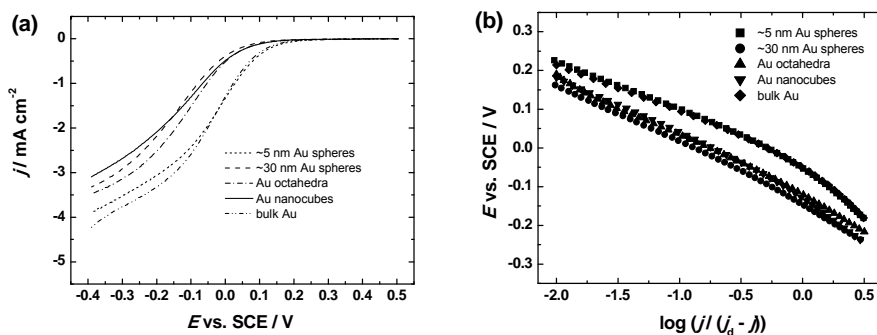


Figure 44. (a) Comparison of RDE voltammetry curves for oxygen reduction on Au/C catalysts and bulk Au in O₂-saturated 0.5 M H₂SO₄ solution and (b) mass-transfer corrected Tafel plots, derived from (a). $\omega = 1900$ rpm, $\nu = 10$ mV s⁻¹.

The SA values for larger Au spheres and Au octahedra are rather similar to that of bulk Au. The smaller Au spheres have a slightly lower SA as compared to larger spheres, which may be related to the particle size effect as demonstrated previously [69]. The considerably higher specific activity of Au nanocubes indicates that the crystallographic orientation of AuNPs has a major contribution to the activity of these catalysts. This is in accordance with the previous results, as it has been determined that the Au(100) is the most active single crystal surface for ORR [56, 57]. As expected, the smallest Au particles (5 nm spheres) demonstrate the highest MA.

On the basis of RDE data shown in Figure 44a the mass-transfer corrected Tafel plots (Figure 44b) were constructed and the values of Tafel slope were determined (Table 11). The absolute values of the Tafel slope are slightly higher than the typical value of -120 mV, which suggests that the rate-determining step is the transfer of the first electron to O₂ molecule. Similarly, higher negative slope values have been previously observed for some Au single-crystal electrodes [56, 57] and Au/C catalysts [paper VIII]. In addition, higher negative Tafel slope values due to the porosity of the catalyst have been obtained in case of very thick catalyst layers [144], however, in this work the catalyst loading is much lower and presumably the reaction is not limited by the thin layer diffusion, as confirmed for Au/C catalysts of various loadings [VIII]. Therefore, the exact reason of the higher slope is not clear at present, but it is expected to be related to the reaction kinetics and not to the diffusion effects.

Table 11. Kinetic parameters for O₂ reduction on Au/C catalysts in 0.5 M H₂SO₄. $\omega = 1900$ rpm.

Catalyst	A _r [cm ²]	Tafel slope [mV]	E _{1/2} vs. SCE [V]	SA at 0 V vs. SCE [mA cm ⁻²]	MA at 0 V vs. SCE [A g ⁻¹]
~5 nm Au spheres	0.67 ± 0.02	-139 ± 2	-0.05 ± 0.01	0.56 ± 0.06	277 ± 24
~30 nm Au spheres	0.12 ± 0.02	-151 ± 6	-0.14 ± 0.02	0.87 ± 0.03	77 ± 15
Au octahedra	0.14 ± 0.01	-150 ± 4	-0.13 ± 0.01	0.82 ± 0.02	86 ± 3
Au nanocubes	0.06 ± 0.01	-166 ± 2	-0.13 ± 0.01	1.81 ± 0.07	78 ± 1
Bulk Au	0.43 ± 0.02	-141 ± 3	-0.05 ± 0.02	0.75 ± 0.01	-

6.7.5. ORR on shape-controlled Au/C catalysts in alkaline solution

The oxygen reduction reaction on shape-controlled Au nanoparticles supported on carbon was also studied in alkaline media. Two-wave ORR polarisation curves were registered for all the Au/C catalysts (Figure 45a) studied. The RDE data was analysed using the K-L equation (Eq. (3)). The value of n depends on electrode potential as usually observed Au-based catalysts in alkaline media [100]. At the current maximum at around -0.4 V the value of n is higher than 3 depending on the Au/C catalyst, but by scanning to more negative potentials it first decreases to until $2 < n < 2.5$ and then increases again to $3 < n < 4$. This behaviour suggests that the main product is hydrogen peroxide, which is further reduced to water at more negative potentials.

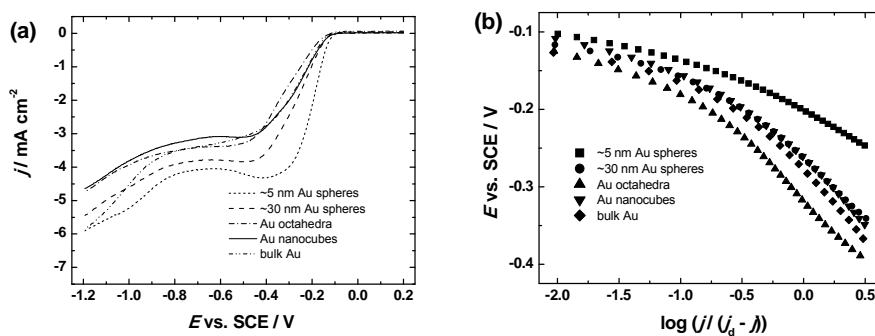


Figure 45. (a) Comparison of RDE voltammetry curves for oxygen reduction on Au/C catalysts and bulk Au in O₂-saturated 0.1 M KOH solution and (b) mass-transfer corrected Tafel plots, derived from (a). $\omega = 1900$ rpm, $\nu = 10$ mV s⁻¹.

From the comparison of the O₂ reduction results (Figure 45a) it can be seen that the overall electrode activity was the highest for smaller Au spheres and that bulk Au has similar ORR activity than that of larger AuNPs. The differences in the $E_{1/2}$ value are more pronounced in alkaline media than in acid, being about 60 and 40 mV between ~5 nm and ~30 nm Au spheres and octahedra, respectively (Table 12). Taking into account that the electroactive surface area of Au nanocubes is considerably smaller than that of 5 nm Au spheres, the half-wave potential does not reflect the intrinsic electrocatalytic activity of Au nanoparticles and thus the SA values were calculated using Eq. (2). The specific activities were slightly lower for smaller Au spheres, as compared to these of larger Au spheres and bulk Au (Table 12). This may be due to the particle size effect on the kinetics of the ORR, which has previously been reported also in alkaline media [75], however, the difference is too small to claim that. The Au octahedra had rather low SA value and similarly to the results obtained in acidic solution, the highest specific activity was determined for Au nanocubes. This order of activities is in agreement with studies on Au single-crystal electrodes [56], which show that Au(111) is the least active and Au(100) the most active single-crystal plane and also confirms the results of previous O₂ reduction studies on shape-controlled AuNPs [100]. As expected, the MA values increased in the following order: Au octahedra \approx Au cubes < 30 nm Au spheres < 5 nm Au spheres.

Table 12. Kinetic parameters for O₂ reduction on Au/C catalysts in 0.1 M KOH. $\omega = 1900$ rpm.

Catalyst	A_r [cm ²]	Tafel slope [mV]	$E_{1/2}$ vs. SCE [V]	SA at -0.15 V vs. SCE [mA cm ⁻²]	MA at -0.15 V vs. SCE [A g ⁻¹]
~5 nm Au spheres	0.67 ± 0.02	-43 ± 9	-0.23 ± 0.03	0.18 ± 0.03	89 ± 9
~30 nm Au spheres	0.12 ± 0.02	-44 ± 4	-0.29 ± 0.02	0.27 ± 0.04	29 ± 9
Au octahedra	0.14 ± 0.01	-60 ± 11	-0.33 ± 0.02	0.15 ± 0.02	16 ± 2
Au nanocubes	0.06 ± 0.01	-48 ± 3	-0.30 ± 0.03	0.36 ± 0.02	15 ± 1
Bulk Au	0.43 ± 0.02	-54 ± 8	-0.27 ± 0.02	0.23 ± 0.02	-

The Tafel slope value remained lower than -60 mV for Au spheres and Au nanocubes, for octahedra it was near -60 mV at low current densities, but it increased up to -170 mV in the high current density region (Figure 45b). The Tafel slope value in the range from -60 to -120 mV suggest that the rate-determining step is the transfer of the first electron to O₂ molecule [189].

The values of the specific and mass activity of Au nanoparticles for O₂ reduction suggest that the particle size of the catalysts should be further reduced for practical applications. On the other hand, the results obtained demonstrate that the surface structure of the AuNPs plays an essential role in the performance of these catalysts, which can therefore be improved by employing new methods of the shape-controlled synthesis.

7. SUMMARY

The electrochemical reduction of oxygen on nanostructured palladium and gold electrodes in sulphuric acid and potassium hydroxide solutions was studied using the rotating disk electrode method.

The nanostructured palladium and gold catalysts were prepared by electron beam evaporation, electrochemical deposition and chemical synthesis.

In the first part of the study the oxygen reduction reaction on thin Pd films with nominal thicknesses of 0.25–10 nm was explored. The films were prepared by electron beam evaporation onto glassy carbon substrate and it was observed that thinner films consisted of small particles. In alkaline media the activity of Pd for ORR was rather constant for all coatings, but in sulphuric acid solution an increase in specific activity with increasing film thickness was observed.

In the second part of the work palladium was electrochemically deposited onto glassy carbon and gold substrates and subsequently their electrocatalytic properties towards the ORR were evaluated. These coatings consisted of larger particles than electron beam evaporated Pd films, but the specific activities showed the same tendencies that were observed for thin Pd films. In addition, for Pd coatings deposited onto gold the SA values surpassed that of bulk Pd, which could be due to alloying effects.

Next, palladium and gold were co-deposited onto glassy carbon substrate. The resulted coating showed uniform distribution of both metals and the particle size was about 6 nm; formation of some larger agglomerates was also observed. The XPS analysis of these coatings suggested alloy formation that was also seen from the cyclic voltammetry studies. The Pd-Au coatings showed relatively low activity towards the ORR in acidic solution, but in alkaline solution the specific activity of the alloy coatings was 3–5 times higher than that of the electrochemically deposited Pd and bulk Pd. The increased activity arises most probably from the alloying effects between Au and Pd.

In the next part cubic Pd nanoparticles were used as the catalyst for ORR. The size of the nanocubes was 26.9 ± 3.9 nm. The XRD analysis showed a prevalence of Pd(100) facet that has highest activity among Pd single-crystal facets. As expected, the specific activity of Pd nanocubes was higher than that of spherical PdNPs and bulk Pd. The nanocubes exhibited up to three times higher SA than the spheres in acid medium and in alkaline medium these were up to four times more active.

The Au/C catalysts with 20 wt% and 30 wt% Au content were used to prepare catalyst layers with different thicknesses (1.5–10 μm). The analysis revealed that the specific activities do not depend on the layer thickness or the metal content in the catalyst. The mass activities were higher for 20 wt% catalyst, as Au particles were smaller in that catalyst.

Finally the ORR was studied on carbon-supported shape-controlled Au nanoparticles, i.e. Au spheres of two different size (~5 and ~30 nm), octahedral (40–45 nm) and cubic AuNPs (40–45 nm). The specific activity of

Au nanocubes was more than two times higher than that of spherical and octahedral AuNPs in acid solution, in alkaline medium the differences were smaller, but Au nanocubes exhibited the highest activity also in that solution.

The RDE data of O₂ reduction was analysed using the Koutecky-Levich equation and the number of electrons transferred per O₂ molecule was found. For most of the palladium-based catalysts it was close to four in both solutions, but for thin Pd films and electrodeposited Pd coatings on glassy carbon substrate this value dropped to 3.5. These values suggest that the oxygen reduction reaction proceeds mainly via four-electron pathway yielding water. For gold catalysts the number of electrons transferred strongly depended on the potential. The Tafel analysis revealed that at low current densities the mechanism of the ORR on nanostructured palladium and gold catalysts studied is the same as on their bulk counterparts, the rate-limiting step being the transfer of the first electron to the oxygen molecule.

8. REFERENCES

- [1] E. Antolini, Palladium in fuel cell catalysis, *Energy & Environmental Science*, 2 (2009) 915–931.
- [2] M. Shao, Palladium-based electrocatalysts for hydrogen oxidation and oxygen reduction reactions, *Journal of Power Sources*, 196 (2011) 2433–2444.
- [3] S. Kondo, M. Nakamura, N. Maki, N. Hoshi, Active sites for the oxygen reduction reaction on the low and high index planes of palladium, *Journal of Physical Chemistry C*, 113 (2009) 12625–12628.
- [4] N.M. Markovic, T.J. Schmidt, V. Stamenkovic, P.N. Ross, Oxygen reduction reaction on Pt and Pt bimetallic surfaces: A selective review, *Fuel Cells*, 1 (2001) 105–116.
- [5] M.R. Tarasevich, A. Sadkowsky, E. Yeager, in: B.E. Conway, J.O'M. Bockris, E. Yeager, S.U.M. Khan, R.E. White (Eds.), *Comprehensive treatise of electrochemistry*. vol. 7, Plenum Press, New York, 1983, pp. 301–398.
- [6] R. Adzic, in: J. Lipkowsky, P.N. Ross (Eds.), *Electrocatalysis*, Wiley-VCH, New York, 1998, pp. 197–242.
- [7] J. Zhang, *PEM fuel cell electrocatalysts and catalyst layers: fundamentals and applications*, Springer, London, 2008.
- [8] J.K. Norskov, J. Rossmeisl, A. Logadottir, L. Lindqvist, J.R. Kitchin, T. Bligaard, H. Jonsson, Origin of the overpotential for oxygen reduction at a fuel-cell cathode, *Journal of Physical Chemistry B*, 108 (2004) 17886–17892.
- [9] L.M. Vracar, D.B. Sepa, A. Damjanovic, Palladium electrode in oxygen-saturated aqueous-solutions – reduction of oxygen in the activation-controlled region, *Journal of the Electrochemical Society*, 133 (1986) 1835–1839.
- [10] L.M. Vracar, D.B. Sepa, A. Damjanovic, Palladium electrode in oxygen-saturated aqueous-solutions – potential dependent adsorption of oxygen containing species and their effect on oxygen reduction, *Journal of the Electrochemical Society*, 136 (1989) 1973–1977.
- [11] I. Srejcic, Z. Rakocevic, M. Nenadovic, S. Strbac, Oxygen reduction on polycrystalline palladium in acid and alkaline solutions: topographical and chemical Pd surface changes, *Electrochimica Acta*, 169 (2015) 22–31.
- [12] R. Rahul, R.K. Singh, B. Bera, R. Devivaraprasad, M. Neergat, The role of surface oxygenated-species and adsorbed hydrogen in the oxygen reduction reaction (ORR) mechanism and product selectivity on Pd-based catalysts in acid media, *Physical Chemistry Chemical Physics*, 17 (2015) 15146–15155.
- [13] A. Hitotsuyanagi, S. Kondo, M. Nakamura, N. Hoshi, Structural effects on the oxygen reduction reaction on n(111)-(100) series of Pd, *Journal of Electroanalytical Chemistry*, 657 (2011) 123–127.
- [14] L.A. Kibler, M. Kleinert, R. Randler, D.M. Kolb, Initial stages of Pd deposition on Au(hkl) - Part I: Pd on Au(111), *Surface Science*, 443 (1999) 19–30.
- [15] L.A. Kibler, M. Kleinert, D.M. Kolb, Initial stages of Pd deposition on Au(hkl) part II: Pd on Au(100), *Surface Science*, 461 (2000) 155–167.
- [16] L.A. Kibler, M. Kleinert, V. Lazarescu, D.M. Kolb, Initial stages of palladium deposition on Au(h k l) Part III: Pd on Au(110), *Surface Science*, 498 (2002) 175–185.
- [17] A.H. Creus, Y. Gimeno, P. Diaz, L. Vazquez, S. Gonzalez, R.C. Salvarezza, A.J. Arvia, Influence of the nanostructure of palladium mesoparticles on the kinetics of

- molecular oxygen electroreduction, *Journal of Physical Chemistry B*, 108 (2004) 10785–10795.
- [18] S. Szunerits, R. Boukherroub, Investigation of the electrocatalytic activity of boron-doped diamond electrodes modified with palladium or gold nanoparticles for oxygen reduction reaction in basic medium, *Comptes Rendus Chimie*, 11 (2008) 1004–1009.
- [19] J.H. Shim, Y.S. Kim, M. Kang, C. Lee, Y. Lee, Electrocatalytic activity of nanoporous Pd and Pt: effect of structural features, *Physical Chemistry Chemical Physics*, 14 (2012) 3974–3979.
- [20] N.A. Al Abass, G. Denuault, D. Pletcher, The unexpected activity of Pd nanoparticles prepared using a non-ionic surfactant template, *Physical Chemistry Chemical Physics*, 16 (2014) 4892–4899.
- [21] G.F. Alvarez, M. Mamlouk, S.M.S. Kumar, K. Scott, Preparation and characterisation of carbon-supported palladium nanoparticles for oxygen reduction in low temperature PEM fuel cells, *Journal of Applied Electrochemistry*, 41 (2011) 925–937.
- [22] K. Jukk, N. Alexeyeva, C. Johans, K. Kontturi, K. Tammeveski, Oxygen reduction on Pd nanoparticle/multi-walled carbon nanotube composites, *Journal of Electroanalytical Chemistry*, 666 (2012) 67–75.
- [23] A. Sarapuu, A. Kasikov, N. Wong, C.A. Lucas, G. Sedghi, R.J. Nichols, K. Tammeveski, Electroreduction of oxygen on gold-supported nanostructured palladium films in acid solutions, *Electrochimica Acta*, 55 (2010) 6768–6774.
- [24] K. Jukk, N. Alexeyeva, P. Ritslaid, J. Kozlova, V. Sammelselg, K. Tammeveski, Electrochemical reduction of oxygen on heat-treated Pd nanoparticle/multi-walled carbon nanotube composites in alkaline solution, *Electrocatalysis*, 4 (2013) 42–48.
- [25] K. Jukk, N. Alexeyeva, A. Sarapuu, P. Ritslaid, J. Kozlova, V. Sammelselg, K. Tammeveski, Electroreduction of oxygen on sputter-deposited Pd nanolayers on multi-walled carbon nanotubes, *International Journal of Hydrogen Energy*, 38 (2013) 3614–3620.
- [26] Y.S. Li, T.S. Zhao, Ultra-low catalyst loading cathode electrode for anion-exchange membrane fuel cells, *International Journal of Hydrogen Energy*, 37 (2012) 15334–15338.
- [27] C. Shao, N. Lu, Z. Deng, DNA-assisted electroless deposition of highly dispersed palladium nanoparticles on glassy carbon surface: Preparation and electrocatalytic properties, *Journal of Electroanalytical Chemistry*, 629 (2009) 15–22.
- [28] I. Srejac, M. Smiljanic, B. Grgur, Z. Rakocevic, S. Strbac, Catalysis of oxygen reduction on Au modified by Pd nanoislands in perchloric acid solution, *Electrochimica Acta*, 64 (2012) 140–146.
- [29] J.J. Salvador-Pascual, S. Citalan-Cigarroa, O. Solorza-Feria, Kinetics of oxygen reduction reaction on nanosized Pd electrocatalyst in acid media, *Journal of Power Sources*, 172 (2007) 229–234.
- [30] L. Jiang, A. Hsu, D. Chu, R. Chen, Size-dependent activity of palladium nanoparticles for oxygen electroreduction in alkaline solutions, *Journal of the Electrochemical Society*, 156 (2009) B643-B649.
- [31] K.J.J. Mayrhofer, B.B. Blizanac, M. Arenz, V.R. Stamenkovic, P.N. Ross, N.M. Markovic, The impact of geometric and surface electronic properties of Pt-catalysts on the particle size effect in electrocatalysis, *Journal of Physical Chemistry B*, 109 (2005) 14433–14440.

- [32] A. Anastasopoulos, J.C. Davies, L. Hannah, B.E. Hayden, C.E. Lee, C. Milhano, C. Mormiche, L. Offin, The particle size dependence of the oxygen reduction reaction for carbon-supported platinum and palladium, *ChemSusChem*, 6 (2013) 1973–1982.
- [33] W. Ju, T. Bruelle, M. Favaro, L. Perini, C. Durante, O. Schneider, U. Stimming, Palladium nanoparticles supported on highly oriented pyrolytic graphite: Preparation, reactivity and stability, *ChemElectroChem*, 2 (2015) 547–558.
- [34] S.M.S. Kumar, J.S. Herrero, S. Irusta, K. Scott, The effect of pretreatment of Vulcan XC-72R carbon on morphology and electrochemical oxygen reduction kinetics of supported Pd nano-particle in acidic electrolyte, *Journal of Electroanalytical Chemistry*, 647 (2010) 211–221.
- [35] M.H. Seo, S.M. Choi, H.J. Kim, W.B. Kim, The graphene-supported Pd and Pt catalysts for highly active oxygen reduction reaction in an alkaline condition, *Electrochemistry Communications*, 13 (2011) 182–185.
- [36] R. Carrera-Cerritos, V. Baglio, A.S. Arico, J. Ledesma-Garcia, M.F. Sgroi, D. Pullini, A.J. Pruna, D.B. Mataix, R. Fuentes-Ramirez, L.G. Arriaga, Improved Pd electro-catalysis for oxygen reduction reaction in direct methanol fuel cell by reduced graphene oxide, *Applied Catalysis B-Environmental*, 144 (2014) 554–560.
- [37] K. Jukk, N. Kongi, L. Matisen, T. Kallio, K. Kontturi, K. Tammeveski, Electro-reduction of oxygen on palladium nanoparticles supported on nitrogen-doped graphene nanosheets, *Electrochimica Acta*, 137 (2014) 206–212.
- [38] D. Ye, R. Zhang, Y. Fu, J. Bu, Y. Wang, B. Liu, J. Kong, Co-calcination-derived Pd budded in N-doped ordered mesoporous graphitic carbon nanospheres for advanced methanol-tolerant oxygen reduction, *Electrochimica Acta*, 160 (2015) 306–312.
- [39] W. Ju, M. Favaro, C. Durante, L. Perini, S. Agnoli, O. Schneider, U. Stimming, G. Granozzi, Pd nanoparticles deposited on nitrogen-doped HOPG: New insights into the Pd-catalyzed oxygen reduction reaction, *Electrochimica Acta*, 141 (2014) 89–101.
- [40] C. Alegre, A. Stassi, E. Modica, C. Lo Vecchio, A.S. Arico, V. Baglio, Investigation of the activity and stability of Pd-based catalysts towards the oxygen reduction (ORR) and evolution reactions (OER) in iron-air batteries, *RSC Advances*, 5 (2015) 25424–25427.
- [41] G. Fu, X. Jiang, L. Tao, Y. Chen, J. Lin, Y. Zhou, Y. Tang, T. Lu, Polyallylamine functionalized palladium icosahedra: One-pot water-based synthesis and their superior electrocatalytic activity and ethanol tolerant ability in alkaline media, *Langmuir*, 29 (2013) 4413–4420.
- [42] Y. Shi, S. Yin, Y. Ma, D. Lu, Y. Chen, Y. Tang, T. Lu, Oleylamine-functionalized palladium nanoparticles with enhanced electrocatalytic activity for the oxygen reduction reaction, *Journal of Power Sources*, 246 (2014) 356–360.
- [43] L. Xiao, L. Zhuang, Y. Liu, J. Lu, H.D. Abruna, Activating Pd by morphology tailoring for oxygen reduction, *Journal of the American Chemical Society*, 131 (2009) 602–608.
- [44] Y. Cai, C. Ma, Y.M. Zhu, J.X. Wang, R.R. Adzic, Low-coordination sites in oxygen-reduction electrocatalysis: Their roles and methods for removal, *Langmuir*, 27 (2011) 8540–8547.
- [45] Y. Luo, J.M. Mora-Hernández, L.A. Estudillo-Wong, E.M. Arce-Estrada, N. Alonso-Vante, Nanostructured palladium tailored via carbonyl chemical route towards oxygen reduction reaction, *Electrochimica Acta*, 173 (2015) 771–778.

- [46] M. Shao, T. Yu, J.H. Odell, M. Jin, Y. Xia, Structural dependence of oxygen reduction reaction on palladium nanocrystals, *Chemical Communications*, 47 (2011) 6566–6568.
- [47] C.L. Lee, H.P. Chiou, C.R. Liu, Palladium nanocubes enclosed by (100) planes as electrocatalyst for alkaline oxygen electroreduction, *International Journal of Hydrogen Energy*, 37 (2012) 3993–3997.
- [48] C.-L. Lee, H.-P. Chiou, Methanol-tolerant Pd nanocubes for catalyzing oxygen reduction reaction in H₂SO₄ electrolyte, *Applied Catalysis B-Environmental*, 117 (2012) 204–211.
- [49] M.H. Shao, J. Odell, M. Humbert, T.Y. Yu, Y.N. Xia, Electrocatalysis on shape-controlled palladium nanocrystals: Oxygen reduction reaction and formic acid oxidation, *Journal of Physical Chemistry C*, 117 (2013) 4172–4180.
- [50] N. Arjona, M. Guerra-Balcazar, L. Ortiz-Frade, G. Osorio-Monreal, L. Alvarez-Contreras, J. Ledesma-Garcia, L.G. Arriaga, Electrocatalytic activity of well-defined and homogeneous cubic-shaped Pd nanoparticles, *Journal of Materials Chemistry A*, 1 (2013) 15524–15529.
- [51] L. Jiang, A. Hsu, D. Chu, R. Chen, Oxygen reduction reaction on carbon supported Pt and Pd in alkaline solutions, *Journal of the Electrochemical Society*, 156 (2009) B370-B376.
- [52] A. Zadick, L. Dubau, A. Zalineeova, C. Coutanceau, M. Chatenet, When cubic nanoparticles get spherical: An identical location transmission electron microscopy case study with Pd in alkaline media, *Electrochemistry Communications*, 48 (2014) 1–4.
- [53] R.R. Adzic, N.M. Markovic, V.B. Vesovic, Structural effects in electrocatalysis – oxygen reduction on the Au(100) single-crystal electrode, *Journal of Electroanalytical Chemistry*, 165 (1984) 105–120.
- [54] N.M. Markovic, R.R. Adzic, V.B. Vesovic, Structural effects in electrocatalysis – oxygen reduction on the gold single-crystal electrodes with (110) and (111) orientations, *Journal of Electroanalytical Chemistry*, 165 (1984) 121–133.
- [55] S. Strbac, R.R. Adzic, The influence of pH on reaction pathways for O₂ reduction on the Au(100) face, *Electrochimica Acta*, 41 (1996) 2903–2908.
- [56] R.R. Adzic, S. Strbac, N. Anastasijevic, Electrocatalysis of oxygen on single-crystal gold electrodes, *Materials Chemistry and Physics*, 22 (1989) 349–375.
- [57] S. Štrbac, R. Adzic, Oxygen reduction on single crystal gold electrodes in acid solutions, *Journal of the Serbian Chemical Society*, 57 (1992) 835–848.
- [58] M.H. Shao, R.R. Adzic, Spectroscopic identification of the reaction intermediates in oxygen reduction on gold in alkaline solutions, *Journal of Physical Chemistry B*, 109 (2005) 16563–16566.
- [59] J.W. Kim, A.A. Gewirth, Mechanism of oxygen electroreduction on gold surfaces in basic media, *Journal of Physical Chemistry B*, 110 (2006) 2565–2571.
- [60] V.M. Andoralov, M.R. Tarasevich, O.V. Tripachev, Oxygen reduction reaction on polycrystalline gold. Pathways of hydrogen peroxide transformation in the acidic medium, *Russian Journal of Electrochemistry*, 47 (2011) 1327–1336.
- [61] Y. Zhang, V. Suryanarayanan, I. Nakazawa, S. Yoshihara, T. Shirakashi, Electrochemical behavior of Au nanoparticle deposited on as-grown and O-terminated diamond electrodes for oxygen reduction in alkaline solution, *Electrochimica Acta*, 49 (2004) 5235–5240.
- [62] A. Kuzume, E. Herrero, J.M. Feliu, E. Ahlberg, R.J. Nichols, D.J. Schiffrin, Electrochemical reactivity in nanoscale domains: O₂ reduction on a fullerene

- modified gold surface, *Physical Chemistry Chemical Physics*, 7 (2005) 1293–1299.
- [63] M.S. El-Deab, T. Ohsaka, Quasi-reversible two-electron reduction of oxygen at gold electrodes modified with a self-assembled submonolayer of cysteine, *Electrochemistry Communications*, 5 (2003) 214–219.
- [64] S. Ben Aoun, Z. Dursun, T. Sotomura, I. Taniguchi, Effect of metal ad-layers on Au(111) electrodes on electrocatalytic reduction of oxygen in an alkaline solution, *Electrochemistry Communications*, 6 (2004) 747–752.
- [65] A. Sarapuu, K. Tammeveski, T.T. Tenno, V. Sammelselg, K. Kontturi, D.J. Schiffrin, Electrochemical reduction of oxygen on thin-film Au electrodes in acid solution, *Electrochemistry Communications*, 3 (2001) 446–450.
- [66] A. Sarapuu, M. Nurmik, H. Mändar, A. Rosental, T. Laaksonen, K. Kontturi, D.J. Schiffrin, K. Tammeveski, Electrochemical reduction of oxygen on nanostructured gold electrodes, *Journal of Electroanalytical Chemistry*, 612 (2008) 78–86.
- [67] I. Yagi, T. Ishida, K. Uosaki, Electrocatalytic reduction of oxygen to water at Au nanoclusters vacuum-evaporated on boron-doped diamond in acidic solution, *Electrochemistry Communications*, 6 (2004) 773–779.
- [68] M. Bron, Carbon black supported gold nanoparticles for oxygen electroreduction in acidic electrolyte solution, *Journal of Electroanalytical Chemistry*, 624 (2008) 64–68.
- [69] T. Inasaki, S. Kobayashi, Particle size effects of gold on the kinetics of the oxygen reduction at chemically prepared Au/C catalysts, *Electrochimica Acta*, 54 (2009) 4893–4897.
- [70] T. Bruelle, W. Ju, P. Niedermayr, A. Denisenko, O. Paschos, O. Schneider, U. Stimming, Size-dependent electrocatalytic activity of gold nanoparticles on HOPG and highly boron-doped diamond surfaces, *Molecules*, 16 (2011) 10059–10077.
- [71] M.J. Rodriguez-Vazquez, M.C. Blanco, R. Lourido, C. Vazquez-Vazquez, E. Pastor, G.A. Planes, J. Rivas, M. Arturo Lopez-Quintela, Synthesis of atomic gold clusters with strong electrocatalytic activities, *Langmuir*, 24 (2008) 12690–12694.
- [72] S. Guerin, B.E. Hayden, D. Pletcher, M.E. Rendall, J.-P. Suchsland, A combinatorial approach to the study of particle size effects on supported electrocatalysts: Oxygen reduction on gold, *Journal of Combinatorial Chemistry*, 8 (2006) 679–686.
- [73] J.S. Jirkovsky, M. Halasa, D.J. Schiffrin, Kinetics of electrocatalytic reduction of oxygen and hydrogen peroxide on dispersed gold nanoparticles, *Physical Chemistry Chemical Physics*, 12 (2010) 8042–8052.
- [74] W. Tang, H. Lin, A. Kleiman-Shwarsctein, G.D. Stucky, E.W. McFarland, Size-dependent activity of gold nanoparticles for oxygen electroreduction in alkaline electrolyte, *Journal of Physical Chemistry C*, 112 (2008) 10515–10519.
- [75] W. Chen, S. Chen, Oxygen electroreduction catalyzed by gold nanoclusters: Strong core size effects, *Angewandte Chemie-International Edition*, 48 (2009) 4386–4389.
- [76] G.-R. Zhang, B.-Q. Xu, Nano-size effect of Au catalyst for electrochemical reduction of oxygen in alkaline electrolyte, *Chinese Journal of Catalysis*, 34 (2013) 942–948.
- [77] C.R. Raj, A.I. Abdelrahman, T. Ohsaka, Gold nanoparticle-assisted electroreduction of oxygen, *Electrochemistry Communications*, 7 (2005) 888–893.

- [78] M.S. El-Deab, T. Sotomura, T. Ohsaka, Size and crystallographic orientation controls of gold nanoparticles electrodeposited on GC electrodes, *Journal of the Electrochemical Society*, 152 (2005) C1-C6.
- [79] M.S. El-Deab, T. Sotomura, T. Ohsaka, Oxygen reduction at electrochemically deposited crystallographically oriented Au(100)-like gold nanoparticles, *Electrochemistry Communications*, 7 (2005) 29–34.
- [80] F.F. Gao, M.S. El-Deab, T. Okajima, T. Ohsaka, Electrochemical preparation of a Au crystal with peculiar morphology and unique growth orientation and its catalysis for oxygen reduction, *Journal of the Electrochemical Society*, 152 (2005) A1226-A1232.
- [81] M.S. El-Deab, T. Sotomura, T. Ohsaka, Morphological selection of gold nanoparticles electrodeposited on various substrates, *Journal of the Electrochemical Society*, 152 (2005) C730-C737.
- [82] A.I. Abdelrahman, A.M. Mohammad, T. Okajima, T. Ohsaka, Fabrication and electrochemical application of three-dimensional gold nanoparticles: Self-assembly, *Journal of Physical Chemistry B*, 110 (2006) 2798–2803.
- [83] M.S. El-Deab, T. Okajima, T. Ohsaka, Fabrication of phase-separated multi-component self-assembled monolayers at gold nanoparticles electrodeposited on glassy carbon electrodes, *Journal of the Electrochemical Society*, 153 (2006) E201-E206.
- [84] M.S. El-Deab, T. Sotomura, T. Ohsaka, Oxygen reduction at Au nanoparticles electrodeposited on different carbon substrates, *Electrochimica Acta*, 52 (2006) 1792–1798.
- [85] J.H. Shim, J. Kim, C. Lee, Y. Lee, Electrocatalytic activity of gold and gold nanoparticles improved by electrochemical pretreatment, *Journal of Physical Chemistry C*, 115 (2011) 305–309.
- [86] W.S. Baker, J.J. Pietron, M.E. Teliska, P.J. Bouwman, D.E. Ramaker, K.E. Swider-Lyons, Enhanced oxygen reduction activity in acid by tin-oxide supported Au nanoparticle catalysts, *Journal of the Electrochemical Society*, 153 (2006) A1702-A1707.
- [87] D.S. Gatewood, D.E. Ramaker, K. Sasaki, K.E. Swider-Lyons, Support effects on water activation and oxygen reduction over Au-SnOx electrocatalysts observed with X-ray absorption spectroscopy, *Journal of the Electrochemical Society*, 155 (2008) B834-B842.
- [88] J.M. Macak, F. Schmidt-Stein, P. Schmuki, Efficient oxygen reduction on layers of ordered TiO2 nanotubes loaded with Au nanoparticles, *Electrochemistry Communications*, 9 (2007) 1783–1787.
- [89] D. Jasin, A. Abu-Rabi, S. Mentus, D. Jovanovic, Oxygen reduction reaction on spontaneously and potentiodynamically formed Au/TiO2 composite surfaces, *Electrochimica Acta*, 52 (2007) 4581–4588.
- [90] M.S. El-Deab, T. Ohsaka, Electrocatalysis by design: Effect of the loading level of Au nanoparticles-MnOx nanoparticles binary catalysts on the electrochemical reduction of molecular oxygen, *Electrochimica Acta*, 52 (2007) 2166–2174.
- [91] Y. Hu, J. Jin, P. Wu, H. Zhang, C. Cai, Graphene-gold nanostructure composites fabricated by electrodeposition and their electrocatalytic activity toward the oxygen reduction and glucose oxidation, *Electrochimica Acta*, 56 (2010) 491–500.
- [92] H. Yin, H. Tang, D. Wang, Y. Gao, Z. Tang, Facile synthesis of surfactant-free Au cluster/graphene hybrids for high-performance oxygen reduction reaction, *ACS Nano*, 6 (2012) 8288–8297.

- [93] N. Alexeyeva, T. Laaksonen, K. Kontturi, F. Mirkhalaf, D.J. Schiffrin, K. Tammeveski, Oxygen reduction on gold nanoparticle/multi-walled carbon nanotubes modified glassy carbon electrodes in acid solution, *Electrochemistry Communications*, 8 (2006) 1475–1480.
- [94] N. Alexeyeva, K. Tammeveski, Electroreduction of oxygen on gold nanoparticle/PDDA-MWCNT nanocomposites in acid solution, *Analytica Chimica Acta*, 618 (2008) 140–146.
- [95] N. Alexeyeva, J. Kozlova, V. Sammelseg, P. Ritslaid, H. Mändar, K. Tammeveski, Electrochemical and surface characterisation of gold nanoparticle decorated multi-walled carbon nanotubes, *Applied Surface Science*, 256 (2010) 3040–3046.
- [96] N. Alexeyeva, L. Matisen, A. Saar, P. Laaksonen, K. Kontturi, K. Tammeveski, Kinetics of oxygen reduction on gold nanoparticle/multi-walled carbon nanotube hybrid electrodes in acid media, *Journal of Electroanalytical Chemistry*, 642 (2010) 6–12.
- [97] J. Hernandez, J. Solla-Gullon, E. Herrero, Gold nanoparticles synthesized in a water-in-oil microemulsion: electrochemical characterization and effect of the surface structure on the oxygen reduction reaction, *Journal of Electroanalytical Chemistry*, 574 (2004) 185–196.
- [98] J. Hernandez, J. Solla-Gullon, E. Herrero, A. Aldaz, J.M. Feliu, Characterization of the surface structure of gold nanoparticles and nanorods using structure sensitive reactions, *Journal of Physical Chemistry B*, 109 (2005) 12651–12654.
- [99] J. Hernandez, J. Solla-Gullon, E. Herrero, A. Aldaz, J.M. Feliu, Electrochemistry of shape-controlled catalysts: Oxygen reduction reaction on cubic gold nanoparticles, *Journal of Physical Chemistry C*, 111 (2007) 14078–14083.
- [100] J. Hernandez, J. Solla-Gullon, E. Herrero, J.M. Feliu, A. Aldaz, In situ surface characterization and oxygen reduction reaction on shape-controlled gold nanoparticles, *Journal of Nanoscience and Nanotechnology*, 9 (2009) 2256–2273.
- [101] C.M. Sanchez-Sanchez, F.J. Vidal-Iglesias, J. Solla-Gullon, V. Montiel, A. Aldaz, J.M. Feliu, E. Herrero, Scanning electrochemical microscopy for studying electrocatalysis on shape-controlled gold nanoparticles and nanorods, *Electrochimica Acta*, 55 (2010) 8252–8257.
- [102] B.K. Jena, C.R. Raj, Shape-controlled synthesis of gold nanoprism and nanoperiwinkles with pronounced electrocatalytic activity, *Journal of Physical Chemistry C*, 111 (2007) 15146–15153.
- [103] H. Naohara, S. Ye, K. Uosaki, Electrocatalytic reactivity for oxygen reduction at epitaxially grown Pd thin layers of various thickness on Au(111) and Au(100), *Electrochimica Acta*, 45 (2000) 3305–3309.
- [104] T.J. Schmidt, V. Stamenkovic, M. Arenz, N.M. Markovic, P.N. Ross, Oxygen electrocatalysis in alkaline electrolyte: Pt(hkl), Au(hkl) and the effect of Pd-modification, *Electrochimica Acta*, 47 (2002) 3765–3776.
- [105] Z. Dursun, S. Ulubay, B. Gelmez, F.N. Ertas, Electrocatalytic reduction of oxygen on a Pd ad-layer modified Au(111) electrode in alkaline solution, *Catalysis Letters*, 132 (2009) 127–132.
- [106] S.R. Brankovic, J.X. Wang, R.R. Adzic, Metal monolayer deposition by replacement of metal adlayers on electrode surfaces, *Surface Science*, 474 (2001) L173–L179.
- [107] A. Kiani, E.N. Fard, Fabrication of palladium coated nanoporous gold film electrode via underpotential deposition and spontaneous metal replacement: A

- low palladium loading electrode with electrocatalytic activity, *Electrochimica Acta*, 54 (2009) 7254–7259.
- [108] M. Palomar-Pardave, E. Garfías-García, M. Romero-Romo, M.T. Ramirez-Silva, N. Batina, Influence of the substrate's surface structure on the mechanism and kinetics of the electrochemical UPD formation of a copper monolayer on gold, *Electrochimica Acta*, 56 (2011) 10083–10092.
- [109] J.S. Jirkovsky, I. Panas, E. Ahlberg, M. Halasa, S. Romani, D.J. Schiffrin, Single Atom Hot-Spots at Au-Pd Nanoalloys for Electrocatalytic H₂O₂ Production, *Journal of the American Chemical Society*, 133 (2011) 19432–19441.
- [110] A. Damjanovic, V. Brusić, Pretreatment of Pt-Au and Pd-Au alloy electrodes in the study of oxygen reduction, *Journal of Electroanalytical Chemistry and Interfacial Electrochemistry*, 15 (1967) 29–33.
- [111] M. Lukaszewski, A. Czerwinski, Electrochemical behavior of palladium-gold alloys, *Electrochimica Acta*, 48 (2003) 2435–2445.
- [112] J.S. Jirkovsky, I. Panas, S. Romani, E. Ahlberg, D.J. Schiffrin, Potential-dependent structural memory effects in Au-Pd nanoalloys, *Journal of Physical Chemistry Letters*, 3 (2012) 315–321.
- [113] C. Koenigsmann, E. Sutter, T.A. Chiesa, R.R. Adzic, S.S. Wong, Highly enhanced electrocatalytic oxygen reduction performance observed in bimetallic palladium-based nanowires prepared under ambient, surfactantless conditions, *Nano Letters*, 12 (2012) 2013–2020.
- [114] C. Koenigsmann, E. Sutter, R.R. Adzic, S.S. Wong, Size- and composition-dependent enhancement of electrocatalytic oxygen reduction performance in ultrathin palladium-gold (Pd_{1-x}Au_x) nanowires, *Journal of Physical Chemistry C*, 116 (2012) 15297–15306.
- [115] J.H. Shim, J. Kim, C. Lee, Y. Lee, Porous Pd layer-coated Au nanoparticles supported on carbon: Synthesis and electrocatalytic activity for oxygen reduction in acid media, *Chemistry of Materials*, 23 (2011) 4694–4700.
- [116] J. Son, S. Cho, C. Lee, Y. Lee, J.H. Shim, Spongelike nanoporous Pd and Pd/Au structures: Facile synthesis and enhanced electrocatalytic activity, *Langmuir*, 30 (2014) 3579–3588.
- [117] A. Cha, J.H. Shim, A. Jo, S.C. Lee, Y. Lee, C. Lee, Facile synthesis of AuPd nanochain networks on carbon supports and their application as electrocatalysts for oxygen reduction reaction, *Electroanalysis*, 26 (2014) 723–731.
- [118] J.-J. Lv, S.-S. Li, A.-J. Wang, L.-P. Mei, J.-R. Chen, J.-J. Feng, Monodisperse Au-Pd bimetallic alloyed nanoparticles supported on reduced graphene oxide with enhanced electrocatalytic activity towards oxygen reduction reaction, *Electrochimica Acta*, 136 (2014) 521–528.
- [119] W.X. Ji, C.W. Zhang, F. Li, P. Li, P.J. Wang, M.J. Ren, M. Yuan, First-principles study of small Pd-Au alloy clusters on graphene, *RSC Advances*, 4 (2014) 55781–55789.
- [120] U.A. Paulus, T.J. Schmidt, H.A. Gasteiger, R.J. Behm, Oxygen reduction on a high-surface area Pt/Vulcan carbon catalyst: a thin-film rotating ring-disk electrode study, *Journal of Electroanalytical Chemistry*, 495 (2001) 134–145.
- [121] W. Niu, Z.-Y. Li, L. Shi, X. Liu, H. Li, S. Han, J. Chen, G. Xu, Seed-mediated growth of nearly monodisperse palladium nanocubes with controllable sizes, *Crystal Growth & Design*, 8 (2008) 4440–4444.

- [122] M.C. Daniel, D. Astruc, Gold nanoparticles: Assembly, supramolecular chemistry, quantum-size-related properties, and applications toward biology, catalysis, and nanotechnology, *Chemical Reviews*, 104 (2004) 293–346.
- [123] B. Lim, M.J. Jiang, J. Tao, P.H.C. Camargo, Y.M. Zhu, Y.N. Xia, Shape-controlled synthesis of Pd nanocrystals in aqueous solutions, *Advanced Functional Materials*, 19 (2009) 189–200.
- [124] M.S. Jin, H.Y. Liu, H. Zhang, Z.X. Xie, J.Y. Liu, Y.N. Xia, Synthesis of Pd nanocrystals enclosed by {100} facets and with sizes < 10 nm for application in CO oxidation, *Nano Research*, 4 (2011) 83–91.
- [125] A. Zalineeva, S. Baranton, C. Coutanceau, G. Jerkiewicz, Electrochemical behavior of unsupported shaped palladium nanoparticles, *Langmuir*, 31 (2015) 1605–1609.
- [126] J. Perez-Juste, L.M. Liz-Marzan, S. Carnie, D.Y.C. Chan, P. Mulvaney, Electric-field-directed growth of gold nanorods in aqueous surfactant solutions, *Advanced Functional Materials*, 14 (2004) 571–579.
- [127] G. Frens, Controlled nucleation for the regulation of the particle size in monodisperse gold suspensions, *Nature Physical Science*, 241 (1973) 20–22.
- [128] D. Kim, J. Heo, M. Kim, Y.W. Lee, S.W. Han, Size-controlled synthesis of monodisperse gold nanooctahedrons and their surface-enhanced Raman scattering properties, *Chemical Physics Letters*, 468 (2009) 245–248.
- [129] J. Heo, D.-S. Kim, Z.H. Kim, Y.W. Lee, D. Kim, M. Kim, K. Kwon, H.J. Park, W.S. Yun, S.W. Han, Controlled synthesis and characterization of the enhanced local field of octahedral Au nanocrystals, *Chemical Communications*, (2008) 6120–6122.
- [130] T.K. Sau, C.J. Murphy, Room temperature, high-yield synthesis of multiple shapes of gold nanoparticles in aqueous solution, *Journal of the American Chemical Society*, 126 (2004) 8648–8649.
- [131] J. Solla-Gullon, V. Montiel, A. Aldaz, J. Clavilier, Electrochemical characterisation of platinum nanoparticles prepared by microemulsion: how to clean them without loss of crystalline surface structure, *Journal of Electroanalytical Chemistry*, 491 (2000) 69–77.
- [132] A. Sarapuu, A. Kasikov, T. Laaksonen, K. Kontturi, K. Tammeveski, Electrochemical reduction of oxygen on thin-film Pt electrodes in acid solutions, *Electrochimica Acta*, 53 (2008) 5873–5880.
- [133] K. Tammeveski, T. Tenno, J. Claret, C. Ferrater, Electrochemical reduction of oxygen on thin-film Pt electrodes in 0.1 M KOH, *Electrochimica Acta*, 42 (1997) 893–897.
- [134] B.E. Hayden, D. Pletcher, J.-P. Suchsland, L.J. Williams, The influence of support and particle size on the platinum catalysed oxygen reduction reaction, *Physical Chemistry Chemical Physics*, 11 (2009) 9141–9148.
- [135] S. Mukerjee, J. McBreen, Effect of particle size on the electrocatalysis by carbon-supported Pt electrocatalysts: an in situ XAS investigation, *Journal of Electroanalytical Chemistry*, 448 (1998) 163–171.
- [136] N. Hoshi, M. Nakamura, N. Maki, S. Yamaguchi, A. Kitajima, Structural effects on voltammograms of the low index planes of palladium and Pd(S)- n(100) x (111) surfaces in alkaline solution, *Journal of Electroanalytical Chemistry*, 624 (2008) 134–138.

- [137] M. Grden, M. Lukaszewski, G. Jerkiewicz, A. Czerwinski, Electrochemical behaviour of palladium electrode: Oxidation, electrodisolution and ionic adsorption, *Electrochimica Acta*, 53 (2008) 7583–7598.
- [138] D.R. Lawson, L.D. Whiteley, C.R. Martin, M.N. Szentirmay, J.I. Song, Oxygen reduction at Nafion film-coated platinum electrodes: Transport and kinetics, *Journal of the Electrochemical Society*, 135 (1988) 2247–2253.
- [139] S.K. Zecevic, J.S. Wainright, M.H. Litt, S.L. Gojkovic, R.F. Savinell, Kinetics of O₂ reduction on a Pt electrode covered with a thin film of solid polymer electrolyte, *Journal of the Electrochemical Society*, 144 (1997) 2973–2982.
- [140] R.E. Davis, G.L. Horvath, C.W. Tobias, The solubility and diffusion coefficient of oxygen in potassium hydroxide solutions, *Electrochimica Acta*, 12 (1967) 287–297.
- [141] D.R. Lide (Ed.), *CRC handbook of chemistry and physics*, CRC Press, Boca Raton, 2001.
- [142] K. Tammeveski, K. Kontturi, R.J. Nichols, R.J. Potter, D.J. Schiffrin, Surface redox catalysis for O₂ reduction on quinone-modified glassy carbon electrodes, *Journal of Electroanalytical Chemistry*, 515 (2001) 101–112.
- [143] Y.F. Yang, Y.H. Zhou, C.S. Cha, Electrochemical reduction of oxygen on small palladium particles supported on carbon in alkaline solution, *Electrochimica Acta*, 40 (1995) 2579–2586.
- [144] J. Perez, E.R. Gonzalez, E.A. Ticianelli, Oxygen electrocatalysis on thin porous coating rotating platinum electrodes, *Electrochimica Acta*, 44 (1998) 1329–1339.
- [145] L. Genies, R. Faure, R. Durand, Electrochemical reduction of oxygen on platinum nanoparticles in alkaline media, *Electrochimica Acta*, 44 (1998) 1317–1327.
- [146] D.B. Sepa, M.V. Vojnovic, A. Damjanovic, Kinetics and mechanism of O₂ reduction at Pt in alkaline solutions, *Electrochimica Acta*, 25 (1980) 1491–1496.
- [147] D.B. Sepa, M.V. Vojnovic, L.M. Vracar, A. Damjanovic, Different views regarding the kinetics and mechanisms of oxygen reduction at Pt and Pd electrodes, *Electrochimica Acta*, 32 (1987) 129–134.
- [148] M.R. Tarasevich, Investigation of the parallel and consecutive steps in the reactions of oxygen and hydrogen peroxide IX. The mechanism of oxygen electroreduction on the platinum metals, *Elektrokhimiya*, 9 (1973) 599–605.
- [149] J.X. Wang, N.M. Markovic, R.R. Adzic, Kinetic analysis of oxygen reduction on Pt(111) in acid solutions: Intrinsic kinetic parameters and anion adsorption effects, *Journal of Physical Chemistry B*, 108 (2004) 4127–4133.
- [150] K.L. Hsueh, E.R. Gonzalez, S. Srinivasan, Electrolyte effects on oxygen reduction kinetics at platinum: A rotating ring-disc electrode analysis, *Electrochimica Acta*, 28 (1983) 691–697.
- [151] N.M. Markovic, H.A. Gasteiger, P.N. Ross, Oxygen reduction on platinum low-index single-crystal surfaces in sulfuric acid solution: Rotating ring-Pt(hkl) disk studies, *Journal of Physical Chemistry*, 99 (1995) 3411–3415.
- [152] M.H. Shao, T. Huang, P. Liu, J. Zhang, K. Sasaki, M.B. Vukmirovic, R.R. Adzic, Palladium monolayer and palladium alloy electrocatalysts for oxygen reduction, *Langmuir*, 22 (2006) 10409–10415.
- [153] H. Yano, E. Higuchi, H. Uchida, M. Watanabe, Temperature dependence of oxygen reduction activity at Nafion-coated bulk Pt and Pt/carbon black catalysts, *Journal of Physical Chemistry B*, 110 (2006) 16544–16549.

- [154] K. Kinoshita, Particle size effects for oxygen reduction on highly dispersed platinum in acid electrolytes, *Journal of the Electrochemical Society*, 137 (1990) 845–848.
- [155] N. Markovic, H. Gasteiger, P.N. Ross, Kinetics of oxygen reduction on Pt(hkl) electrodes: Implications for the crystallite size effect with supported Pt electrocatalysts, *Journal of the Electrochemical Society*, 144 (1997) 1591–1597.
- [156] S. Bliznakov, M. Vukmirovic, E. Sutter, R. Adzic, Electrodeposition of Pd nanowires and nanorods on carbon nanoparticles, *Macedonian Journal of Chemistry and Chemical Engineering*, 30 (2011) 19–27.
- [157] H. Duncan, A. Lasia, Separation of hydrogen adsorption and absorption on Pd thin films, *Electrochimica Acta*, 53 (2008) 6845–6850.
- [158] M.H. Martin, A. Lasia, Study of the hydrogen absorption in Pd in alkaline solution, *Electrochimica Acta*, 53 (2008) 6317–6322.
- [159] L.C. Nagle, S. Garbarino, L.D. Burke, Active site and electrocatalytic behaviour at palladium electrode surfaces, *ECS Transactions*, 25 (2010) 3–12.
- [160] F. Maroun, F. Ozanam, O.M. Magnussen, R.J. Behm, The role of atomic ensembles in the reactivity of bimetallic electrocatalysts, *Science*, 293 (2001) 1811–1814.
- [161] V. Climent, N.M. Markovic, P.N. Ross, Kinetics of oxygen reduction on an epitaxial film of palladium on Pt(111), *Journal of Physical Chemistry B*, 104 (2000) 3116–3120.
- [162] A.J. Bard, L.R. Faulkner, *Electrochemical Methods*, 2nd ed., Wiley, New York, 2001.
- [163] R.R. Adzic, J. Wang, B.M. Ocko, Structure of metal adlayers during the course of electrocatalytic reactions: O₂ reduction on Au(111) with Tl adlayers in acid solutions, *Electrochimica Acta*, 40 (1995) 83–89.
- [164] N. Alexeyeva, K. Tammeveski, Electrochemical reduction of oxygen on multiwalled carbon nanotube modified glassy carbon electrodes in acid media, *Electrochemical and Solid-State Letters*, 10 (2007) F18-F21.
- [165] D. Cao, L. Sun, G. Wang, Y. Lv, M. Zhang, Kinetics of hydrogen peroxide electroreduction on Pd nanoparticles in acidic medium, *Journal of Electroanalytical Chemistry*, 621 (2008) 31–37.
- [166] A. Sarapuu, K. Vaik, D.J. Schiffrin, K. Tammeveski, Electrochemical reduction of oxygen on anthraquinone-modified glassy carbon electrodes in alkaline solution, *Journal of Electroanalytical Chemistry*, 541 (2003) 23–29.
- [167] J.S. Spendelow, A. Wieckowski, Electrocatalysis of oxygen reduction and small alcohol oxidation in alkaline media, *Physical Chemistry Chemical Physics*, 9 (2007) 2654–2675.
- [168] J.B. Xu, T.S. Zhao, Y.S. Li, W.W. Yang, Synthesis and characterization of the Au-modified Pd cathode catalyst for alkaline direct ethanol fuel cells, *International Journal of Hydrogen Energy*, 35 (2010) 9693–9700.
- [169] K. Sasaki, H. Naohara, Y.M. Choi, Y. Cai, W.F. Chen, P. Liu, R.R. Adzic, Highly stable Pt monolayer on PdAu nanoparticle electrocatalysts for the oxygen reduction reaction, *Nature Communications*, 3 (2012) 9.
- [170] M.H. Shao, K. Sasaki, P. Liu, R.R. Adzic, Pd₃Fe and Pt monolayer-modified Pd₃Fe electrocatalysts for oxygen reduction, *Zeitschrift Fur Physikalische Chemie-International Journal of Research in Physical Chemistry & Chemical Physics*, 221 (2007) 1175–1190.

- [171] N.M. Markovic, H.A. Gasteiger, P.N. Ross, Oxygen reduction on platinum low-index single-crystal surfaces in alkaline solution: Rotating ring disk(Pt(hkl)) studies, *Journal of Physical Chemistry*, 100 (1996) 6715–6721.
- [172] T.C. Nagaiah, D. Schaefer, W. Schuhmann, N. Dimcheva, Electrochemically deposited Pd-Pt and Pd-Au codeposits on graphite electrodes for electrocatalytic H₂O₂ reduction, *Analytical Chemistry*, 85 (2013) 7897–7903.
- [173] M. Kang, Y. Yang, J.H. Shim, S.C. Lee, Y. Lee, C. Lee, Simple electrodeposition of dendritic Pd without supporting electrolyte and its electrocatalytic activity toward oxygen reduction and H₂O₂ sensing, *Electroanalysis*, 25 (2013) 2691–2699.
- [174] W. Niu, L. Zhang, G. Xu, Shape-controlled synthesis of single-crystalline palladium nanocrystals, *ACS Nano*, 4 (2010) 1987–1996.
- [175] L. Zhang, W. Niu, G. Xu, Seed-mediated growth of palladium nanocrystals: The effect of pseudo-halide thiocyanate ions, *Nanoscale*, 3 (2011) 678–682.
- [176] F.-R. Fan, A. Attia, U.K. Sur, J.-B. Chen, Z.-X. Xie, J.-F. Li, B. Ren, Z.-Q. Tian, An effective strategy for room-temperature synthesis of single-crystalline palladium nanocubes and nanodendrites in aqueous solution, *Crystal Growth & Design*, 9 (2009) 2335–2340.
- [177] Y. Yu, Y. Zhao, T. Huang, H. Liu, Microwave-assisted synthesis of palladium nanocubes and nanobars, *Materials Research Bulletin*, 45 (2010) 159–164.
- [178] N. Hoshi, K. Kagaya, Y. Hori, Voltammograms of the single-crystal electrodes of palladium in aqueous sulfuric acid electrolyte: Pd(S)- n(111) x (111) and Pd(S)- n(100) x (111), *Journal of Electroanalytical Chemistry*, 485 (2000) 55–60.
- [179] N. Hoshi, M. Kuroda, Y. Hori, Voltammograms of stepped and kinked stepped surfaces of palladium: Pd(S)- n(111) x (100) and Pd(S)- n(100) x (110), *Journal of Electroanalytical Chemistry*, 521 (2002) 155–160.
- [180] R. Woods, in: A.J. Bard (Ed.), *Electroanalytical chemistry a series of advances*. Vol. 9, Marcel Dekker, New York, 1976.
- [181] M.D. Macia, J.M. Campina, E. Herrero, J.M. Feliu, On the kinetics of oxygen reduction on platinum stepped surfaces in acidic media, *Journal of Electroanalytical Chemistry*, 564 (2004) 141–150.
- [182] A. Kuzume, E. Herrero, J.M. Feliu, Oxygen reduction on stepped platinum surfaces in acidic media, *Journal of Electroanalytical Chemistry*, 599 (2007) 333–343.
- [183] N. Hoshi, M. Kuroda, O. Koga, Y. Hori, Infrared reflection absorption spectroscopy of the sulfuric acid anion on low and high index planes of palladium, *Journal of Physical Chemistry B*, 106 (2002) 9107–9113.
- [184] C. Wang, H. Daimon, Y. Lee, J. Kim, S. Sun, Synthesis of monodisperse Pt nanocubes and their enhanced catalysis for oxygen reduction, *Journal of the American Chemical Society*, 129 (2007) 6974–6975.
- [185] N. Alexeyeva, A. Sarapuu, K. Tammeveski, F.J. Vidal-Iglesias, J. Solla-Gullon, J.M. Feliu, Electroreduction of oxygen on Vulcan carbon supported Pd nanoparticles and Pd-M nanoalloys in acid and alkaline solutions, *Electrochimica Acta*, 56 (2011) 6702–6708.
- [186] N. Naresh, F.G.S. Wasim, B.P. Ladewig, M. Neergat, Removal of surfactant and capping agent from Pd nanocubes (Pd-NCs) using tert-butylamine: its effect on electrochemical characteristics, *Journal of Materials Chemistry A*, 1 (2013) 8553–8559.

- [187] M. Goral-Kurbiel, A. Drelinkiewicz, R. Kosydar, J. Gurgul, B. Dembinska, P.J. Kulesza, The effect of Nafion ionomer on electroactivity of palladium-polypyrrole catalysts for oxygen reduction reaction, *Journal of Solid State Electrochemistry*, 18 (2014) 639–653.
- [188] H. Angerstein-Kozłowska, in: E. Yeager, J.O'M. Bockris, B.E. Conway, S. Sarangapani (Eds.) *Comprehensive treatise of electrochemistry*, vol. 9, Plenum Press, New York, 1984, pp. 15–61.
- [189] R.W. Zurilla, R.K. Sen, E. Yeager, The kinetics of the oxygen reduction reaction on gold in alkaline solution, *Journal of The Electrochemical Society*, 125 (1978) 1103–1109.
- [190] N. Tian, Z.-Y. Zhou, S.-G. Sun, Platinum metal catalysts of high-index surfaces: From single-crystal planes to electrochemically shape-controlled nanoparticles, *Journal of Physical Chemistry C*, 112 (2008) 19801–19817.
- [191] Z.-Y. Zhou, N. Tian, Z.-Z. Huang, D.-J. Chen, S.-G. Sun, Nanoparticle catalysts with high energy surfaces and enhanced activity synthesized by electrochemical method, *Faraday Discussions*, 140 (2009) 81–92.
- [192] J. Solla-Gullon, F.J. Vidal-Iglesias, J.M. Feliu, Shape dependent electrocatalysis, *Annual Reports Section "C" (Physical Chemistry)*, 107 (2011) 263–297.
- [193] P. Rodriguez, J.M. Feliu, M.T.M. Koper, Unusual adsorption state of carbon monoxide on single-crystalline gold electrodes in alkaline media, *Electrochemistry Communications*, 11 (2009) 1105–1108.
- [194] P. Rodriguez, N. Garcia-Araez, A. Koverga, S. Frank, M.T.M. Koper, CO electrooxidation on gold in alkaline media: A combined electrochemical, spectroscopic, and DFT study, *Langmuir*, 26 (2010) 12425–12432.
- [195] D. Geng, G. Lu, Size effect of gold nanoparticles on the electrocatalytic oxidation of carbon monoxide in alkaline solution, *Journal of Nanoparticle Research*, 9 (2007) 1145–1151.
- [196] G. Vazquez-Huerta, G. Ramos-Sanchez, A. Rodriguez-Castellanos, D. Meza-Calderon, R. Antano-Lopez, O. Solorza-Feria, Electrochemical analysis of the kinetics and mechanism of the oxygen reduction reaction on Au nanoparticles, *Journal of Electroanalytical Chemistry*, 645 (2010) 35–40.
- [197] K.R. Ward, M. Gara, N.S. Lawrence, R.S. Hartshorne, R.G. Compton, Nanoparticle modified electrodes can show an apparent increase in electrode kinetics due solely to altered surface geometry: The effective electrochemical rate constant for non-flat and non-uniform electrode surfaces, *Journal of Electroanalytical Chemistry*, 695 (2013) 1–9.

9. SUMMARY IN ESTONIAN

Hapniku elektrokeemiline redutseerumine nanostruktuursetel pallaadium- ja kuldkatalüsaatoritel

Doktoritöö eesmärk oli uurida hapniku elektrokeemilist redutseerumist pallaadiumil ja kullal põhinevatel nanostruktuursetel metallkatalüsaatoritel, milleks olid vaakumaurustamise teel valmistatud õhukesed pallaadiumkiled [I], elektrokeemiliselt sadestatud pallaadiumkatted [II, III], elektrokeemiliselt sadestatud PdAu sulamid [IV], Pd nanokuubid [V, VI, VII], kommertsiaalsed Au/C katalüsaatorid [VIII] ja suurepinnalisele süsinikule kantud erikujulised Au nanoosakesed [IX]. Elektrokeemilised mõõtmised viidi läbi nii väävelhappe kui ka kaaliumhüdroksiidi lahuses, kasutades pöörleva ketaselektroodi meetodit.

Töö esimeses osas uuriti hapniku redutseerumist õhukestel pallaadiumkiledel nominaalse paksusega 0,25–10 nm. Läbistuselektronmikroskoopia abil tuvastati, et kiled kasvavad saarekestena, mis kile paksenedes liituvad ja katavad kogu alusmaterjali pinna. Leeliselises lahuses uuritud elektroodide eriaktiivsus ei sõltunud kile paksusest, kuid happelises lahuses kasvas see kile paksuse suurenedes. Saadud andmeid analüüsiti kasutades Koutecky-Levichi võrrandit, mille abil leiti üleminevate elektronide arv hapniku molekuli kohta (n). Leeliselises lahuses õhematel kiledel oli see 3,5–3,7, kuid paksematel oli n ligikaudu 4; happes jäi see suurus 3,6 ja 3,9 vahele. Tafeli analüüs näitas, et kiirust limiteerivaks staadiumiks on esimese elektroni aeglane ülekanne hapniku molekulile.

Töö teises osas kasutati elektrokeemilist sadestamist Pd-katete valmistamiseks. Skaneeriva elektronmikroskoobi abil uuriti klaassüsinikule sadestatud pallaadiumkatteid ja leiti, et väiksemate osakeste suurus on 3–10 nm, kuid mõnede osakeste suurus küündis ka 100 nm-ni. Sadestusaja pikenedes osakeste arv ja nende mõõtmed suurenesid. Kuldalusele sadestatud Pd osakesed olid pigem ühtlaste mõõtmetega (ligi 20 nm) ja nende suurus ei sõltunud sadestusajast. Hapniku redutseerumisel happelises lahuses oli Pd katete eriaktiivsus kompaktsel pallaadiumiga võrreldav, välja arvatud kuldalusele sadestatud kõige paksema katte puhul, mille eriaktiivsus oli ligikaudu kaks korda suurem kui teistel uuritud katetel. Leeliselises lahuses olid klaassüsinikule sadestatud Pd katete eriaktiivsused mõnevõrra väiksemad kui kompaktsel pallaadiumil, kuid kuldalusel olid kõik elektrosadestatud katetega elektroodid kompaktselt pallaadiumielektroodist aktiivsemad. Suurem eriaktiivsus kuldalusele sadestatud katetel tuleneb sulami moodustumisest, mida uuriti töö järgmises osas.

Seejärel sadestati Pd ja Au üheskoos, varieerides metallide lähteainete sisaldust sadestuslahuses. Saadud osakesed olid läbimõõduga 6 ± 2 nm, kuid võis ka täheldada suuremate aglomeraatide moodustumist. Röntgenfotoelektron-spektroskoopia ja tsükliline voltamperomeetria näitasid sulami moodustumist. Uuritud PdAu sulamite elektrokatalüütiline aktiivsus happelises lahuses oli väiksem kui puhtal pallaadiumil. Seevastu leeliselises keskkonnas saavutati

3–5 korda suuremad eriaktiivsuse väärtused kui puhtal pallaadiumil, mis tuleneb ilmselt sulami moodustumisega kaasnevatest efektidest.

Töö järgmises osas uuriti hapniku elektrokeemilist redutseerumist kuubikujulistel Pd nanoosakestel mõõtmega $26,9 \pm 3,9$ nm ja võrreldi saadud tulemusi sfääriliste osakeste ($2,8 \pm 0,4$ nm) vastavate andmetega. Uuritud nanoosakeste eelistatud struktuur tehti kindlaks röntgendifraktsioonanalüüsiga. Selgus, et sfäärilistel osakestel ei ole eelistatud orientatsiooni, kuid kuubikujulistel osakestel on pinnal ülekaalus Pd(100) tahk, mida kinnitasid ka tsüklilise voltamperomeetria andmed. Hapniku redutseerumisel oli kuubikujulistel Pd nanoosakestel kõige suurem eriaktiivsus, mis ületas sfääriliste osakeste eriaktiivsuse happelises lahuses ligi kolm korda ja leeliselises keskkonnas ligi neli korda. Pallaadiumi nanokuupide suurem aktiivsus tulenebki nende eelistatud kristallograafilisest orientatsioonist.

Järgmisena uuriti kommertsiaalse päritoluga erineva kullasisaldusega Au/C katalüsaatoreid. Uuritud katalüsaatorid erinesid peale kullasisalduse ka osakeste suuruse poolest. Elektrokeemilistest mõõtmistest selgus, et eriaktiivsus ei sõltu katalüsaatorikihi paksusest vahemikus $1,5\text{--}10$ μm , mis näitab, et hapniku difusioon läbi katalüsaatorikihi on piisavalt efektiivne ega limiteeri hapniku redutseerumisprotsessi.

Töö viimases osas uuriti hapniku elektrokeemilist redutseerumist süsinikandjale kantud erikujulistel Au nanoosakestel. Uuriti kahes mõõdus Au sfäärilisi osakesi, Au oktaeedreid ning Au kuupe. Nagu Pd nanokuupidel, oli ka kulla nanokuupidel peamine pinnal esinev tahk (100), mis on kõige aktiivsem kulla monokristalli tahk hapniku redutseerumisel. Hapniku redutseerumise uurinutest selgus, et kulla nanokuupide eriaktiivsus väävelhappe lahuses on üle kahe korra kõrgem kui kompaktsel kullal ning sfäärilistel ja oktaeedrilistel Au nanoosakestel. Kaaliumhüdroksiidi lahuses olid erinevused väiksemad, kuid kulla nanokuupide eriaktiivsus oli ka tolles lahuses suurim. Massaktiivsus oli mõlemas uuritud lahuses ootuspäraselt suurim ~ 5 nm sfääridel.

Kokku võttes võib öelda, et hapniku redutseerumine pallaadiumil põhinevatel materjalidel kulgeb peamiselt neljaelektronilise protsessina vee moodustumiseni ning kullal põhinevatel katalüsaatoritel on peamiseks saaduseks vesinikperoksiid. Tafeli analüüs näitas, et madalatel volutihedustel on hapniku redutseerumisreaktsiooni mehhanism nii happelises kui ka leeliselises lahuses sama, mis vastavatel kompaktsel metallektroodidel ning reaktsiooni limiteerivaks staadiumiks on esimese elektroni aeglane ülekande hapniku molekulile.

10. ACKNOWLEDGEMENTS

First I would like to thank my supervisors Dr. Ave Sarapuu and Assoc. Prof. Kaido Tammeveski for their continuous support, advices, patience and investment of time to guide me throughout my academic studies.

I would like to thank the staff at the Institute of Physics, Dr. Aarne Kasikov for preparation of thin Pd films, Prof. Väino Sammelselg and his co-workers Jekaterina Kozlova for SEM and EDX measurements, Dr. Margus Marandi for AFM studies, Dr. Leonard Matisen for XPS measurements. Also Dr. Christoffer Johans and Prof. Kyösti Kontturi from Aalto University and Dr. Robert J. Potter from Johnson Matthey Technology Centre are greatly acknowledged for their contribution.

I am truly grateful to Dr. Jose Solla-Gullón and Prof. Juan M. Feliu for the preparation of shape-controlled Pd and Au nanoparticles and also for the knowledge acquired from my stay at the University of Alicante, Spain.

I would also like to thank my colleagues, and former colleagues from the Institute of Chemistry. Special gratitude goes to Dr. Nadezda Kongi, Dr. Ivar Kruusenberg, Dr. Elo Kibena, Kristel Jukk, Madis Liik, Eve Toomsalu and Jaan Saame.

This work has been supported by Estonian Research Council (Grant Nos. 7546, 8380 and 9323), CRDF-ETF grant (Project No. ESC2-2975-TR-09), institutional research funding of the Estonian Ministry of Education and Research (IUT20-16 and IUT02-24), Archimedes Foundation (project no. 3.2.0501.10-0015), European Union Framework VI programme, NENA project Contract No. NMP3-CT-2004-505906 and graduate school “Functional materials and technologies” receiving funding from the European Social Fund under project 1.2.0401.09-0079 in University of Tartu, Estonia.

Most importantly I am grateful to my parents and grandparents for their support.

II. PUBLICATIONS

CURRICULUM VITAE

Name: Heiki Erikson
Born: October 12, 1986
Citizenship: Estonian
Address: Ravila 14a, 50411 Tartu, Eesti
Phone: +372 737 5277
E-mail: heiki.erikson@ut.ee

Education:

2011– University of Tartu, Faculty of Science and Technology, PhD student
2009–2011 University of Tartu, Faculty of Science and Technology, MSc (chemistry) 2011
2006–2009 University of Tartu, Faculty of Science and Technology, BSc (chemistry) 2009

Professional employment:

2010 University of Tartu, Institute of Chemistry, chemist (0.5)

Major scientific publications:

1. H. Erikson, G. Jürmann, A. Sarapuu, R. J. Potter, K. Tammeveski, Electroreduction of oxygen on carbon-supported gold catalysts, *Electrochimica Acta* 54 (2009) 7483–7489.
2. H. Erikson, A. Kasikov, C. Johans, K. Kontturi, K. Tammeveski, A. Sarapuu, Oxygen reduction on Nafion-coated thin-film palladium electrodes, *Journal of Electroanalytical Chemistry* 652 (2011) 1–7.
3. H. Erikson, A. Sarapuu, K. Tammeveski, J. Solla-Gullón, J. M. Feliu, Enhanced electrocatalytic activity of cubic Pd nanoparticles towards the oxygen reduction reaction in acid media, *Electrochemistry Communications* 13 (2011) 734–737.
4. H. Erikson, A. Sarapuu, N. Alexeyeva, K. Tammeveski, J. Solla-Gullón, J. M. Feliu, Electrochemical reduction of oxygen on palladium nanocubes in acid and alkaline solutions, *Electrochimica Acta* 59 (2012) 329–335.
5. L. Tammeveski, H. Erikson, A. Sarapuu, J. Kozlova, P. Ritslaid, V. Sammelseg, K. Tammeveski, Electrocatalytic oxygen reduction on silver nanoparticle/multi-walled carbon nanotube modified glassy carbon electrodes in alkaline solution, *Electrochemistry Communications* 20 (2012) 15–18.
6. H. Erikson, M. Liik, A. Sarapuu, J. Kozlova, V. Sammelseg, K. Tammeveski, Oxygen reduction on electrodeposited Pd coatings on glassy carbon, *Electrochimica Acta* 88 (2013) 513–518.
7. H. Erikson, M. Liik, A. Sarapuu, M. Marandi, V. Sammelseg, K. Tammeveski, Electrocatalysis of oxygen reduction on electrodeposited Pd coatings on gold, *Journal of Electroanalytical Chemistry* 691 (2013) 35–41.

8. H. Erikson, A. Sarapuu, K. Tammeveski, J. Solla-Gullón, J. M. Feliu, Shape-dependent electrocatalysis: oxygen reduction on carbon-supported gold nanoparticles, *ChemElectroChem* 1 (2014) 1338–1347.
9. H. Erikson, A. Sarapuu, J. Kozlova, L. Matisen, V. Sammelselg, K. Tammeveski, Oxygen electroreduction on electrodeposited PdAu nanoalloys, *Electrocatalysis* 6 (2015) 77–85.

ELULOOKIRJELDUS

Nimi: Heiki Erikson
Sünniaeg: 12. oktoober, 1986
Kodakondsus: Eesti
Aadress: Ravila 14a, 50411 Tartu, Eesti
Telefon: +372 737 5277
E-post: heiki.erikson@ut.ee

Haridus:

2011– Tartu Ülikool, Loodus- ja tehnoloogiateaduskond, doktori-õppe üliõpilane
2009–2011 Tartu Ülikool, Loodus- ja tehnoloogiateaduskond, MSc (keemia) 2011
2006–2009 Tartu Ülikool, Loodus- ja tehnoloogiateaduskond, BSc (keemia) 2009

Teenistuskäik:

2010– Tartu Ülikool, Keemia instituut, keemik (0,5)

Olulisemad publikatsioonid:

1. H. Erikson, G. Jürmann, A. Sarapuu, R. J. Potter, K. Tammeveski, Electro-reduction of oxygen on carbon-supported gold catalysts, *Electrochimica Acta* 54 (2009) 7483–7489.
2. H. Erikson, A. Kasikov, C. Johans, K. Kontturi, K. Tammeveski, A. Sarapuu, Oxygen reduction on Nafion-coated thin-film palladium electrodes, *Journal of Electroanalytical Chemistry* 652 (2011) 1–7.
3. H. Erikson, A. Sarapuu, K. Tammeveski, J. Solla-Gullón, J. M. Feliu, Enhanced electrocatalytic activity of cubic Pd nanoparticles towards the oxygen reduction reaction in acid media, *Electrochemistry Communications* 13 (2011) 734–737.
4. H. Erikson, A. Sarapuu, N. Alexeyeva, K. Tammeveski, J. Solla-Gullón, J. M. Feliu, Electrochemical reduction of oxygen on palladium nanocubes in acid and alkaline solutions, *Electrochimica Acta* 59 (2012) 329–335.
5. L. Tammeveski, H. Erikson, A. Sarapuu, J. Kozlova, P. Ritslaid, V. Sammelselg, K. Tammeveski, Electrocatalytic oxygen reduction on silver nanoparticle/multi-walled carbon nanotube modified glassy carbon electrodes in alkaline solution, *Electrochemistry Communications* 20 (2012) 15–18.
6. H. Erikson, M. Liik, A. Sarapuu, J. Kozlova, V. Sammelselg, K. Tammeveski, Oxygen reduction on electrodeposited Pd coatings on glassy carbon, *Electrochimica Acta* 88 (2013) 513–518.

7. H. Erikson, M. Liik, A. Sarapuu, M. Marandi, V. Sammelselg, K. Tammeveski, Electrocatalysis of oxygen reduction on electrodeposited Pd coatings on gold, *Journal of Electroanalytical Chemistry* 691 (2013) 35–41.
8. H. Erikson, A. Sarapuu, K. Tammeveski, J. Solla-Gullón, J. M. Feliu, Shape-dependent electrocatalysis: oxygen reduction on carbon-supported gold nanoparticles, *ChemElectroChem* 1 (2014) 1338–1347.
9. H. Erikson, A. Sarapuu, J. Kozlova, L. Matisen, V. Sammelselg, K. Tammeveski, Oxygen electroreduction on electrodeposited PdAu nanoalloys, *Electrocatalysis* 6 (2015) 77–85.

DISSERTATIONES CHIMICAE UNIVERSITATIS TARTUENSIS

1. **Toomas Tamm.** Quantum-chemical simulation of solvent effects. Tartu, 1993, 110 p.
2. **Peeter Burk.** Theoretical study of gas-phase acid-base equilibria. Tartu, 1994, 96 p.
3. **Victor Lobanov.** Quantitative structure-property relationships in large descriptor spaces. Tartu, 1995, 135 p.
4. **Vahur Mäemets.** The ^{17}O and ^1H nuclear magnetic resonance study of H_2O in individual solvents and its charged clusters in aqueous solutions of electrolytes. Tartu, 1997, 140 p.
5. **Andrus Metsala.** Microcanonical rate constant in nonequilibrium distribution of vibrational energy and in restricted intramolecular vibrational energy redistribution on the basis of Slater's theory of unimolecular reactions. Tartu, 1997, 150 p.
6. **Uko Maran.** Quantum-mechanical study of potential energy surfaces in different environments. Tartu, 1997, 137 p.
7. **Alar Jänes.** Adsorption of organic compounds on antimony, bismuth and cadmium electrodes. Tartu, 1998, 219 p.
8. **Kaido Tammeveski.** Oxygen electroreduction on thin platinum films and the electrochemical detection of superoxide anion. Tartu, 1998, 139 p.
9. **Ivo Leito.** Studies of Brønsted acid-base equilibria in water and non-aqueous media. Tartu, 1998, 101 p.
10. **Jaan Leis.** Conformational dynamics and equilibria in amides. Tartu, 1998, 131 p.
11. **Toonika Rinken.** The modelling of amperometric biosensors based on oxidoreductases. Tartu, 2000, 108 p.
12. **Dmitri Panov.** Partially solvated Grignard reagents. Tartu, 2000, 64 p.
13. **Kaja Orupõld.** Treatment and analysis of phenolic wastewater with microorganisms. Tartu, 2000, 123 p.
14. **Jüri Ivask.** Ion Chromatographic determination of major anions and cations in polar ice core. Tartu, 2000, 85 p.
15. **Lauri Vares.** Stereoselective Synthesis of Tetrahydrofuran and Tetrahydropyran Derivatives by Use of Asymmetric Horner-Wadsworth-Emmons and Ring Closure Reactions. Tartu, 2000, 184 p.
16. **Martin Lepiku.** Kinetic aspects of dopamine D_2 receptor interactions with specific ligands. Tartu, 2000, 81 p.
17. **Katrin Sak.** Some aspects of ligand specificity of P2Y receptors. Tartu, 2000, 106 p.
18. **Vello Pällin.** The role of solvation in the formation of iotsitch complexes. Tartu, 2001, 95 p.

19. **Katrin Kollist.** Interactions between polycyclic aromatic compounds and humic substances. Tartu, 2001, 93 p.
20. **Ivar Koppel.** Quantum chemical study of acidity of strong and superstrong Brønsted acids. Tartu, 2001, 104 p.
21. **Viljar Pihl.** The study of the substituent and solvent effects on the acidity of OH and CH acids. Tartu, 2001, 132 p.
22. **Natalia Palm.** Specification of the minimum, sufficient and significant set of descriptors for general description of solvent effects. Tartu, 2001, 134 p.
23. **Sulev Sild.** QSPR/QSAR approaches for complex molecular systems. Tartu, 2001, 134 p.
24. **Ruslan Petrukhin.** Industrial applications of the quantitative structure-property relationships. Tartu, 2001, 162 p.
25. **Boris V. Rogovoy.** Synthesis of (benzotriazolyl)carboximidamides and their application in relations with *N*- and *S*-nucleophiles. Tartu, 2002, 84 p.
26. **Koit Herodes.** Solvent effects on UV-vis absorption spectra of some solvatochromic substances in binary solvent mixtures: the preferential solvation model. Tartu, 2002, 102 p.
27. **Anti Perkson.** Synthesis and characterisation of nanostructured carbon. Tartu, 2002, 152 p.
28. **Ivari Kaljurand.** Self-consistent acidity scales of neutral and cationic Brønsted acids in acetonitrile and tetrahydrofuran. Tartu, 2003, 108 p.
29. **Karmen Lust.** Adsorption of anions on bismuth single crystal electrodes. Tartu, 2003, 128 p.
30. **Mare Piirsalu.** Substituent, temperature and solvent effects on the alkaline hydrolysis of substituted phenyl and alkyl esters of benzoic acid. Tartu, 2003, 156 p.
31. **Meeri Sassian.** Reactions of partially solvated Grignard reagents. Tartu, 2003, 78 p.
32. **Tarmo Tamm.** Quantum chemical modelling of polypyrrole. Tartu, 2003. 100 p.
33. **Erik Teinmaa.** The environmental fate of the particulate matter and organic pollutants from an oil shale power plant. Tartu, 2003. 102 p.
34. **Jaana Tammiku-Taul.** Quantum chemical study of the properties of Grignard reagents. Tartu, 2003. 120 p.
35. **Andre Lomaka.** Biomedical applications of predictive computational chemistry. Tartu, 2003. 132 p.
36. **Kostyantyn Kirichenko.** Benzotriazole – Mediated Carbon–Carbon Bond Formation. Tartu, 2003. 132 p.
37. **Gunnar Nurk.** Adsorption kinetics of some organic compounds on bismuth single crystal electrodes. Tartu, 2003, 170 p.
38. **Mati Arulepp.** Electrochemical characteristics of porous carbon materials and electrical double layer capacitors. Tartu, 2003, 196 p.

39. **Dan Cornel Fara.** QSPR modeling of complexation and distribution of organic compounds. Tartu, 2004, 126 p.
40. **Riina Mahlapuu.** Signalling of galanin and amyloid precursor protein through adenylate cyclase. Tartu, 2004, 124 p.
41. **Mihkel Kerikmäe.** Some luminescent materials for dosimetric applications and physical research. Tartu, 2004, 143 p.
42. **Jaanus Kruusma.** Determination of some important trace metal ions in human blood. Tartu, 2004, 115 p.
43. **Urmas Johanson.** Investigations of the electrochemical properties of polypyrrole modified electrodes. Tartu, 2004, 91 p.
44. **Kaido Sillar.** Computational study of the acid sites in zeolite ZSM-5. Tartu, 2004, 80 p.
45. **Aldo Oras.** Kinetic aspects of dATP α S interaction with P2Y₁ receptor. Tartu, 2004, 75 p.
46. **Erik Mölder.** Measurement of the oxygen mass transfer through the air-water interface. Tartu, 2005, 73 p.
47. **Thomas Thomborg.** The kinetics of electroreduction of peroxodisulfate anion on cadmium (0001) single crystal electrode. Tartu, 2005, 95 p.
48. **Olavi Loog.** Aspects of condensations of carbonyl compounds and their imine analogues. Tartu, 2005, 83 p.
49. **Siim Salmar.** Effect of ultrasound on ester hydrolysis in aqueous ethanol. Tartu, 2006, 73 p.
50. **Ain Uustare.** Modulation of signal transduction of heptahelical receptors by other receptors and G proteins. Tartu, 2006, 121 p.
51. **Sergei Yurchenko.** Determination of some carcinogenic contaminants in food. Tartu, 2006, 143 p.
52. **Kaido Tamm.** QSPR modeling of some properties of organic compounds. Tartu, 2006, 67 p.
53. **Olga Tšubrik.** New methods in the synthesis of multisubstituted hydrazines. Tartu. 2006, 183 p.
54. **Lilli Sooväli.** Spectrophotometric measurements and their uncertainty in chemical analysis and dissociation constant measurements. Tartu, 2006, 125 p.
55. **Eve Koort.** Uncertainty estimation of potentiometrically measured pH and pK_a values. Tartu, 2006, 139 p.
56. **Sergei Kopanchuk.** Regulation of ligand binding to melanocortin receptor subtypes. Tartu, 2006, 119 p.
57. **Silvar Kallip.** Surface structure of some bismuth and antimony single crystal electrodes. Tartu, 2006, 107 p.
58. **Kristjan Saal.** Surface silanization and its application in biomolecule coupling. Tartu, 2006, 77 p.
59. **Tanel Tätte.** High viscosity Sn(OBu)₄ oligomeric concentrates and their applications in technology. Tartu, 2006, 91 p.

60. **Dimitar Atanasov Dobchev.** Robust QSAR methods for the prediction of properties from molecular structure. Tartu, 2006, 118 p.
61. **Hannes Hagu.** Impact of ultrasound on hydrophobic interactions in solutions. Tartu, 2007, 81 p.
62. **Rutha Jäger.** Electroreduction of peroxodisulfate anion on bismuth electrodes. Tartu, 2007, 142 p.
63. **Kaido Viht.** Immobilizable bisubstrate-analogue inhibitors of basophilic protein kinases: development and application in biosensors. Tartu, 2007, 88 p.
64. **Eva-Ingrid Rõõm.** Acid-base equilibria in nonpolar media. Tartu, 2007, 156 p.
65. **Sven Tamp.** DFT study of the cesium cation containing complexes relevant to the cesium cation binding by the humic acids. Tartu, 2007, 102 p.
66. **Jaak Nerut.** Electroreduction of hexacyanoferrate(III) anion on Cadmium (0001) single crystal electrode. Tartu, 2007, 180 p.
67. **Lauri Jalukse.** Measurement uncertainty estimation in amperometric dissolved oxygen concentration measurement. Tartu, 2007, 112 p.
68. **Aime Lust.** Charge state of dopants and ordered clusters formation in CaF₂:Mn and CaF₂:Eu luminophors. Tartu, 2007, 100 p.
69. **Iiris Kahn.** Quantitative Structure-Activity Relationships of environmentally relevant properties. Tartu, 2007, 98 p.
70. **Mari Reinik.** Nitrates, nitrites, N-nitrosamines and polycyclic aromatic hydrocarbons in food: analytical methods, occurrence and dietary intake. Tartu, 2007, 172 p.
71. **Heili Kasuk.** Thermodynamic parameters and adsorption kinetics of organic compounds forming the compact adsorption layer at Bi single crystal electrodes. Tartu, 2007, 212 p.
72. **Erki Enkvist.** Synthesis of adenosine-peptide conjugates for biological applications. Tartu, 2007, 114 p.
73. **Svetoslav Hristov Slavov.** Biomedical applications of the QSAR approach. Tartu, 2007, 146 p.
74. **Eneli Härk.** Electroreduction of complex cations on electrochemically polished Bi(*hkl*) single crystal electrodes. Tartu, 2008, 158 p.
75. **Priit Möller.** Electrochemical characteristics of some cathodes for medium temperature solid oxide fuel cells, synthesized by solid state reaction technique. Tartu, 2008, 90 p.
76. **Signe Viggor.** Impact of biochemical parameters of genetically different pseudomonads at the degradation of phenolic compounds. Tartu, 2008, 122 p.
77. **Ave Sarapuu.** Electrochemical reduction of oxygen on quinone-modified carbon electrodes and on thin films of platinum and gold. Tartu, 2008, 134 p.
78. **Agnes Kütt.** Studies of acid-base equilibria in non-aqueous media. Tartu, 2008, 198 p.

79. **Rouvim Kadis.** Evaluation of measurement uncertainty in analytical chemistry: related concepts and some points of misinterpretation. Tartu, 2008, 118 p.
80. **Valter Reedo.** Elaboration of IVB group metal oxide structures and their possible applications. Tartu, 2008, 98 p.
81. **Aleksei Kuznetsov.** Allosteric effects in reactions catalyzed by the cAMP-dependent protein kinase catalytic subunit. Tartu, 2009, 133 p.
82. **Aleksei Bredihhin.** Use of mono- and polyanions in the synthesis of multisubstituted hydrazine derivatives. Tartu, 2009, 105 p.
83. **Anu Ploom.** Quantitative structure-reactivity analysis in organosilicon chemistry. Tartu, 2009, 99 p.
84. **Argo Vonk.** Determination of adenosine A_{2A}- and dopamine D₁ receptor-specific modulation of adenylyl cyclase activity in rat striatum. Tartu, 2009, 129 p.
85. **Indrek Kivi.** Synthesis and electrochemical characterization of porous cathode materials for intermediate temperature solid oxide fuel cells. Tartu, 2009, 177 p.
86. **Jaanus Eskusson.** Synthesis and characterisation of diamond-like carbon thin films prepared by pulsed laser deposition method. Tartu, 2009, 117 p.
87. **Marko Lätt.** Carbide derived microporous carbon and electrical double layer capacitors. Tartu, 2009, 107 p.
88. **Vladimir Stepanov.** Slow conformational changes in dopamine transporter interaction with its ligands. Tartu, 2009, 103 p.
89. **Aleksander Trummal.** Computational Study of Structural and Solvent Effects on Acidities of Some Brønsted Acids. Tartu, 2009, 103 p.
90. **Eerold Vellemäe.** Applications of mischmetal in organic synthesis. Tartu, 2009, 93 p.
91. **Sven Parkel.** Ligand binding to 5-HT_{1A} receptors and its regulation by Mg²⁺ and Mn²⁺. Tartu, 2010, 99 p.
92. **Signe Vahur.** Expanding the possibilities of ATR-FT-IR spectroscopy in determination of inorganic pigments. Tartu, 2010, 184 p.
93. **Tavo Romann.** Preparation and surface modification of bismuth thin film, porous, and microelectrodes. Tartu, 2010, 155 p.
94. **Nadežda Aleksejeva.** Electrocatalytic reduction of oxygen on carbon nanotube-based nanocomposite materials. Tartu, 2010, 147 p.
95. **Marko Kullapere.** Electrochemical properties of glassy carbon, nickel and gold electrodes modified with aryl groups. Tartu, 2010, 233 p.
96. **Liis Siinor.** Adsorption kinetics of ions at Bi single crystal planes from aqueous electrolyte solutions and room-temperature ionic liquids. Tartu, 2010, 101 p.
97. **Angela Vaasa.** Development of fluorescence-based kinetic and binding assays for characterization of protein kinases and their inhibitors. Tartu 2010, 101 p.

98. **Indrek Tulp.** Multivariate analysis of chemical and biological properties. Tartu 2010, 105 p.
99. **Aare Selberg.** Evaluation of environmental quality in Northern Estonia by the analysis of leachate. Tartu 2010, 117 p.
100. **Darja Lavõgina.** Development of protein kinase inhibitors based on adenosine analogue-oligoarginine conjugates. Tartu 2010, 248 p.
101. **Laura Herm.** Biochemistry of dopamine D₂ receptors and its association with motivated behaviour. Tartu 2010, 156 p.
102. **Terje Raudsepp.** Influence of dopant anions on the electrochemical properties of polypyrrole films. Tartu 2010, 112 p.
103. **Margus Marandi.** Electroformation of Polypyrrole Films: *In-situ* AFM and STM Study. Tartu 2011, 116 p.
104. **Kairi Kivirand.** Diamine oxidase-based biosensors: construction and working principles. Tartu, 2011, 140 p.
105. **Anneli Kruve.** Matrix effects in liquid-chromatography electrospray mass-spectrometry. Tartu, 2011, 156 p.
106. **Gary Urb.** Assessment of environmental impact of oil shale fly ash from PF and CFB combustion. Tartu, 2011, 108 p.
107. **Nikita Oskolkov.** A novel strategy for peptide-mediated cellular delivery and induction of endosomal escape. Tartu, 2011, 106 p.
108. **Dana Martin.** The QSPR/QSAR approach for the prediction of properties of fullerene derivatives. Tartu, 2011, 98 p.
109. **Säde Viirlaid.** Novel glutathione analogues and their antioxidant activity. Tartu, 2011, 106 p.
110. **Ülis Sõukand.** Simultaneous adsorption of Cd²⁺, Ni²⁺, and Pb²⁺ on peat. Tartu, 2011, 124 p.
111. **Lauri Lipping.** The acidity of strong and superstrong Brønsted acids, an outreach for the “limits of growth”: a quantum chemical study. Tartu, 2011, 124 p.
112. **Heisi Kurig.** Electrical double-layer capacitors based on ionic liquids as electrolytes. Tartu, 2011, 146 p.
113. **Marje Kasari.** Bisubstrate luminescent probes, optical sensors and affinity adsorbents for measurement of active protein kinases in biological samples. Tartu, 2012, 126 p.
114. **Kalev Takkis.** Virtual screening of chemical databases for bioactive molecules. Tartu, 2012, 122 p.
115. **Ksenija Kisseljova.** Synthesis of aza-β³-amino acid containing peptides and kinetic study of their phosphorylation by protein kinase A. Tartu, 2012, 104 p.
116. **Riin Rebane.** Advanced method development strategy for derivatization LC/ESI/MS. Tartu, 2012, 184 p.

117. **Vladislav Ivaništšev.** Double layer structure and adsorption kinetics of ions at metal electrodes in room temperature ionic liquids. Tartu, 2012, 128 p.
118. **Irja Helm.** High accuracy gravimetric Winkler method for determination of dissolved oxygen. Tartu, 2012, 139 p.
119. **Karin Kipper.** Fluoroalcohols as Components of LC-ESI-MS Eluents: Usage and Applications. Tartu, 2012, 164 p.
120. **Arno Ratas.** Energy storage and transfer in dosimetric luminescent materials. Tartu, 2012, 163 p.
121. **Reet Reinart-Okugbeni.** Assay systems for characterisation of subtype-selective binding and functional activity of ligands on dopamine receptors. Tartu, 2012, 159 p.
122. **Lauri Sikk.** Computational study of the Sonogashira cross-coupling reaction. Tartu, 2012, 81 p.
123. **Karita Raudkivi.** Neurochemical studies on inter-individual differences in affect-related behaviour of the laboratory rat. Tartu, 2012, 161 p.
124. **Indrek Saar.** Design of GalR2 subtype specific ligands: their role in depression-like behavior and feeding regulation. Tartu, 2013, 126 p.
125. **Ann Laheäär.** Electrochemical characterization of alkali metal salt based non-aqueous electrolytes for supercapacitors. Tartu, 2013, 127 p.
126. **Kerli Tõnurist.** Influence of electrospun separator materials properties on electrochemical performance of electrical double-layer capacitors. Tartu, 2013, 147 p.
127. **Kaija Põhako-Esko.** Novel organic and inorganic ionogels: preparation and characterization. Tartu, 2013, 124 p.
128. **Ivar Kruusenberg.** Electroreduction of oxygen on carbon nanomaterial-based catalysts. Tartu, 2013, 191 p.
129. **Sander Piiskop.** Kinetic effects of ultrasound in aqueous acetonitrile solutions. Tartu, 2013, 95 p.
130. **Iлона Faustova.** Regulatory role of L-type pyruvate kinase N-terminal domain. Tartu, 2013, 109 p.
131. **Kadi Tamm.** Synthesis and characterization of the micro-mesoporous anode materials and testing of the medium temperature solid oxide fuel cell single cells. Tartu, 2013, 138 p.
132. **Iva Bozhidarova Stoyanova-Slavova.** Validation of QSAR/QSPR for regulatory purposes. Tartu, 2013, 109 p.
133. **Vitali Grozovski.** Adsorption of organic molecules at single crystal electrodes studied by *in situ* STM method. Tartu, 2014, 146 p.
134. **Santa Veikšina.** Development of assay systems for characterisation of ligand binding properties to melanocortin 4 receptors. Tartu, 2014, 151 p.
135. **Jüri Liiv.** PVDF (polyvinylidene difluoride) as material for active element of twisting-ball displays. Tartu, 2014, 111 p.

136. **Kersti Vaarmets.** Electrochemical and physical characterization of pristine and activated molybdenum carbide-derived carbon electrodes for the oxygen electroreduction reaction. Tartu, 2014, 131 p.
137. **Lauri Tõntson.** Regulation of G-protein subtypes by receptors, guanine nucleotides and Mn^{2+} . Tartu, 2014, 105 p.
138. **Aiko Adamson.** Properties of amine-boranes and phosphorus analogues in the gas phase. Tartu, 2014, 78 p.
139. **Elo Kibena.** Electrochemical grafting of glassy carbon, gold, highly oriented pyrolytic graphite and chemical vapour deposition-grown graphene electrodes by diazonium reduction method. Tartu, 2014, 184 p.
140. **Teemu Näykki.** Novel Tools for Water Quality Monitoring – From Field to Laboratory. Tartu, 2014, 202 p.
141. **Karl Kaupmees.** Acidity and basicity in non-aqueous media: importance of solvent properties and purity. Tartu, 2014, 128 p.
142. **Oleg Lebedev.** Hydrazine polyanions: different strategies in the synthesis of heterocycles. Tartu, 2015, 118 p.
143. **Geven Piir.** Environmental risk assessment of chemicals using QSAR methods. Tartu, 2015, 123 p.
144. **Olga Mazina.** Development and application of the biosensor assay for measurements of cyclic adenosine monophosphate in studies of G protein-coupled receptor signaling. Tartu, 2015, 116 p.
145. **Sandip Ashokrao Kadam.** Anion receptors: synthesis and accurate binding measurements. Tartu, 2015, 116 p.
146. **Indrek Tallo.** Synthesis and characterization of new micro-mesoporous carbide derived carbon materials for high energy and power density electrical double layer capacitors. Tartu, 2015, 148 p.